BLAST ENERGY DISSIPATION USING VISCOELASTIC DAMPING PAD AND DESIGN OF A BLAST RESISTANT WALL

A DISSERTATION

Submitted in partial fulfilment of the

requirements for the award of the degree

of

MASTER OF TECHNOLOGY

in

EARTHQUAKE ENGINEERING

(With Specialisation in Structural Dynamics)

By

ARKA MAITY

(17526004)

DEPARTMENT OF EARTHQUAKE ENGINEERING

INDIAN INSTITUTE OF TECHNOLOGY ROORKEE

ROORKEE – 247 667 (INDIA)

JUNE, 2019

CANDIDATE'S DECLARATION

I hereby declare that the work carried out in this thesis entitled **Blast Energy Dissipation Using Viscoelastic Damping Pad and Design of a Blast Resistant Wall**, is being submitted to the department of Earthquake Engineering, IIT Roorkee towards partial fulfilment for the requirements of the award of degree of Master of Technology in Earthquake Engineering with specialisation in STRUCTURAL DYNAMICS. This is an authentic report of my work prepared by myself during the period of May, 2018 to June, 2019 under expert guidance of the supervisor **Dr. Manish Shrikhande**, Professor, Department of Earthquake Engineering, IIT Roorkee.

The matter embodied in this thesis report, to the best of our knowledge, has not been submitted by me for the award of any other degree of this institute or any other institutes.

Place: Roorkee   Arka Maity

Dt.– . . . .   Enrolment No.- 17526004

CERTIFICATE

This is to certify that the above statement made by the candidate is correct to best of my knowledge and belief.

Dr. Manish Shrikhande

Professor

Dept. of Earthquake Engg.

IIT, Roorkee

ACKNOWLEDGEMENT

ABSTRACT

This end term evaluation report gives an overview of the blast phenomenon and subsequent effects on structures, behaviour of elastomer (viscoelastic materials) under cyclic loading, and an idea about blast energy dissipation using viscoelastic damping pads. It also gives idea of how a blast resistant wall can be designed despite being subjected to high impact loading. It has been seen that with suitable thickness of elastomer pad we can significantly reduce the blast pressure. Hence we can think about a proper blast resistant wall by dissipating blast pressure before it hits the wall. A linear spring – dashpot model has been built up and implemented in a common purpose finite element software ABAQUS. A parametric study of pressure reduction for different thickness of elastomer has been carried out for a particular type of viscoelastic material. Then using the transferred pressure for a specific thickness of pad, a preliminary analysis and design has been carried out in SAP2000. However, the shear stress at base is much higher than the permissible value for the considered concrete grade and hence we have used a composite section of embedded I sections in concrete for the vulnerable ground support. Then again a rigorous modelling of the blast wall is done in ABAQUS with blast loading transferred through the pad. This includes constitutive modelling of concrete and steel. For steel elastic – perfectly plastic behaviour is chosen. Concrete Damaged Plasticity (CDP) model has been opted in ABAQUS to model brittle concrete material. A mesh convergence study has been performed to check the mesh sensitivity for the stress at a critical position on wall. Finally, full analysis is run and the damage contour is observed after one cycle of blast loading. To make the reinforced concrete structure safe, we have to make sure that there is no compression damage in the structure. Moreover, the valuable equipments inside the building have to be safeguarded against the surface blast induced ground vibration. For this purpose a trenching technique is adopted in between point of detonation and the face of the building. The trench is found to be very effective even for a small constructable depth to reduce the shock ground acceleration by a great extent. This composite section with supporting shear walls along with a trench in between the detonation point and the face of the building make the whole structure stand safely after the explosion occurs.

Contents

List of Figures

List of Tables

Chapter 1

Introduction and Literature Review

An explosion represents a large scale of energy released in a very short time which creates a gust of wind known as blast. Unlike earthquake or other dynamic loads blast is an impact type of load and under such loading structure behaves differently. Rather than the integrated action and load transfer in a building or structure for a blast or any impact type of loading, local flexibility governs the behaviour of structure. For example, if a bullet strikes a brittle material (like glass or concrete) instead of crushing of materials, indentation or penetration takes place. Now, blast load comes in form of huge air pressure. It is difficult to save a structure if the full air pressure strikes any face of the building (for closer point of detonation). Hence we should think about some external damping source that will reduce the blast pressure first and then it will transfer to the building. There are many damping sources like friction damper, viscous damper, etc. but one of the innovative solution is using viscoelastic damping materials (rubbers or elastomers).

Typically the engineering approach to resist blast effects has been through improving the energy storage capacity. Malvar et al. [28] proposed to strengthen structural elements using composites such that their capacities meet the demand and insure the integrity of the structure avoiding local failure in case of blast. Salim et al. [37] and [36] used steel-studs for providing anchorage to the infill wall against out of plane pressure due to blast. Hamburger and Whittaker [14] report use of a structural steel framing system to avoid progressive collapse of building due to severe damage in limited vertical load carrying elements. The moment resistant connections at each floor level help to redistribute the loads away from damaged elements. These methods of structural strengthening do not perform satisfactorily in the case of blast due to high explosive yield and/or short stand-

off distances. In such cases some external passive energy dissipation system are necessary to reduce the impact. Smith [38] studied possibility of using frangible walls for blast resistant design. Sand or water filled panels were found to be efficient in dissipating blast pressure in addition to leading to non-destructive and non-lethal debris in case of blast. Amadio and Bedon [2] have numerically modelled glass curtain walls with viscoelastic dissipative devices and compared with experimental results given by Kranzer et al. [22]. These reflects the effectiveness and usefulness of viscoelastic dampers in a blast resistant system. However, these simulations and experiments are conducted in such a way that viscoelastic dampers are subjected to shear stresses. But if a large wall to be secured against blast mobilising shear stiffness of elastomer will be difficult since the self-weight transfer will be a problem. In order to model in under compressive or bearing pressure we have to go through related literatures. For example, Fediuc et al. [10] have shown the behaviour of elastomers under compressive pressure for different viscoelastic materials or elastomers. It is seen that there is an increasing slope of stress vs strain curve indicating hyperelastic behaviour of rubber under compression. They have compared many empirical or semi empirical relations to find out effective compression modulus and bearing stiffness of elastomers. The most useful one is the relation given by Lindley (1970) which is mentioned by Fediuc et al. [10]. Gent [12] has also followed those relations and has given a calibrated table to find the parameters.

Again, the most important issue is damping by elastomers. Any viscoelastic material shows good quality of hysteretic damping due to its viscous component apart from the elastic one. This property is also known as loss property of materials which is prominent for viscoelastic materials. Connor [6], Genta [13] and many others have elaborated the way viscoelastic materials dissipates energy. The most common and simplest model is the Kelvin (Voigt) model consisting a spring and dashpot in parallel and it gives a reasonable approximation of behaviour of elastomers (using linear system approximation). The parameters can be found out using these previously mentioned literatures.

Blast load modelling is another challenge. It is a high pressure load which loses its strength with time. For rigorous modelling of blast load, modified forms of Friedlander's decay equation is almost everywhere used [11]. The parameters required for this equation can be found from several literatures, codes etc. IS:4991 [17], UFC 3-340-02, 2008 [40] etc. are such codes which are predominantly used. Empirical relations for overpressure

given by Brode [5], Newmark and Hansen [32], Mills [31] etc. are also used to characterize the decay equations.

Another issue is modelling the concrete for a finite element software. It is a little complex because the concrete behaviour is itself complex showing different behaviour under compression and tension. For ABAQUS, a common purpose FEA software, the most commonly used constitutive model is the 'Damaged Plasticity' model. In this model compressive and tensile behaviour in terms of cracking and crushing strain has to be given along with plasticity parameters for modified Drucker Prager failure criterion given by Lubliner et al. [26] with further modifications made by Lee and Fenves [25]. The detailed discussion of modelling CDP (concrete damaged plasticity) is given in literatures by Kmiecik and Kamiński [21], Jankowiak and Lodygowski [20] etc. The concrete stress strain models are very much abundant from different literatures and codes. The most commonly used is the one given by Mander et al. [29].

Moreover blast induced ground vibration can be controlled using trenching since it is a well established technique for vibration isolation especially in case of machine foundation where machine induced vibration of the ground is reduced to a great extent just by digging a trench in around the vibrating machine. Hence it can be an interesting solution to reduce the ground acceleration due to surface blast a few metres away from the face of the structure.

This is the briefing about the literature and detailed discussions will be coming in respective sections. Using these we can proceed to the solution of our problem of designing a blast resistant wall system using viscoelastic damping pads.

Chapter 2

Objectives

Our problem is to initially dissipate the blast pressure before it strikes the wall of a building. And then it becomes a design problem with different trial configuration of structure. Hence the major objectives are:

1. To model the elastomer bearing pad (mount on the blast wall) following Voigt's model (linear springdashpot model). For this it is required to model equivalent bearing stiffness (k_c) and equivalent dashpot coefficient (C_{eq}).

2. To model the blast pressure decay equation for specific size of charge and stand-off distance given in problem statement.

3. To prepare the model including springs and dashpots representing the elastomer pad in ABAQUS and get the reduced load that is getting transferred to the wall.

4. To use this reduced load to analyse and design a suitable blast resisting reinforced concrete wall system in SAP2000.

5. To rigorously model the blast resisting wall system with required reinforcements (predicted by analysis in SAP2000) with proper constitutive modelling of concrete and steel in ABAQUS.

6. Applying the reduced blast load (by viscoelastic pad) on the face of the blast resistant wall and analyse for it.

7. Looking into the damage contour predicted by ABAQUS.

8. Modelling a soil domain using Mohr Coulomb with different depth of trenches in around the mid point between the face of the blast wall and the point of detonation for ground surface explosion.

9. Applying the blast pressure vertically downward on the ground surface for surface explosion and analyse for different trench depths.

10. Comparing the reduction in horizontal ground acceleration due to trenching of different depths and assess the effectiveness of trenches.

Chapter 3

Properties and Modelling of Blast Pressure

3.1.   Introduction to Blast Phenomenon

An explosion is a large-scale sudden and rapid energy release which can be a consequence of a physical, chemical or nuclear event. In case of nuclear events, the energy is released from the formation of different atomic nuclei due to the redistribution of the neutrons and protons within the interacting nuclei. However, in case of a chemical explosion, rapid oxidation of fuel elements (Carbon and Hydrogen atoms) is the main cause. When the explosion takes place, a huge amount of energy is released within microseconds. The velocity in a detonation process can be as high as 10 km/s in case of solid explosives. The expanding detonation products within the explosives hit the surrounding undisturbed air particles and compress them suddenly within microseconds. Hence at the detonation point the air pressure instantaneously increases to a huge order (even up to 300 kilobars while ambient air pressure is 1.013 bar). Now due to this sudden increase in pressure, following the laws of thermodynamics, air heats up and temperature gets elevated to a huge extent (even up to 5000 °C at the point of detonation). The increase of pressure above the ambient static pressure is known as overpressure. But this overpressure dissipates with time quickly, hence making the blast pressure an impact type of loading.

Now a shock wave is generated at the detonation point which travels in space rapidly and dissipates energy as it goes away from the detonation point. Hence with traversing more distance, the amplitude of shock wave front gets reduced as shown in Figure 3.1 It

7
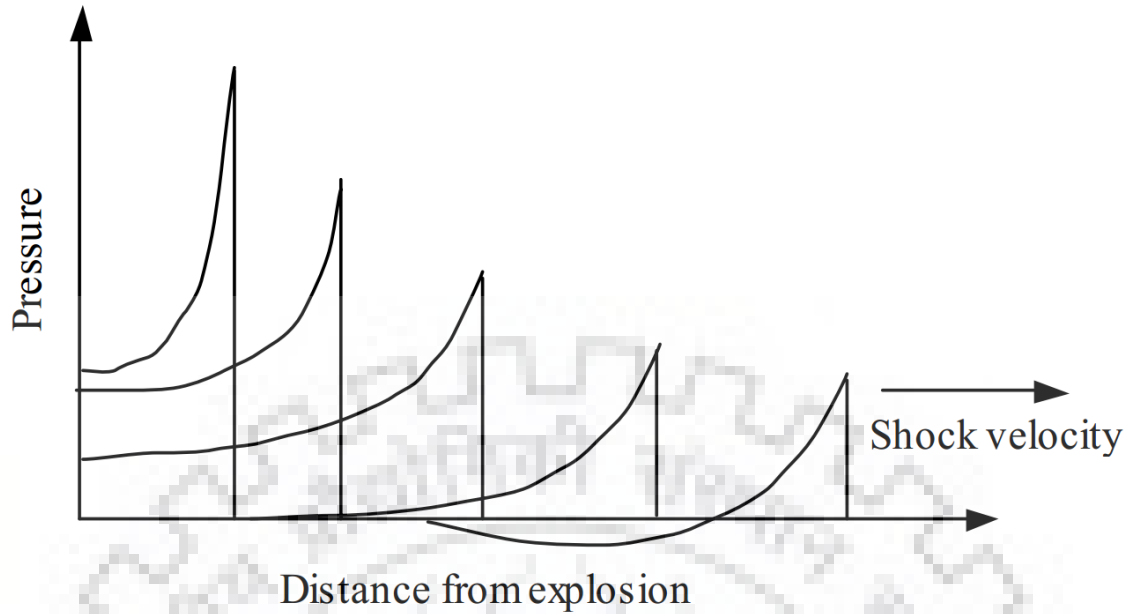
Figure 3.1: Shock wave propagation in blast (Ngo et al. [33])

is also observed that behind the shock wave front, after very short time, the pressure falls below the ambient atmospheric air pressure, thus creating a negative phase of blast. During the negative phase, suction wind is created which carries debris from long distances. Hence the profile of blast pressure consists of an overpressure in the positive phase and a suction in the negative phase (very small amplitude compared to the positive phase overpressure). The amplitude of the overpressure and suction pressure depends on the distance of the detonation point from the point of interest and the weight of the charge.

Hence, in a nutshell during detonation very rapid chemical reaction takes place and it proceeds in a supersonic velocity (known as detonation velocity, it can be as high as 6.5-8 km/s) inside the explosive. This detonation wave rapidly converts solid or liquid constituents of the explosive to very hot, dense and high- pressure gas and creates a shock wave front which is known as the blast wave. This wave front expands from the surface of the explosive and as it goes away from the source, it decays in strength, lengthens the duration and this phenomenon is known as the **spherical divergence**. However, if a structure obstructs the path of the shock wave front, the structure is subjected to a very high pressure, known as **Reflected Overpressure** which is quite a few times higher than the static overpressure. The magnitude and distribution of blast pressure on a structure depends on:

- Type and weight of the explosive material.

- The distance of the point of detonation from the structure.

- Interaction of the blast wave with ground creates certain amplification. This also depends on the height of detonation, because if the reflected wave from the ground merges with incident wave (forming Mach Stem) then the effect will be much more. Hence near ground blast yields much more detrimental effect compared to the free air blast.

3.2.   Some Basic definitions Related to Air Blast

- **Blast Wave:** It is a shock wave which propagates away from source with decaying energy. It is nothing but an air pressure wave in which immediately peak is attained and then amplitude is decayed. In all of the pressure components, i.e. static overpressure, reflected overpressure and dynamic pressure, this sort of decaying behaviour is observed, though the decay rate may be different.

- **Overpressure (p_s):** The excess pressure that is developed in the vicinity of blast, above the ambient atmospheric air pressure is known as overpressure or static overpressure, or side –on overpressure, or incident pressure or gauge pressure.

- **Dynamic Pressure (q_s):** Dynamic pressure develops due to the movement of the air (wind) around the structure, for example drag on a building. Due to blast wind a considerable dynamic pressure is acted on any structure.

- **Reflected Overpressure (p_r):** When the shock pressure wave in terms of blast wind is obstructed by a structure, then the blast wave gets reflected, subjecting the front wall of the structure to a much more elevated pressure than the static overpressure (even more than 8 times). Reflected overpressure (p_r) to peak incident or static overpressure (p_{so}) ratio for free air blast is given in UFC 3-340-02, 2008 [40] which is shown in Figure 3.2.

- **Flow Mach Number (M):** It is the ratio of flow velocity to the local speed of sound. Though it is unitless, its direction is specified as the direction of the flow.

- **Specific Heat Ratio (γ):** It is the ratio of the constant pressure specific heat (C_p) to the constant volume specific heat (C_v). this parameter is always greater than 1 as stated in thermodynamics.
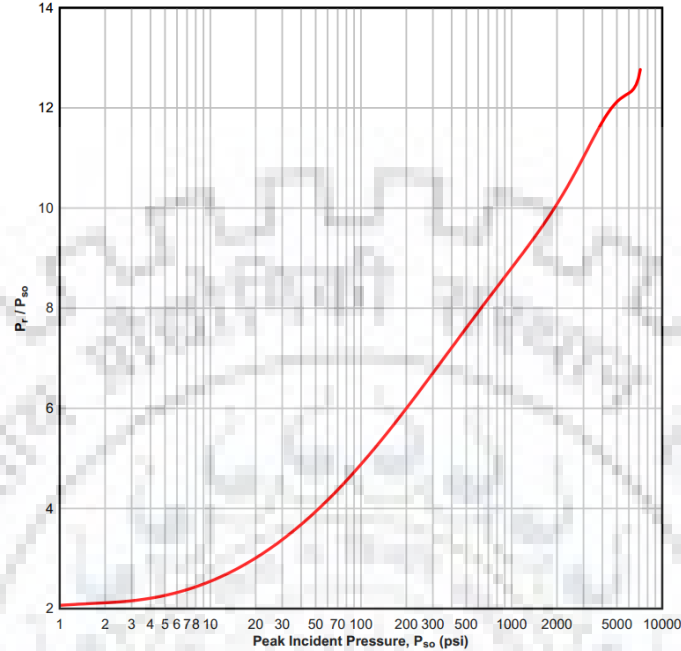
Figure 3.2: Peak incident pressure vs the ratio of peak reflected pressure to peak incident pressure or overpressure for free air blast (UFC 3-340-02, 2008 [40])

- **Transit Time:** It is the time required for the shock wave or blast wave front to travel across the structure or the member under consideration.

- **Scaled Distance (Z):** It is given by the following expression:

$$Z = \frac{R}{W^{1/3}} \tag{3.1}$$

Where, R is the actual distance (Stand-off distance) from detonation point to the point of concern in meters, W is the mass of the charge expressed as mass of a standard explosive (Generally TNT). W is generally considered in kg unit. However, in IS:4991 [17], W is considered in tonnes, and instead of TNT, the reference explosive is considered as an explosive that releases 1.5×10^9 calories heat during explosion of one tonne of the same.

- **Scaled Time (t_0):** It is also given in the similar manner:

$$t_0 = \frac{t}{W^{1/3}} \tag{3.2}$$

Where, t is the actual time, and W is the equivalent mass of charge expressed as mass of reference explosive.

- **TNT Equivalency:** Since most of the available data regarding blast are empirical in nature (either in form of chart or in form of empirical equations), and any empirical relation or chart can be used for only that explosive material which was used to derive the expressions or calibrate the chart or table, we have to find some measure so that we can use these available data for other explosives too. Therefor an effective charge weight is used by comparing the energy released in one explosive with a reference explosive (mostly TNT). The effects of energy output of an explosive material are compared to that of TNT by a function of the heat of detonation, as given by UFC 3-340-02, 2008 [40]:

$$W_E = \frac{H_{EXP}^d}{H_{TNT}^d} \times W_{EXP} \tag{3.3}$$

Where, W_E is the effective charge weight (TNT equivalent), W_{EXP} is the actual weight of explosive concerned, H_{EXP}^d is the heat of detonation of the explosive in question and H_{TNT}^d is the heat of detonation of TNT.

3.3. Characteristics of Blast Pressure Profile

Blast load profile is mostly described by its peak side-on or static overpressure (p_{so}), peak reflected overpressure (p_{ro}), dynamic pressure (q_o), caused by specific equivalent amount (mass) of reference explosive at a certain distance from the structure. The other defining parameters are the positive phase duration (t_o) and positive phase duration in idealised equivalent linear decay of blast pressure profile (t_{of} or t_d). A typical pressure variation due to a free air blast (the effect is almost double in contact blast as one dimensional shock front is created instead of spherical one) at a scaled distance Z is given in the Figure 3.3. The negative phase is ignored by the most people. But in our study we have assumed a triangular pulse shown in Figure 3.3. The details of the decay equation in positive and negative phase will be discussed later.

It is noticeable that just after blast static overpressure increases suddenly, and then it decays exponentially until it reaches the negative phase. After the negative phase is covered finally the static overpressure gets diminished and the air pressure becomes equal
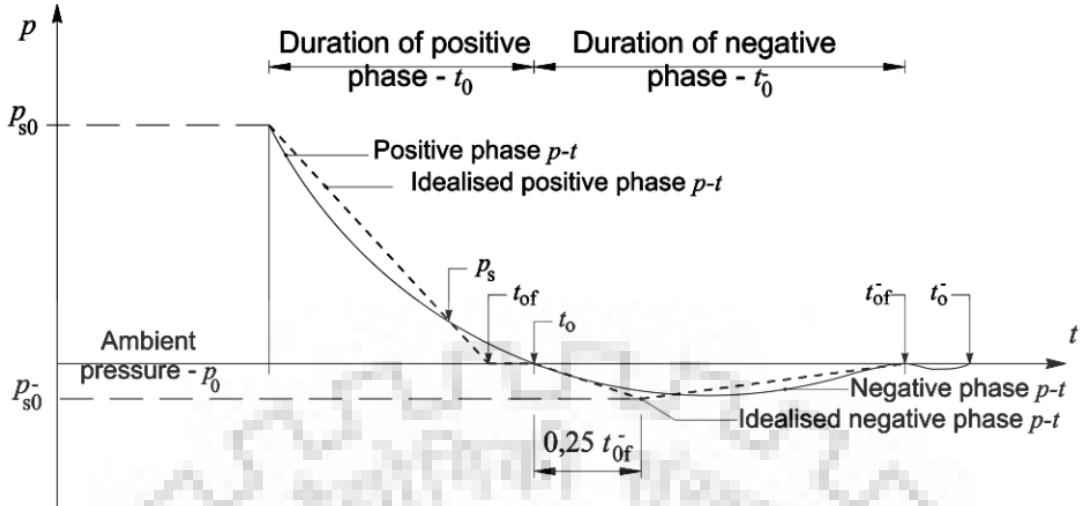
Figure 3.3: Typical static overpressure time history at a scaled distance Z (Draganić and Sigmund [8])

to the ambient atmospheric pressure. The piecewise linear approximation of blast pressure profile is also shown in the Figure 3.3

The decay equation for static overpressure can be described by a semi-empirical relation known as 'Modified Friedlander equation':

$$p_s(t) = p_{so}\left(1 - \frac{t}{t_0}\right)\exp\left(-\frac{bt}{t_0}\right) \tag{3.4}$$

Where b (sometimes termed as α) is known as the decay constant which is a parameter of the waveform. The rest parameters are defined earlier. Modified Friedlander equation can also be used for defining Reflected Overpressure History. Only instead of p_{so} we have to use the peak reflected overpressure value (p_{ro}).

Similarly, when the shock wave hits the structure, reflected overpressure on the front face of the structure develops which is much higher than the static overpressure. Typical idealised piecewise linear reflected overpressure (p_r) time history is given in Figure 3.4.

However, Figure 3.4 is not always the same and changeable in terms of shape or values. The pressure on the front face (closest to blast) of structure at any instance of time is the maximum of p_r and ($p_s + C_D q$), where C_D is the drag coefficient of the structure.

Again t_c is the clearance time, which is defined by the time required for attaining reflected overpressure of ($p_s + C_D q$) from the peak value of reflected over pressure p_{ro}. The clearance time (t_c) is evaluated by the following equation:
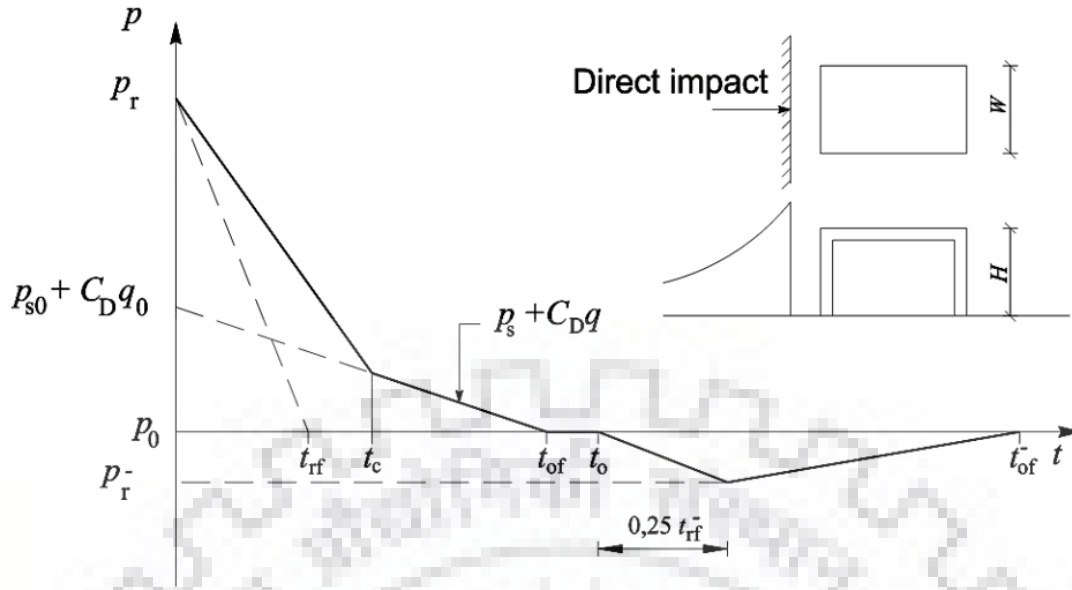
Figure 3.4: Typical idealised reflected overpressure time history at a scaled distance Z
(Draganić and Sigmund [8])

$$t_c = \frac{3S}{U} \quad \text{or} \quad t_d \text{ (also denoted as } t_{fo}) \quad \text{whichever is less} \tag{3.5}$$

Where S is equal to H (height) or $B/2$ (B is the width of structure) (Figure 3.5) whichever is less. The dimensions of above ground building with front face is given in the Figure 3.5.
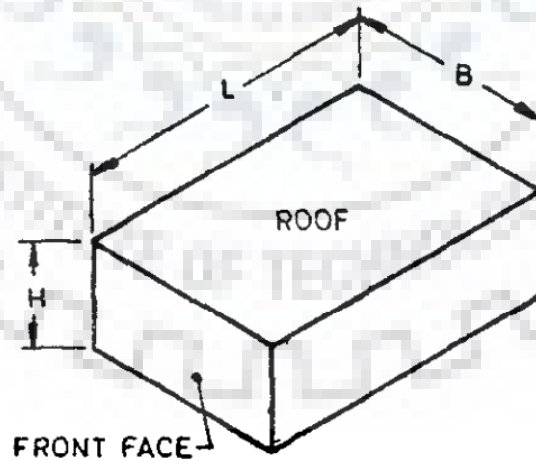
Figure 3.5: Above ground rectangular structure (IS:4991 [17])

And U is the Shock Front Velocity and it's a product of Mach number (M) and velocity of sound in air (a) ($U = M. \, a$). IS:4991 [17] also gives recommendation for a as $344 \, m/s$ at mean sea level (MSL) at a temperature of $20 \, °C$. Mach number is defined by

the following equation:

$$M = \sqrt{\left(1 + \frac{6p_{so}}{7p_a}\right)} \tag{3.6}$$

Where p_{so} is the peak static overpressure and p_a is the ambient air pressure.

From eq: (3.5) it is evident that Figure 3.4 is only true when clearance time (t_c) is less than the positive phase duration for idealised pressure decay plot $(t_d$ (or t_{fo})) so that the slope of decay changes its slope. However, if clearance time (t_c) equal or greater than the idealised positive phase duration (t_d), then the reflected overpressure decay plot becomes a triangular pulse similar to the idealised static overpressure history. Figure 3.6 and Figure 3.7 gives this comparison it the plot of pressure history.
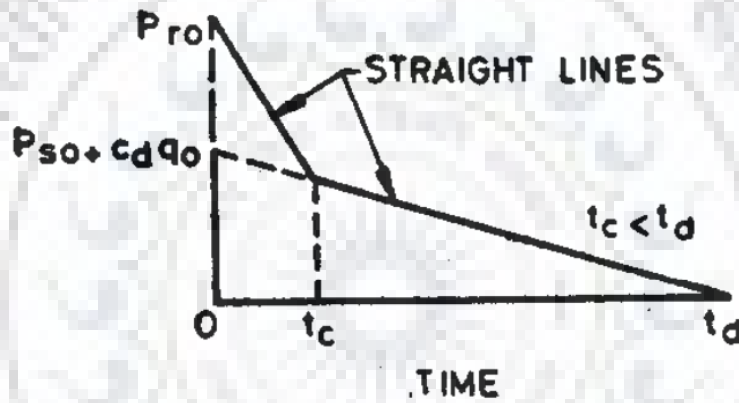
Figure 3.6: Reflected Overpressure History if $t_c < t_d$ (IS:4991 [17])
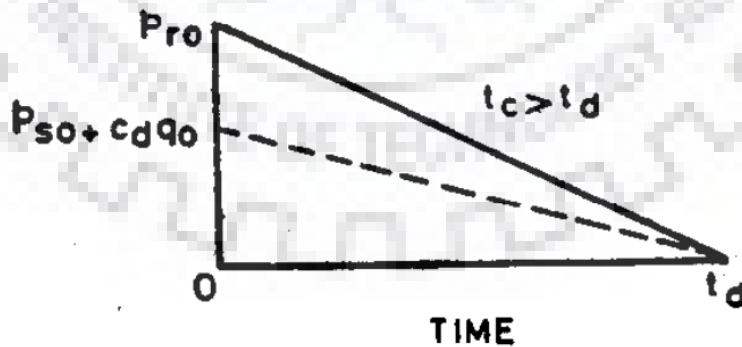
Figure 3.7: Reflected Overpressure History if $t_c > t_d$ (IS:4991 [17])

Another parameter is the dynamic pressure (q), which develops due to dynamic effects of blast induced wind with the structures (such as drag). It decays at a higher rate than the static and reflected overpressure. IS:4991 [17] gives the decay equation for dynamic

pressure:

$$q(t) = q_o \left(1 - \frac{t}{t_0}\right)^2 \exp\left(-2\alpha \frac{t}{t_0}\right) \tag{3.7}$$

Where α (or b) is the same decay constant in Friedlander equation used for static over-pressure. IS:4991 [17] also gives decay equation for static overpressure:

$$p_s(t) = p_{so} \left(1 - \frac{t}{t_0}\right) \exp\left(-\alpha \frac{t}{t_0}\right) \tag{3.8}$$

Where α (or b) is the same decay constant for static overpressure.

3.4.   Evaluation of defining parameters for Blast Pressure Profile

There have been a number of literature available for the calculation of incident overpressure at a scaled stand-off distance Z. some of are given in this section.

Brode [5] gives the following values for the peak static overpressure for the near ($p_s >$ 10 bar) and medium to far field ($p_s <$ 10 bar):

$$p_{so} = \begin{cases} \frac{6.7}{Z^3} + 1 \quad \text{bar} & \text{if } p_{so} > 10\,\text{bar} \\ \frac{0.975}{Z} + \frac{1.455}{Z^2} + \frac{5.85}{Z^3} - 0.019 \quad \text{bar} & \text{if } 0.1 < p_{so} < 10\,\text{bar} \end{cases} \tag{3.9}$$

Where Z is the scaled stand-off distance in m/kg$^{1/3}$.

Newmark and Hansen [32] proposed the following expressions:

$$p_{so} = 6784 \frac{W}{R^3} + 93 \sqrt{\frac{W}{R^3}} \quad \text{bar} \tag{3.10}$$

Where W is the mass of TNT equivalent in kg and R is the distance from point of detonation.

Mills [31] proposed the following:

$$p_{so} = \frac{1772}{Z^3} - \frac{114}{Z^2} + \frac{108}{Z} \quad \text{bar} \tag{3.11}$$

Where Z is the scaled stand-off distance in m/kg$^{1/3}$

Mays et al. [30] proposed the following expression for wave front speed (U) and maximum dynamic pressure (q_s):

$$U = a_0 \sqrt{\frac{6p_s + 7p_0}{7p_0}} \quad \text{m/s} \tag{3.12}$$

$$q_s = \frac{5p_s^2}{2\left(p_s + 7p_0\right)} \quad \text{bar} \tag{3.13}$$

Where, p_s is the static waveferont overpressure (bar), p_0 is the ambient pressure (bar), and a_0 is the speed of sound in air (m/s). It is noted that the same expression is given in IS:4991 [17] for wave front velocity. Rankine et al. [34] and Huguenot [30] derived the equation for reflected peak overpressure:

$$p_r = 2p_s + (\gamma + 1)q_s \tag{3.14}$$

For $\gamma = 1.4$ after substituting eq: (3.13) in this eq: (3.14) we get following most used equation:

$$p_r = \frac{2p_s\left(7p_0 + 4p_s\right)}{7p_0 + p_s} \tag{3.15}$$

However, in this study we will follow the chart given in IS:4991 [17] for determination of static and reflected overpressure, dynamic pressure, positive phase duration, etc. Although, IS:4991 [17] does not dictate anything upon the modelling of negative phase and hence for modelling negative phase we have to go for some other literature which is discussed later. The Table-1 of IS:4991 [17] for determination of blast pressure parameters are given in Table 3.1.

Table 3.1: Blast Parameters for Ground Blast for 1 Tonne of Reference Explosive [17]

Distance (x) (m)	Peak side-on over-pressure (p_{so}/p_a)	Mach No. (M)	Positive phase duration (t_0) (milliseconds)	Duration of equivalent triangular pulse (t_d or t_{fo}) (milliseconds)	Dynamic pressure ratio (q_0/p_a)	Peak reflected overpressure ratio (p_{r0}/p_a)
15	8.00	2.80	9.50	5.39	10.667	41.60
18	5.00	2.30	11.00	7.18	5.208	22.50
21	3.30	1.96	16.38	9.33	2.643	12.94
24	2.40	1.75	18.65	11.22	1.532	8.48
27	1.80	1.60	20.92	13.30	0.920	5.81
30	1.40	1.48	22.93	15.39	0.583	4.20
33	1.20	1.42	24.95	16.31	0.439	3.45
36	1.00	1.36	26.71	17.94	0.312	2.75
39	0.86	1.32	28.22	19.20	0.235	2.28
42	0.76	1.28	29.74	20.20	0.186	1.97
45	0.68	1.25	31.25	21.60	0.142	1.66
48	0.59	1.23	32.26	22.70	0.115	1.46
51	0.53	1.20	33.52	23.70	0.093	1.28
54	0.48	1.19	34.52	24.70	0.077	1.14
57	0.43	1.17	35.53	26.40	0.062	1.01
60	0.40	1.16	36.29	26.60	0.054	0.93
63	0.37	1.15	37.30	27.80	0.046	0.85
66	0.34	1.14	38.05	28.76	0.039	0.77
69	0.32	1.13	38.81	29.25	0.035	0.72
72	0.30	1.12	38.96	29.87	0.031	0.67
75	0.28	1.11	40.32	30.71	0.027	0.62
78	0.26	1.104	40.82	31.85	0.023	0.58
81	0.25	1.10	41.58	31.92	0.022	0.55

Note regarding Table 3.1:

1. The ambient air pressure p_a is taken as 1 kg/cm^2 (100 kPa) at the MSL.

2. One tonne of standard explosive is equivalent to 1.5×10^9 calories (IS:4991 [17]).

3. This table is used for surface blast only. The decay equations given in IS:4991 [17] is already given in eq: (3.7) and eq: (3.8).

Moreover, this table used actual stand-off distance instead of scaled distance because this is only for unit weight of explosive (1 tonne). It has to be noted that the unit used to get scaled distance and scaled time as per IS:4991 [17] is tonne instead of kg.

Hence using the scaled distance (Z m/tonne$^{1/3}$) we get the rest parameters. It is also noted that the time that we read from this literature is scaled time (t s/tonne$^{1/3}$) as defined in eq: (3.2). In order to get the actual time, we must multiply it by cube root of weight of reference explosive.

3.5.   Equivalent Piecewise Linearization of Blast Pressure Profile

In the eq: (3.4) if we use b (or α) $= 0$, we get a linear profile. Hence in idealised linear decay, the decay constant is assumed to be zero. But in order to idealise the pressure profile we have to equate the actual curve with that of the idealised curve.

Following the decay equation given in IS:4991-1968 using eq: (3.8):

Impulse under actual profile:

$$I = I_{max} = \int_0^{t_0} p_s\left(t\right) dt = p_{so} t_0 \left(\frac{1}{\alpha} - \frac{1 - e^{-\alpha}}{\alpha^2}\right) \tag{3.16}$$

While idealised profile gives impulse:

$$I = I_{ideal} = \frac{1}{2} p_{so} t_d \tag{3.17}$$

Equating eq: (3.16) and eq: (3.17) we get the time duration in idealised blast profile:

$$t_d = t_{of} = \frac{2I}{p_{so}} \tag{3.18}$$

These sources and empirical relations or charts let us define several parameters using which we can draw the profile of blast pressure which is discussed in the next section.

3.6.   Modelling Blast Profile for Reflected Overpressure on Blast Wall

So far we have discussed how to get the salient features that are required to get the blast profile. Now we will try to look into the process to draw the profile using those features for both positive and negative phase.

3.6.1   Modelling Positive phase of blast pressure on wall

The positive phase is modelled using the parameters given in different literatures, in our case it is IS:4991 [17]. Then these parameters are fit into modified Friedlander's equation (Friedlander [11]) as proposed by Rigby et al. [35]:

$$p_r\left(t\right) = p_{ro}\left(1 - \frac{t}{t_0}\right)\exp\left(-\frac{\alpha t}{t_0}\right)$$

(3.19)

Where all the parameters denote the same entity as it has been used for earlier. The only unknown in this equation is decay constant (α or b), since all others can be found using IS:4991 [17].

We can obtain peak reflected pressure (p_{ro}), positive phase duration (to) and time duration of idealised positive phase with linear decay (t_d or t_{of}) using Table 3.1 (obtained from IS:4991 [17]). Now we can evaluate the impulse from the ideal pressure profile using eq: (3.17) since all the parameters on the right hand side are known.

Now, impulse (I) is a known quantity and it has to be equal for the actual blast profile too. So we can equate the known impulse with eq: (3.16):

$$I = I_{max} = \int_0^{t_0} p_r\left(t\right)dt = p_{ro}t_0\left(\frac{1}{\alpha} - \frac{1 - e^{-\alpha}}{\alpha^2}\right)$$

Again all the parameters are known in this equation except the decay constant which can be easily evaluated by solving this equation in a trial and error method. Thus the positive phase of blast pressure on wall is modelled.

Note- IS:4991 [17] only gives parameters for surface blast only.

3.6.2   Modelling Negative Phase of Blast Pressure on Wall

Since IS:4991 [17] does not give any recommendation on the negative phase of a blast profile, we will follow the negative phase modelled reviewed by Rigby et al. [35] by compiling theories from different literatures. In this literature, simplified expression for peak

negative phase pressure (p_{ro}^- or $p_{r,min}$) and impulse in the negative phase (I_r^-) are obtained by digitizing the negative phase data (shown in Figure 3.8) presented in UFC 3-340-02, 2008 [40] and fitting curves through the data points. The equations for peak negative pressure(p_{ro}^- or $p_{r,min}$) (in kPa) are given in eq: (3.20) for scaled distance Z (in m/kg$^{1/3}$). Similarly, we can use simplified expressions given by Rigby et al. [35] for negative phase impulse (I_r^-) (in kPa.ms or Pa.s) are given in eq: (3.21).
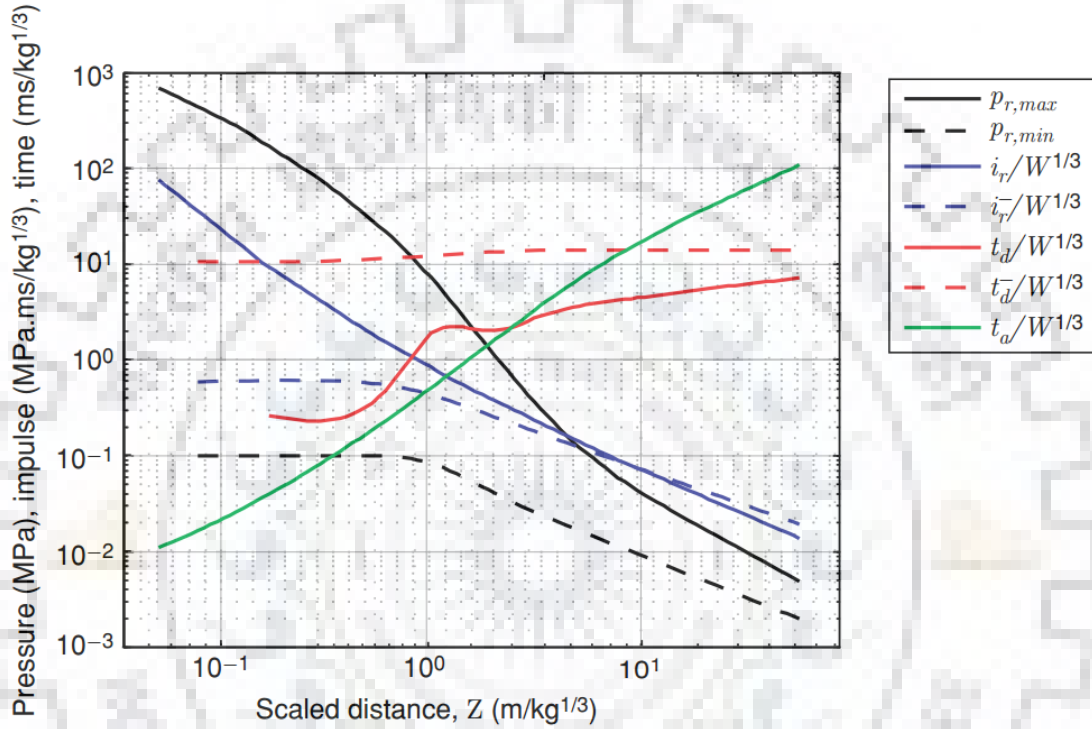
Figure 3.8: Positive and negative phase reflected blast wave parameters for hemispherical charges of TNT on the surface [17]

$$p_{r,min}\,(Z)\,(in\,\mathrm{kPa}) = \begin{cases} 101 & \text{if } 0.071 < Z \le 0.668 \\ -32.9Z^2 + 13.0Z + 106 & \text{if } 0.668 < Z \le 1.27 \\ 93.0Z^{-1.22} & \text{if } 1.27 < Z \le 2.78 \\ 73.0Z^{-0.978} & \text{if } 2.78 < Z \le 37.6 \end{cases} \quad (3.20)$$

$$I_r^-\,(Z)\,(in\,\mathrm{kPa.ms}) = \sqrt[3]{W} \times \begin{cases} -724Z^2 + 445Z + 553 & \text{if } 0.071 < Z \le 0.580 \\ 11.4Z^2 - 315Z + 752 & \text{if } 0.580 < Z \le 1.19 \\ 462Z^{-0.880} & \text{if } 1.19 < Z \le 5.25 \\ 434Z^{-0.842} & \text{if } 5.25 < Z \le 37.6 \end{cases} \quad (3.21)$$

Note- eq: (3.20) and eq: (3.20) are given by Rigby et al. [35] and the pressure is in kPa and impulse is in kPa.ms or Pa.s unit. W is the weight of equivalent TNT charge in kg.

Now, let's have an approximated triangular phase of the negative phase as shown in Figure 3.3, which is also proposed by Rigby et al. [35] in reference of Krauthammer and Altenberg [23]. In this linear approximation, we consider the negative phase to reach the peak at time $(t_0 + 0.25t_d^-)$, where t_d^- or t_{of}^- is the total duration of negative phase in the idealised triangular profile.

This negative phase duration (t_d^- or t_{of}^-) can be obtained by equating impulse:

$$I_r^- = \frac{1}{2}p_{r,min}t_d^-$$

(3.22)

In the eq: (3.22), all parameters are known from eq: (3.20) and eq: (3.21). Hence the negative phase duration (t_d^- or t_{of}^-) is found out. Now we can find out equation of the linear model using simple equations of straight line in the time vs pressure plane:

$$p_r^-(t) = \begin{cases} -p_{r,min}\left(\frac{t-t_0}{0.25t_d^-}\right) & \text{if } t_0 < t \leq t_0 + 0.25t_d^- \\ -p_{r,min}\left(1 - \frac{t-\left(t_0+0.25t_d^-\right)}{0.75t_d^-}\right) & \text{if } t_0 + 0.25t_d^- < t \leq t_0 + t_d^- \end{cases}$$

(3.23)

Thus, blast load profile modelling for negative phase is also done. Now, we can go into our problem for this study.

Chapter 4

Properties and Modelling of Viscoelastic Materials

4.1. Introduction to Rheological Models

The term **'viscoelastic'** is evolved from two terms associated to the properties of materials, i.e. 'viscous' and 'elastic'. Hence it is evident that a viscoelastic material exhibits properties of both elastic solids as well as viscous fluids. Rubbers and many other polymers are the most common examples of such type of materials. Since these materials exhibits complex behaviour in terms of response to loading, the load vs deformation model is mostly converged from material testing. However, there are a few numerical models given by the physicists which can be selectively used for defining a viscoelastic material using some combinations of simple linear springs and dashpots. These idealised models are known as **Rheological Models or Mechanical Models**. There can be two, three or multiple element models available which are used in accordance to the most suitable purpose. **Maxwell and Kelvin (Voigt) Model** are two of the most common two element models (i.e. only one spring and one dashpot). Sometimes depending on our interest we go for the most generalised multi-element models such as **Generalised Maxwell and Generalised Kelvin Model**.

However, in dynamics problems the most suitable way to model a viscoelastic material is by the **Kelvin (Voigt) Model**. It consists of a spring and a dashpot in parallel which is just similar to the way we represent a dynamics problem. All we have to do is to find out the spring and dashpot coefficient consciously so that it convincingly replicates the

behaviour of viscoelastic materials. Figure 4.1 shows the schematic representation of
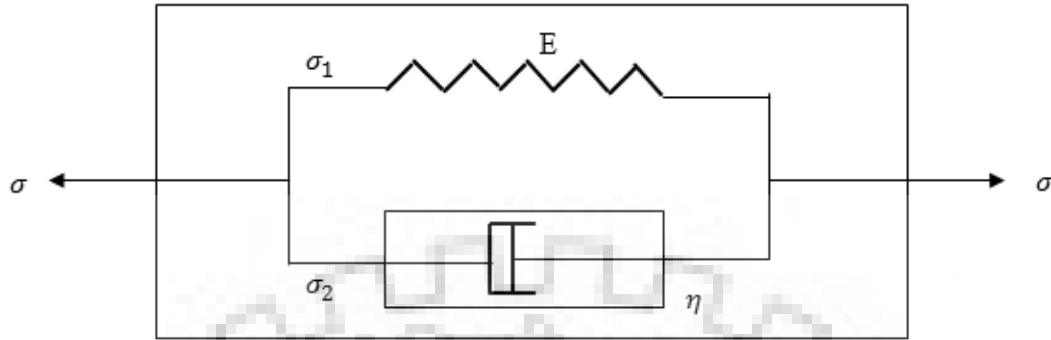
Figure 4.1: Kelvin (Voigt) Model

the Voigt's model, where E is the elastic stiffness of the spring, η is the viscosity of the material, σ is the applied pressure on the material. Since the spring and dashpot are in parallel they will be having the same deformation and strain. For the elastic spring, we can write $\epsilon = \frac{1}{E}\sigma_1$, where σ_1 is the stress taken up by the spring. For the dashpot, we can write, $\dot{\epsilon} = \frac{1}{\eta}\sigma_2$, where σ_2 is the dashpot stress. Hence for the parallel connection, constitutive law for Voigt's model becomes:

$$\sigma = E\epsilon + \eta\dot{\epsilon} \tag{4.1}$$

Though we mostly go for material constitutive model in terms of stress vs strain response, using suitable parameters for spring and dashpot, for accurate study we must go for a creep response test of viscoelastic materials with proper laboratory set-up.

4.2. Constitutive Modelling and Damping in Viscoelastic Material for Dynamics Problem

Genta [13] has compared the viscoelastic model proposed by Kelvin (Voigt) with the simple one degree of freedom system for dynamics problem.

The spring force is defined by the equation:

$$F = kx \tag{4.2}$$

Similarly, the linear viscous damper force (on an assumption that the material reacts to a force that depends only on the strain rate):

$$F = C\dot{x} \tag{4.3}$$

Here x, and $\dot{x}$ are representing displacement and velocity respectively. This linear viscous damping model is also known as the Newton's Model.

Hence for a viscoelastic material represented by a parallel connection of a linear spring and a linear dashpot follows the force-displacement and stress-strain relationships:

$$F = kx + C\dot{x} \tag{4.4}$$

$$\sigma = E\epsilon + C\dot{\epsilon} \tag{4.5}$$

Where σ is the stress, ϵ is the strain, $\dot{\epsilon}$ is the linear strain rate, k is the spring constant, C is the dashpot coefficient.

However, this type of model is not really applicable to the viscoelastic materials in a straight forward manner. Over the past few years it is observed in experiments that many materials under cyclic loading show an internal damping causing energy loss per cycle proportional to the square of the amplitude and independent of frequency. This behaviour is known as Hysteretic or Structural Damping. Rubbers (or other viscoelastic materials) are most commonly known for such kind of energy dissipation under reversible oscillations even within the elastic limit (unlike concrete or steel which exhibit energy dissipation by hysteresis after yielding) due to the viscous portion in the material stiffness. Since in cyclic loading test it has been seen that the rubber like materials follows an elliptical path in the stress-strain curve though the area of ellipse is generally found small (Figure 4.2). Hence the damping properties of such kind of materials come from the energy dissipation in hysteresis cycle. Hence in order to use the Voigt's model, we have to find out some sort of equivalent viscous damping. Before that we will have a look at the elliptical nature of the stress strain curves and its defining properties. Hence we can infer that the structural damping can only be observed if the stress changes its direction (shows cyclic behaviour). Moreover, since the material is linear the displacement time history has to be similar too. However, since in a viscoelastic material we have an elliptical stress-strain path (and also from the eq: (4.5)), we observe a phase lag between strain and stress (Figure 4.3) Now if we try to write the mathematical form of the stress and strain as function of time for
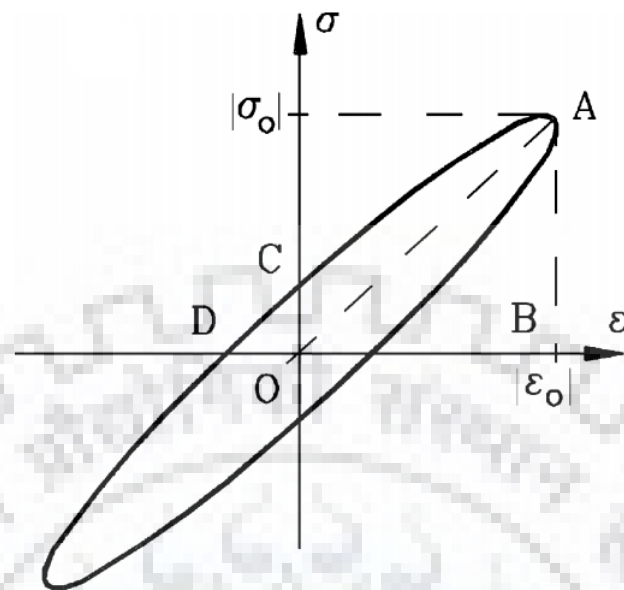
Figure 4.2: Stress-Strain (σ-ϵ) behaviour of viscoelastic material (Genta [13])
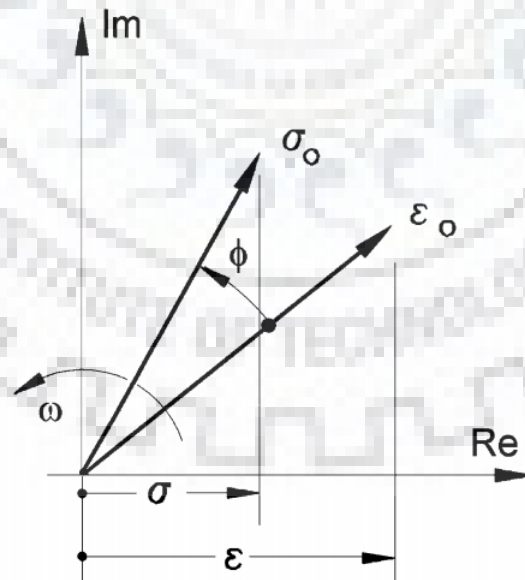
Figure 4.3: Stress-Strain (σ-ϵ) vectors of viscoelastic material in complex plane (Genta [13])

operating frequency ω and assuming maximum strain ϵ_0 is occurring at time $t = 0$:

$$\text{Strain} \Rightarrow \epsilon = \epsilon_0 \cos(\omega t) \tag{4.6}$$

$$\text{Stress} \Rightarrow \sigma = \sigma_0 \cos(\omega t + \phi) \tag{4.7}$$

In complex notation (as in Figure 4.3) it is written as:

$$\text{Strain} \Rightarrow \epsilon = \epsilon_0 \, e^{i\,\omega t} \tag{4.8}$$

$$\text{Stress} \Rightarrow \sigma = \sigma_0 \, e^{i\,(\omega t + \phi)} \tag{4.9}$$

Where σ_0 and ϵ_0 are amplitudes of stress and strain respectively and are represented by real numbers.

Now, for an elastic material the ratio between stress and strain is known as the Young's Modulus or Elastic Modulus (E). For a viscoelastic material, in a similar passion we can define Complex Modulus as:

$$E^* = \frac{\sigma}{\epsilon} = \frac{\sigma_0}{\epsilon_0} e^{i\,\phi} = E(\cos\phi + i\,\sin\phi) \tag{4.10}$$

The real part of the complex modulus represents the elastic properties of the viscoelastic material and gives the measure of Elastic Stiffness (E'). It is most commonly known as In-phase Modulus or Storage modulus:

$$E' = E\cos\phi \tag{4.11}$$

The complex part of the complex modulus represents the viscous behaviour of the viscoelastic material. Since this part is responsible for damping, it is known as In-quadrature Modulus or **Loss Modulus** (E''):

$$E'' = E\sin\phi \tag{4.12}$$

The ratio of loss modulus to the storage modulus is known as **Loss Factor** (η):

$$\eta = \frac{E''}{E'} = \tan\phi \tag{4.13}$$

In the similar manner we can also have Shear Storage Modulus (G') as well as Shear Loss Modulus (G'').

However, in the industry viscoelastic materials are defined by only **Shear Storage Modulus** and the **Loss factor**. These are given in a calibrated chart or plot in a semi-logarithmic scale for different operating frequencies and different operating temperatures. This plot or chart is known as **Nomograph**.
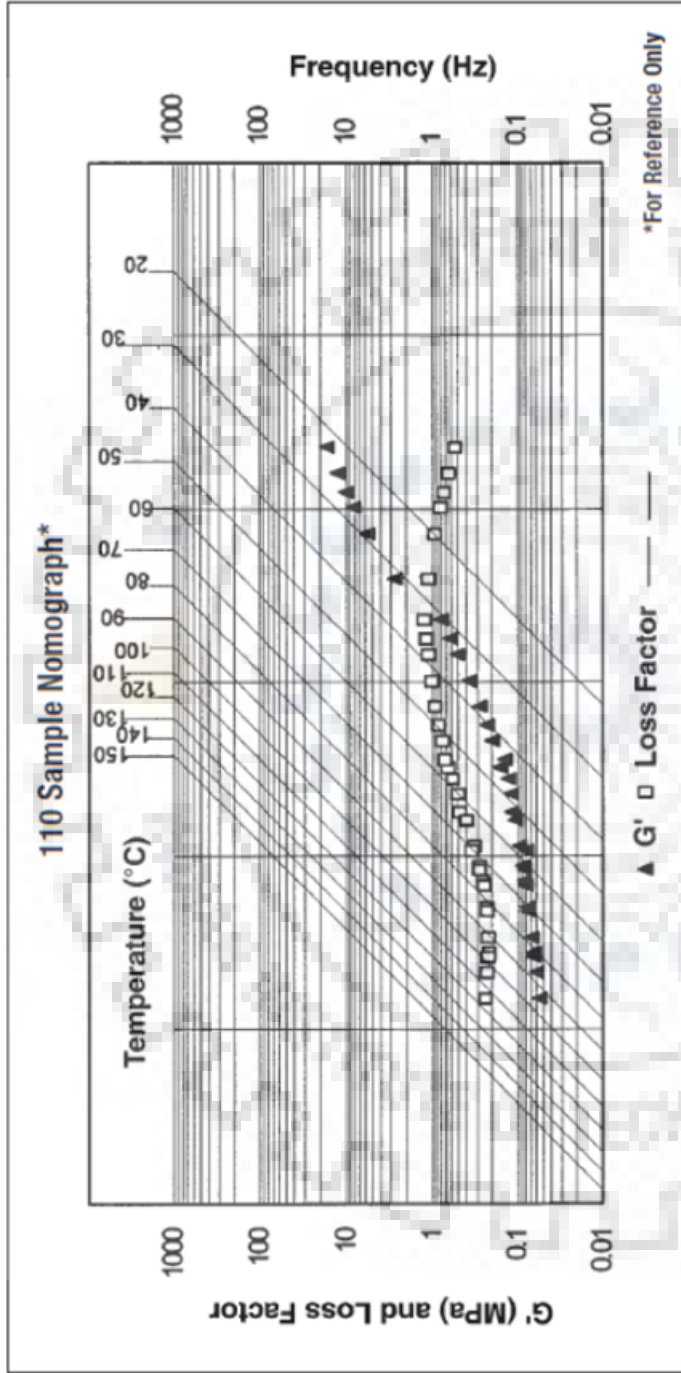
Figure 4.4: Sample nomograph for 110 series viscoelastic damping polymer (Technical Data, 3M Products [39])

In Figure 4.4, a sample nomograph of 110 series of viscoelastic damping material by 3M Products (obtained from the catalogue) has been given. From this nomograph one can find out the Loss Factor (η) and the Shear Storage Modulus (G'). The only thing that has to be known prior to the reading of data from nomograph is the operating temperature and the operating frequency. All the nomographs are calibrated using the experimental results already conducted by the manufacturer itself, the details of which can be found in the catalogue provided by the manufacturer of polymer.

However, there is a proper sequence to read the property corresponding to the existing condition. The sequence to follow for determining loss factor and shear storage modulus:

- Desired operating frequency is located on the right hand scale first.

- Horizontally the chosen frequency line is followed until the isotherm for the desired temperature is intersected.

- Now from the intersect we move up or down vertically until both loss factor curve and the shear storage modulus curve is crossed.

- Finally, the loss factor and shear storage modulus are read from the left hand scale.

Now, from the nomograph we are able to get the major properties for the viscoelastic polymer from which we can derive other parameters either by standard expressions or some charts. Once we can find the stiffness we can express it in the two components – the elastic stiffness part and the viscous stiffness part in the complex plane:

$$k = k' + i\,k'' \tag{4.14}$$

Where k' is the in-phase or storage stiffness and k'' is the in-quadrature or loss stiffness. Hence the loss factor is also defined as:

$$\eta = \frac{k''}{k'} = \tan\phi \tag{4.15}$$

Sometimes another parameter is used to describe the damping which is the ratio of the energy dissipated per cycle to the maximum elastic energy stored during maximum amplitude. The area of ellipse in Figure 4.2 is denoting the dissipated energy in one cycle. The area of triangle OAB from the same figure represents the maximum elastic energy stored in the system. This ratio is expressed as:

$$\psi = \frac{\pi\sigma_0\epsilon_0\sin\phi}{\frac{1}{2}\sigma_0\epsilon_0} = 2\pi\sin\phi \tag{4.16}$$

This is also known as hysteretic damping. Unlike the viscous damping it is evident that the hysteretic damping is independent of frequency.

The area of the hysteretic loop within the elastic limit is very small for most of the engineering materials except some viscoelastic materials or elastomers. Hence the following approximations can be made if the damping is small (i.e. except elastomers):

$$k' \approx k \quad \text{and} \quad k'' = \eta k' \approx \eta k \tag{4.17}$$

$$\text{Hence,} \quad k = k' + i\,\eta k' \approx k\,(1 + i\,\eta) \tag{4.18}$$

$$\text{Also,} \quad \eta \approx \phi \quad \text{and} \quad \psi \approx 2\pi\phi \approx 2\pi\eta \tag{4.19}$$

Some of the loss factors of the common engineering materials are enlisted in the Table 4.1.

Table 4.1: Loss Factors for Common Materials [13]

Material	Loss Factor (η)
Aluminium Alloy	$0.0001 - 0.001$
Cast Iron	$0.001 - 0.08$
Steel	$0.01 - 0.06$
Rubber/ Elastomer	**$0.01 - 3$**

From Table 4.1 we can observe that the rubbers and such viscoelastic materials possess very high value of the loss factor, hence the energy dissipation per cycle is quite high compared to the other materials. This is why viscoelastic materials dissipate major energy in case of cyclic loading by the hysteresis cycle. And for the same reason the viscous characteristics are prominent in elastomers or rubbers, and not so much observed in elastic materials like steel, aluminium etc. **Since the loss factor is high in the viscoelastic materials (mostly it is found to be in the range of 1 to 1.5 for the viscoelastic materials and rubbers) we make an approximation to use the simplified expression for stiffness and damping as given in eq: (4.17) to eq: (4.19).**

4.3. Evaluation of Equivalent Viscous Damping for Viscoelastic Damping Pad

The complex modulus and complex stiffness has already been introduced in Section 4.2 for harmonic loading. Now if we neglect any viscous damping, we can write the equation of motion for a Single Degree of Freedom (SDOF) system as:

$$m\ddot{x}\left(t\right) + kx\left(t\right) = f\left(t\right) \tag{4.20}$$

Where x is the displacement variable, k is the effective stiffness of the system and f is the external force variable applied. Naturally, x and f are function of time.

Now if we consider harmonic loading, we expect harmonic response in the system. Hence We can write:

$$f\left(t\right) = f_0 \cos \omega t \tag{4.21}$$

$$x\left(t\right) = x_0 \cos \omega t \tag{4.22}$$

Also if the stiffness component coming from the viscoelastic material, we will have the complex stiffness (from eq: (4.18)) consisting of elastic as well as the viscous part with a time lag:

$$k_{eq} = k\left(1 + i\,\eta\right) \tag{4.23}$$

Using eq. (4.21), (4.22) and (4.23) we can rewrite eq: (4.20) in the form of the equation of motion in frequency domain:

$$\left[-\omega^2 m + k\left(1 + i\,\eta\right)\right] x_0 = f_0 \tag{4.24}$$

Now, for a SDOF system with viscous damping, we can write the equation as :

$$m\ddot{x}\left(t\right) + C\dot{x}\left(t\right) + kx\left(t\right) = f\left(t\right) \tag{4.25}$$

Where C is the viscous damping coefficient. Similar to the previous case we can write the equation in the frequency domain using eq (4.21) and (4.22) as:

$$\left[-\omega^2 m + i\,\omega C + k\right] x_0 = f_0 \tag{4.26}$$

Now we can see a component of hysteresis damping is being acted in eq: (4.24) for the presence of the viscoelastic material. If we want to find the corresponding Voight's model,

we have to find the equivalent stiffness and dashpot coefficient. To find the equivalent dashpot coefficient, we have to equate the imaginary part of eq: (4.24) and (4.26):

$$i\,\omega C = i\,\eta k \tag{4.27}$$

$$\text{Hence,} \quad C_{eq} \approx \frac{\eta k}{\omega} \tag{4.28}$$

From eq: (4.28), we get an approximation of the Equivalent Viscous Damping Coefficient (C_{eq}). However, this equation is dependent on the loading frequency or the frequency of the hysteresis cycle. But the other damping measure for hysteretic damping ψ given in eq: (4.16) shows that the hysteresis damping is independent of frequency, while eq: (4.28) shows that the damping is as high as infinite when the operating frequency approaches zero, making it frequency dependent.

To remove the frequency dependency, universally approved equation (modified from eq: (4.28)) is:

$$\text{Hence,} \quad C_{eq} \approx \frac{\eta k}{\omega_r} \tag{4.29}$$

Where ω_r is the reference frequency at which equivalent viscous damping dissipates the same energy as the hysteretic damping. It is seen that for $\omega_r = \omega_n$ i.e. the natural frequency, a reasonable approximation is found (Genta [13]):

$$\text{Hence,} \quad C_{eq} \approx \frac{\eta k}{\omega_n} \tag{4.30}$$

Eq: (4.30) is mostly used for viscoelastic material models. Again, it has to be remembered that it's only an approximation assuming that the system is linear and the hysteresis damping is the same as the equivalent viscous one if the reference frequency is the same as the natural frequency of the system. Moreover, the elastic moduli and the loss factors for most of the engineering materials are only approximated to be frequency independent, but truly they are not.

4.4.   Evaluation of Compressive Stiffness for Elastomeric Damping Pad

Rubbers and other elastomeric materials behave like hyperelastic material, the constitutive model of which comes from strain energy density function, and which is sometimes described by non-linear elastic models. Hence it is evident that the stiffness does not

remain the same in such material models. In case of shear stiffness, the stiffness is simply dependent on the shear modulus (G) of the specimen:

$$k_s = \frac{AG}{t} \tag{4.31}$$

Where, k_s is the shear stiffness of the material, G is the shear modulus, A is the loading area, and t is the elastomer specimen thickness. Hence, by getting the shear modulus value from the catalogue of the elastomer, we can simply work out the shear stiffness of the material. But this is only true if there is no compression on the pad. If there is compression strain in the pad and loading area is greater than the bulging area (Shape factor > 1) then the shear modulus increases too considerably.

However, we are only interested in the **bearing stiffness** or the **compression stiffness** of the elastomer pad which is relevant in this project. Under compression, we cannot directly evaluate bearing stiffness directly using the elastic modulus at zero strain, since the property of the material gets enhanced in the presence of compressive loading, as in the case of hyperelastic materials. Many experimental results also show that the slope of the stress strain curve eventually increase with increasing compressive strain value. An example is given below.

Fediuc et al. [10] have used Chloroprene/neoprene rubber (CR) and Natural rubber (NR) specimens for compression tests and recorded several results. Some of which is attached in Figure 4.5 and 4.6. they have followed elastomer compression test procedures given in ASTM D 395-03 [4], using specimen thickness 12.5 ± 0.5 mm and diameter 29.0 ± 0.5 mm and loading at a rate of 0.05 kN/s and a maximum value of 0.2 kN using universal testing machine. They have observed that the stiffness increases with increasing compressive strain for all specimens (Figure 4.5 and 4.6). It is also observed that the increased compression modulus value is dependent upon the hardness of the elastomer and the shape factor (ratio of loading area to the bulging area). If the shape factor is high the effective compression modulus is very much higher than the elastic modulus at zero compressive strain. They have also noticed that the effective compression modulus best converges to the expression of effective compression modulus given by Gent [12].

Hence it is evident that for compression stiffness of elastomer, instead of using elastic modulus at zero strain, we have to use an effective compression modulus which is generally higher than elastic modulus at zero strain if shape factor is high). Since the expression
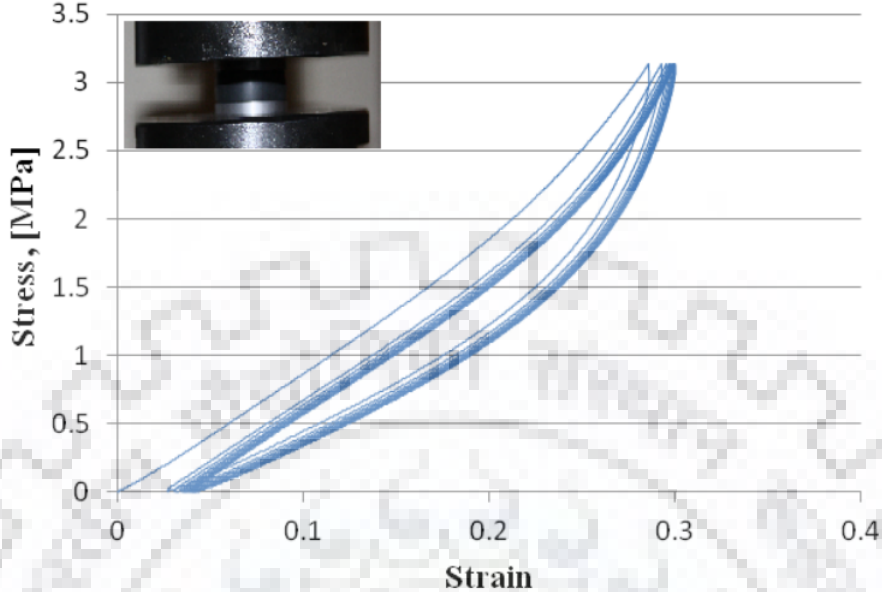
Figure 4.5: Stress- Strain curve of CR specimen (10 cycles) (Fediuc et al. [10])
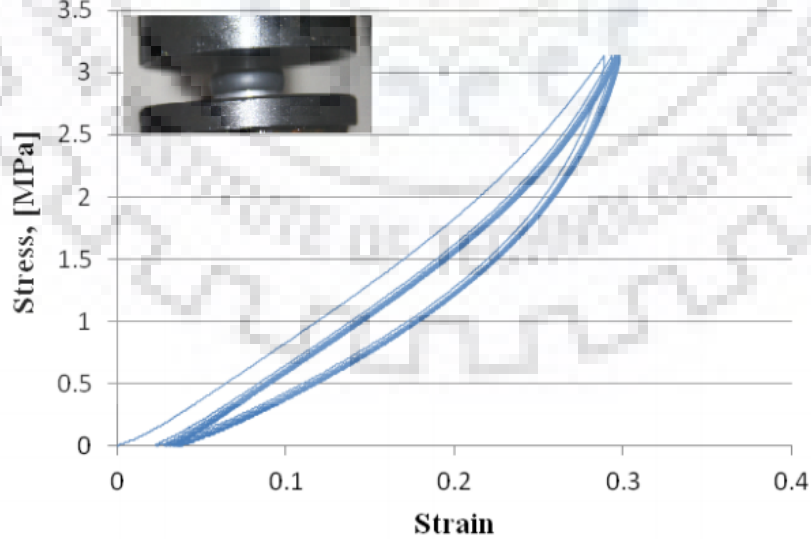
Figure 4.6: Stress- Strain curve of NR specimen (10 cycles) (Fediuc et al. [10])

given by Gent [12] gave a reasonable approximation of effective compression modulus, we will use this for further calculations.

The Effective Compression Modulus (E_c) proposed by Gent [12] for flat sandwich block:

For bidirectional strain blocks:

$$E_c = E_0 \left(1 + 2\phi S^2\right) \tag{4.32}$$

For one dimensional strain strips:

$$E_c = 1.33 E_0 \left(1 + \phi S^2\right) \tag{4.33}$$

Where E_0 is the Young's modulus (i.e. elastic modulus at zero strain), ϕ is the elastomer compressibility coefficient (see Table 4.2) and S is the shape factor.

Shape Factor (S) is defined by the ratio of loaded area to bulge area:

$$S = \frac{load\,area}{bulge\,area} = \frac{A_l}{A_b} \tag{4.34}$$

For example, for a rectangular block with dimensions l (length) × w (width) × t (thickness), shape factor becomes:

$$S = \frac{lw}{2t\left(l + w\right)} \tag{4.35}$$

For having the other parameters, Gent [12] has used Design Handbook, Lord [7] and the chart is given in Table 4.2.

Hence, we can evaluate the effective compression modulus value for an elastomer using eq: (4.32) and (4.33) by extracting the catalogue data (from nomograph given in the catalogue of an elastomer we obtain the shear modulus) and getting the parameters such as Young's modulus, compressibility coefficient from Table 4.2. Now the stiffness of a elastomer pad can simply be expressed as:

$$k_c = \frac{E_c A}{t} \tag{4.36}$$

Where, k_c is the compression stiffness, A is the loading area and t is the pad thickness.

Note– This expression for compression modulus stands for incompressible rubber. If bulk compressibility is taken into account, the effective compression modulus has to be multiplied by a factor $1/\left(1 + \frac{E_0}{E_b}\right)$, where E_0 is the Young's Modulus and E_b is the bulk modulus of the elastomer.

Table 4.2: Elastomer Material Properties [7]

Shear Modulus (G) (kPa)	Young's Modulus (E_0) (kPa)	Bulk Modulus (E_b) (MPa)	Elastomer Compressibility Coefficient (ϕ)
296	896	979	0.93
365	1158	979	0.89
441	1469	979	0.85
524	1765	979	0.80
621	2137	1007	0.73
793	3172	1062	0.64
1034	4344	1124	0.57
1344	5723	1179	0.54
1689	7170	1241	0.53
2186	9239	1303	0.52

4.5.   Steps for Modelling Elastomeric Damping Pad (Summary)

1. The operating temperature and the operating frequency are pre-requisites.

2. Then, the catalogue of the elastomer has to be studied and from the nomograph, the shear storage modulus (G_s) and the loss factor (η) corresponding to the operating temperature and frequency are extracted. The procedure of reading nomograph is given in section: 4.2.

3. Using section: 4.4, effective compression modulus is found and hence the compression stiffness (k_c) is evaluated as per eq: (4.36).

4. Finally, an approximate estimation of equivalent damping coefficient (C_{eq}) is obtained as per eq: (4.30).

The stiffness coefficient (k_c) and the dashpot coefficient (C_{eq}) are the main parameters in the linear model of the elastomeric damping pad.

Chapter 5

Description of Problem

5.1.   Brief Definition of the Concerned Problem

It is to design a **Pulse Radiographic Equipment Arrangement Building** of plan dimension of 24.7 m × 23.0 m. However, the main challenge lies in building up the front wall of the building a blast resistant one. Moreover, protection for the integrated building against blast will also have to be ensured. Again, the blast loads will be coming from testing of explosions outside the structure, and hence we cannot allow any damage inside the permanent structural elements (structural members like wall, beam, columns etc.). We will consider 4000 times of recurrence of the blast loading due to 60 kg TNT equivalent explosive at a minimum distance of 5 m from the building face. However, we cannot predict the exact location of blasting along the height. Hence we will consider the most detrimental situation, i.e. the ground surface blast.

Hence, we have to design a building of plan dimension 24.7 m × 23.0 m with a blast resistant front wall of dimension 24.7 m (width) × 12.6 m (height) to withstand 4000 discrete cycles of blast load due to 60 kg TNT equivalent explosive at a distance of 5 m on the ground surface from the front face of the wall.

5.2.   Possible Approach for Solution of the Concerned Problem

First of all, we will think of separating the whole building into two segments – **first one is a blast resisting wall supported by shear wall and the rest half is a frame**

building that will not carry any of the blast pressure. These two parts will be separated by a separation joint which will be designed against the maximum displacement occurred in the blast resisting system (to avoid pounding). The frame building design is quite a regulatory one. The real challenge is to design the blast resistant wall system of the building by some energy dissipative mechanism.

We now know that the elastomers or rubbers are viscoelastic materials which has quite good loss properties. Hence, within elastic limit itself it dissipates quite some energy by hysteresis cycles. So the main dissipative system that will be introduced in this problem is a viscoelastic pad (elastomer pad). It is sandwiched between the blast wall and a sacrificial steel plate.

A schematic diagram of the blast resistant system for the blast wall is shown in Figure 5.1. Our problem will be a two-step one–
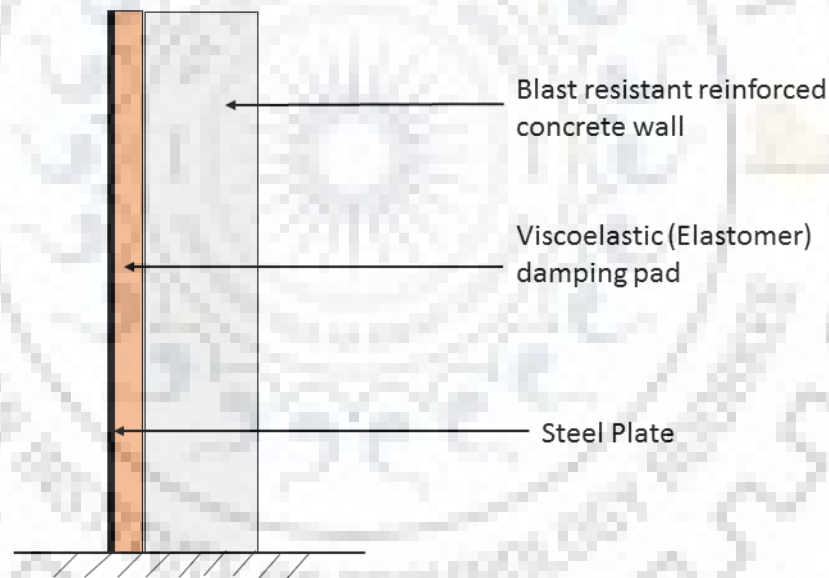
Figure 5.1: Blast pressure reduction arrangement

- **Blast pressure dissipation study using viscoelastic damping pad under compression.**

- **Design of the blast resistant mechanism using the reduced blast pressure that is already obtained in the last step.**

Chapter 6

Blast Pressure Dissipation Using Viscoelastic Damping Pad

6.1. Introduction

It has already been discussed that we will focus on using viscoelastic damping pad to reduce the incoming blast pressure. We will model the elastomer pad using Voigt's model i.e. parallel combination of springs and dashpots uniformly distributed all over the surface of the blast wall. To find the reduced force that is acting on the wall, we will consider the wall to be rigid base of a spring-mass-dashpot system. The schematic diagram for the model of the blast pressure dissipation system is given in Figure 6.1. In order to get the reduced load, we need to model the incoming blast profile first and then followed by modelling the spring and dashpot coefficients for different thickness of the elastomer pad. Finally, we will discuss about the analytical model that will give us the result of reduction in blast pressure due to the viscoelastic damping pad.

6.2. Blast Profile Determination for the Given Condition

For our problem we have 60 kg TNT equivalent explosive. We have to convert it to reference explosive as specified in IS:4991 [17]. But before that we have to remember that explosion is a thermodynamic process. For proper estimation of the pressure and other parameters we have to use thermodynamic principles and model it as a Computational
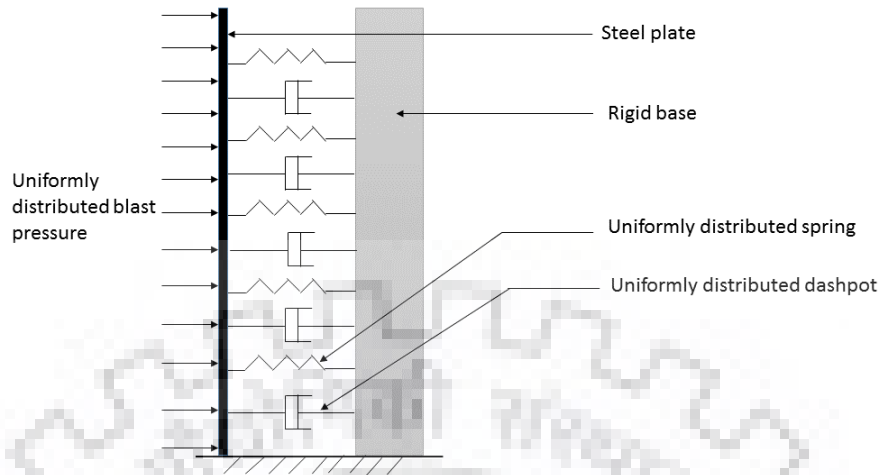
Figure 6.1: Schematic diagram of model for blast pressure reduction problem

Fluid Dynamics (CFD) problem. Instead we are using a simplified decay equation. Hence many uncertainties can arise in blast load modelling. For example, the heat generated from an explosion depends on many parameters if we look into from a point of view of a thermodynamics problem, but in exercise we do not consider these parameters. Hence we have to use a factor of safety on the charge weight for being on the safe side to eliminate the requirement of considering these uncertainties. As per UFC 3-340-02, 2008 [40], a factor of safety of 1.2 has to be considered on the equivalent TNT charge weight (In this handbook, reference explosive is TNT). Hence for our problem effective TNT equivalent design mass of charge becomes –

$$W_{TNT} = 1.2 \times 60 = 72 \, \text{kg}$$

Now this charge weight is considered to be causing the blast on ground surface (which gives the most critical case) at a distance of $R = 5$ m from the blast resistant wall face.

Another assumption is adopted which is uniformly distributed pattern of the blast pressure on the surface of the wall as specified in IS:4991 [17] (specified as vertical wave front for blast pressure). This assumption is mostly adopted in a design problem since we never know where the blast will actually happen in front of the wall. It can happen on the ground surface, or it can happen at any height. We can never exactly predict blast and hence for safety of a structure in such cases IS:4991 [17] also considered a vertical

wave front on the wall face creating a uniformly distributed blast pressure.

6.2.1   Positive Phase Characterisation

For positive phase modelling for blast pressure we will use the Table 3.1 which is adopted from IS:4991 [17]. But before that we have to calculate the effective equivalent mass of the reference explosive as specified in IS:4991 [17].

The reference explosive as per IS:4991 [17] produces heat of explosion of 1.5×10^9 calories per tonne of explosive which is equal to 6276 kJ/kg of explosive (Q_{IS}). Draganić and Sigmund [8] has given an estimate of heat of explosion for TNT as 4520 kJ/kg of TNT (Q_{TNT}).

Hence using eq: (3.3) (adopted from UFC 3-340-02, 2008 [40]) we can get the equivalent weight of the reference explosive defined in IS:4991 [17] for 72 kg of TNT equivalent:

$$W_{E_{IS}} = W_{TNT} \times \frac{Q_{TNT}}{Q_{IS}} = 72 \times \frac{4520}{6276} = 52\,\mathrm{kg} = 0.052\,\mathrm{tonne}$$

Hence, scaled distance defined in eq: (3.1) is obtained as:

$$Z = \frac{R}{W^{1/3}} = 13.394\,\mathrm{m/tonne}^{1/3}$$

Now using Table 3.1 and fitting curves through the data set we interpolate the blast characterisation parameters for the calculated scaled distance. These parameters are enlisted in Table 6.1.

Table 6.1: Positive Phase Parameters for Blast Pressure for Given Condition

Scaled distance (Z)(m/tonne$^{1/3}$)	13.394
Peak side on overpressure (p_{so}) (MPa)	0.974
Mach no. (M)	3.04
Scaled positive phase duration (t_{0s}) (milliseconds/tonne$^{1/3}$)	7.702
Positive phase duration ($t_0 = t_{0s} \times W_E^{1/3}$) (milliseconds)	**2.875**
Duration of equivalent triangular pulse (t_{ds} or t_{fos}) (milliseconds/tonne$^{1/3}$)	4.007
Duration of equivalent triangular pulse (t_d or $t_{fo} = t_{ds} \times W_E^{1/3}$) (milliseconds)	**1.496**
Peak dynamic pressure (q_0) (MPa)	1.435
Peak reflected overpressure (p_{ro}) (MPa)	**5.47**

Note– Ambient pressure has been considered as 1.013×10^5 Pa for the overpressure calculations. Velocity of sound in air (a) given in IS:4991 [17]:

$$a = 331.5 + 0.607\, T \tag{6.1}$$

Where T is the ambient temperature in Celsius. For our problem we assume that the operating temperature is $40\,°\mathrm{C}$. Hence the velocity of sound becomes $a = 356\,\mathrm{m/s}$.

Hence the blast wave velocity becomes: $U = M \cdot a = 3.04 \times 356 = 1028.84$ m/s. Now lets us eq: (3.5) to get the clearance time (t_c). For that, $S = \min\{H, B/2\} = \min\{12.6, 24.7/2\} = 12.35\,\mathrm{m}$, where H is the height and B is the width of the building and the dimensions are specified in section 5.1. Now we can find clearance time:

$$t_c = \min\left\{\frac{3S}{U}, t_d\right\} = \min\left\{3 \times \frac{12.35}{1028.84}, 1.496 \times 10^{-3}\right\} = \min\{0.036, 1.496 \times 10^{-3}\}$$

$$\text{or,} \quad t_c = t_d = 1.496 \times 10^{-3} \quad \text{s}$$

Now, we are mainly interested in reflected overpressure profile as it is giving pressure on the front wall of the building and observing the clearance time, using theory given in section 3.3 we can infer that the idealised reflected overpressure history will be a triangular pulse (single straight line with constant decay) which is given in Figure 6.2. Now, total impulse is same for both idealised as well as actual blast pressure profile. We can calculate impulse for reflected overpressure from eq: (3.17):

$$I = I_{ideal} = \frac{1}{2}p_{ro}t_d = \frac{1}{2} \times 5.47 \times 10^6 \times 1.496 \times 10^{-3} = 4092 \quad \text{Pa.s}$$

Let's fit this impulse value in eq: (3.16) by using theory of section 3.6:

$$I = 4092 = p_{ro}t_0\left(\frac{1}{\alpha} - \frac{1 - e^{-\alpha}}{\alpha^2}\right) \tag{6.2}$$

Where α (or b) is the decay constant in the modified Friedlander equation (eq: (3.19)) which can be evaluated from the above equation in any iterative manner. The other parameters are already known in this equation. Hence solving eq: (6.2) we get the value of the decay constant, $\boldsymbol{\alpha = 2.36}$.

Hence, modified Friedlander equation for positive phase given in eq: (3.19) can be written as:

$$p_r(t) = p_{ro}\left(1 - \frac{t}{t_0}\right)\exp\left(-\frac{2.36\,t}{t_0}\right) \tag{6.3}$$

Where all the notations are standing for usual notations defining blast parameter. All the parameters in the equation are known. Hence the final exponential decay curve for
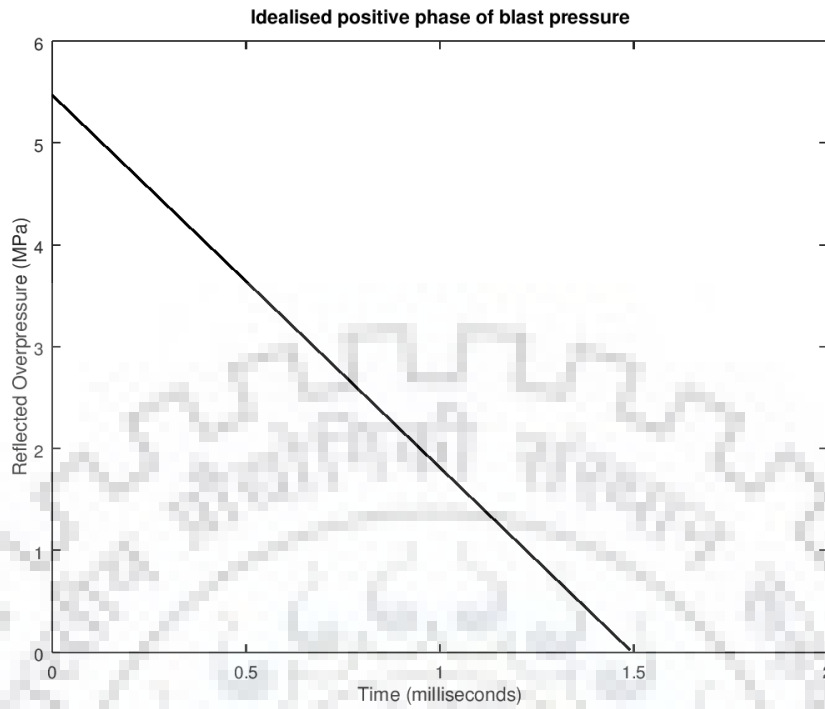
Figure 6.2: Idealised positive phase time history of reflected overpressure (p_r)
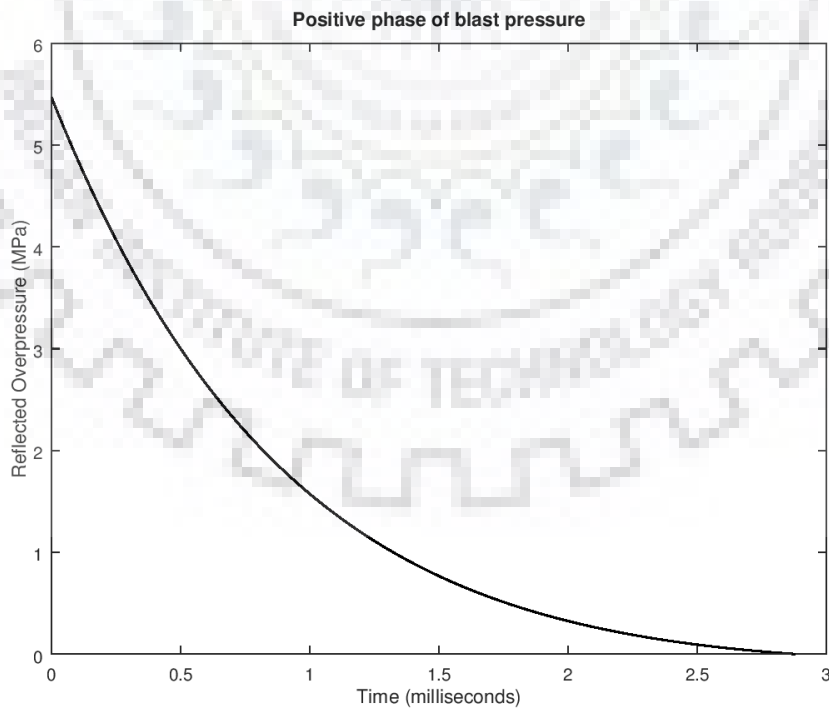
Figure 6.3: Time history of positive phase reflected overpressure (p_r)

positive phase of blast pressure has been derived. The plot of positive phase is given in Figure 6.3.

6.2.2 Negative Phase Characterisation

We will find parameters for the negative phase in the manner given in section 3.6.2 in which simplified expressions for peak negative pressure and negative phase impulse is given by Rigby et al. [35] who used plots given in UFC 3-340-02, 2008 [40] (Figure 3.8). For using these expressions, we need to have input of scaled distance in m/kg$^{1/3}$ where reference explosive is TNT. The scaled distance is given as:

$$Z = \frac{5}{72^{1/3}} = 1.2 \quad \text{m/kg}^{1/3}$$

Using this scaled distance of explosion, we get the negative phase defining parameters using expressions given in eq: (3.20) and (3.21):

$$p_{r,min} = 74.3 \quad \text{kPa} = 74.3 \times 10^3 \quad \text{Pa}$$

$$I_r^- = 1614 \quad \text{kPa} \cdot \text{ms} = 1614 \quad \text{Pa.s}$$

Now, using eq: (3.22):

$$I_r^- = 1614 \quad \text{Pa} \cdot \text{s} = \frac{1}{2} p_{r,min} t_d^- \tag{6.4}$$

We already know the value of $P_{r,min}$ and hence solving eq: (6.4) we get the negative phase duration as $t_d^- = \mathbf{0.043}$ s. Hence all parameters for negative phase characterisation is known and we can now plot the negative phase of the blast pressure (Figure 6.4).

The complete time history of the reflected overpressure profile of blast load is found by combining Figure 6.3 and 6.4. The complete time history of reflected blast pressure is given in Figure 6.5. We can see that the positive phase is much more predominant and that is why most of the cases we neglect negative phase. The exaggerated reflected overpressure history can be visualised from Figure 3.3.

Now since in order to read the loss properties from nomograph we need to have operating frequency, we have conducted a Fast Fourier Transform (FFT) using Matlab 2017. The portion of the peak amplitude and fundamental frequency is shown in Figure 6.6 to visualise properly instead of the whole plot.
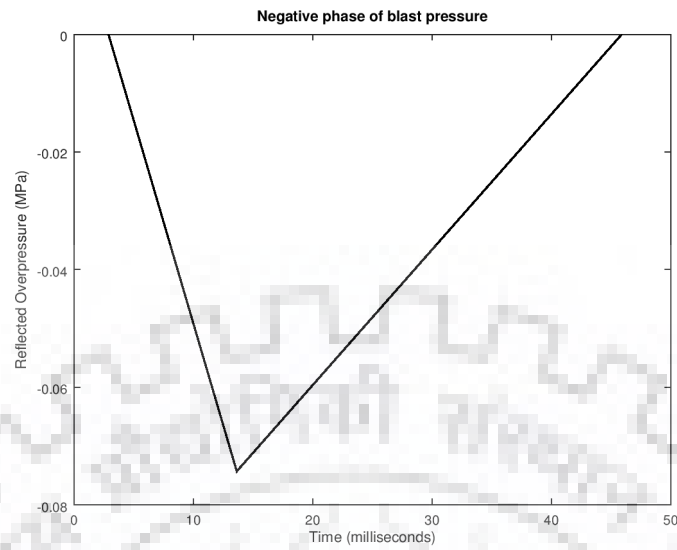
Figure 6.4: Time history of negative phase reflected overpressure
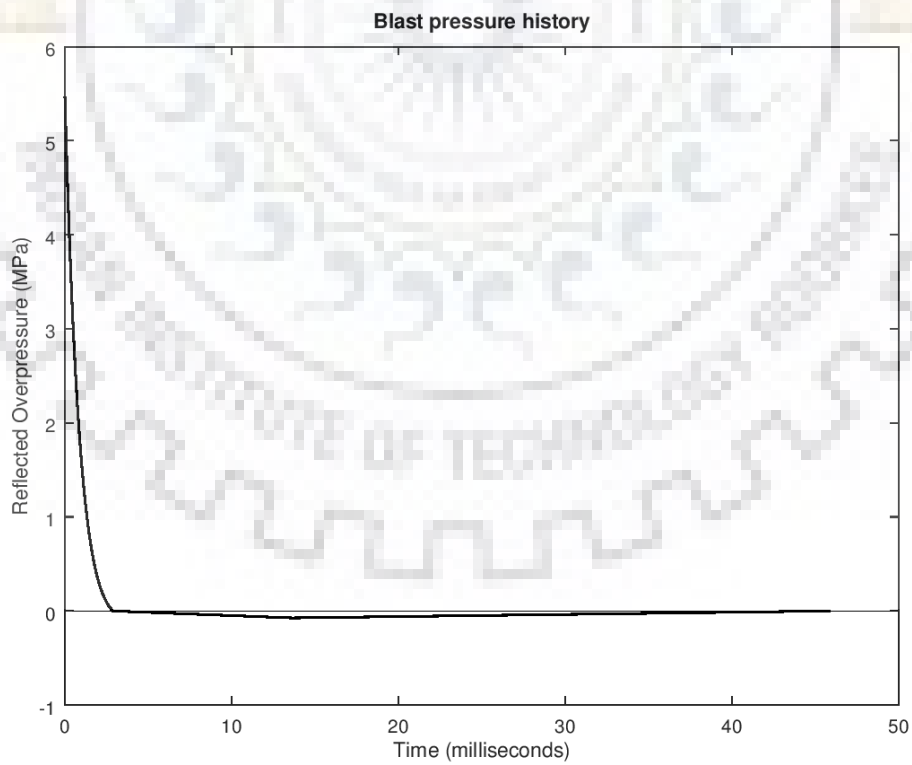
Figure 6.5: Time history of reflected overpressure due to given blast
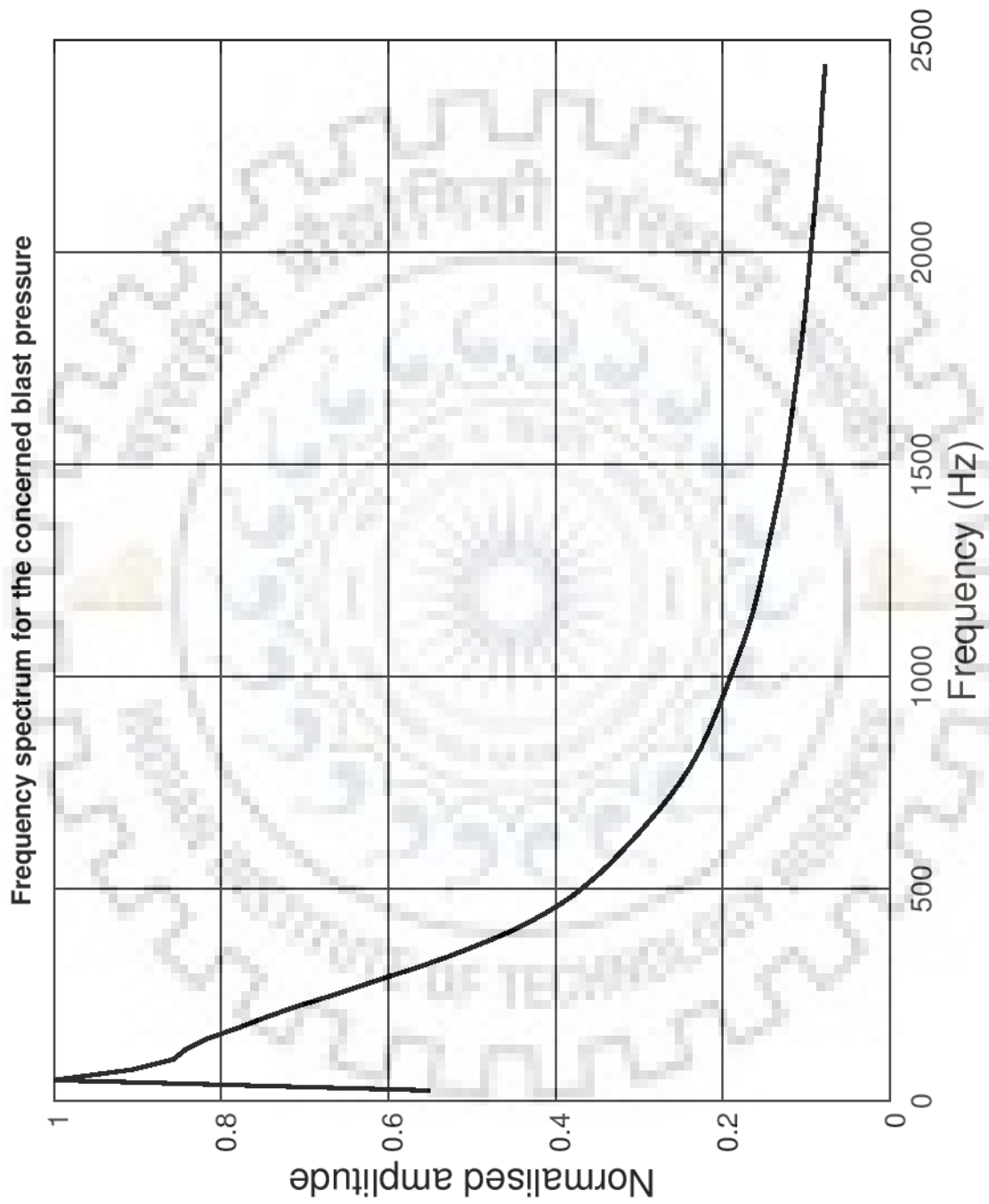
Figure 6.6: Frequency Content in the considered blast pressure

6.3. Elastomeric (Viscoelastic) Damping Pad Characterisation

We have already seen how to model a viscoelastic pad using parallel connection of spring and dashpot (Voigt's Model). If a viscoelastic material or elastomer is kept as a pad between two elements such that it takes compression or bearing type of pressures, we can model the pad using uniformly distributed springs and dashpots as shown in Figure 6.1, the coefficients of which will be calculated in this section for various thickness of elastomer. We will follow the procedure described in section 4.5.

The first thing which is required is the operating frequency and temperature. The temperature is assumed to be **40 °C** (only a little elevation from ambient temperature due to blast is considered because it will take time to reach much higher temperature while the blast pressure is acting instantaneously). The operating frequency can be assumed to be the frequency at which the first major peak comes up in the frequency spectrum obtained from FFT of the blast pressure profile and it is given in Figure 6.6. Hence from Figure 6.6, we can infer that the predominant operating frequency is $f = 49\,\mathrm{Hz}$ (however the range is quite wide from 10 to 1000 Hz).

Now in the next step lets fix the viscoelastic material to be `3M 112 series` viscoelastic damping pad, produced by 3M Products. Using temperature of $40\,°\mathrm{C}$ and operating frequency range of 10 to 1000 Hz we can obtain the loss properties of the 112 series damping polymer (notable property of this pad is that it has same damping property for a wide range of operating frequency) from its nomograph given in its product catalogue (Figure 6.7). **We can read the shear storage modulus (G_s) to be 0.6 MPa and the loss factor (η) to be 1.0**. Hence we can get the shear modulus (G) (using section-4.2 and literature of Connor [6]) as the following:

$$G = \sqrt{G_s^2 + G_l^2} = G_s\sqrt{1 + \eta^2} = 0.6\sqrt{1 + 1^2} = 0.8486 \quad \mathrm{MPa} \qquad (6.5)$$

Now for our problem the pad is sandwiched between the wall and the steel plate. For the time being, wall is considered to be fixed in order to find out the reduced load that is getting transferred to the wall. Hence the pad is having same dimension as the front wall i.e. $24.7\,\mathrm{m}\,(\text{width}\,B) \times 12.6\,\mathrm{m}\,(\text{height}\,H)$.
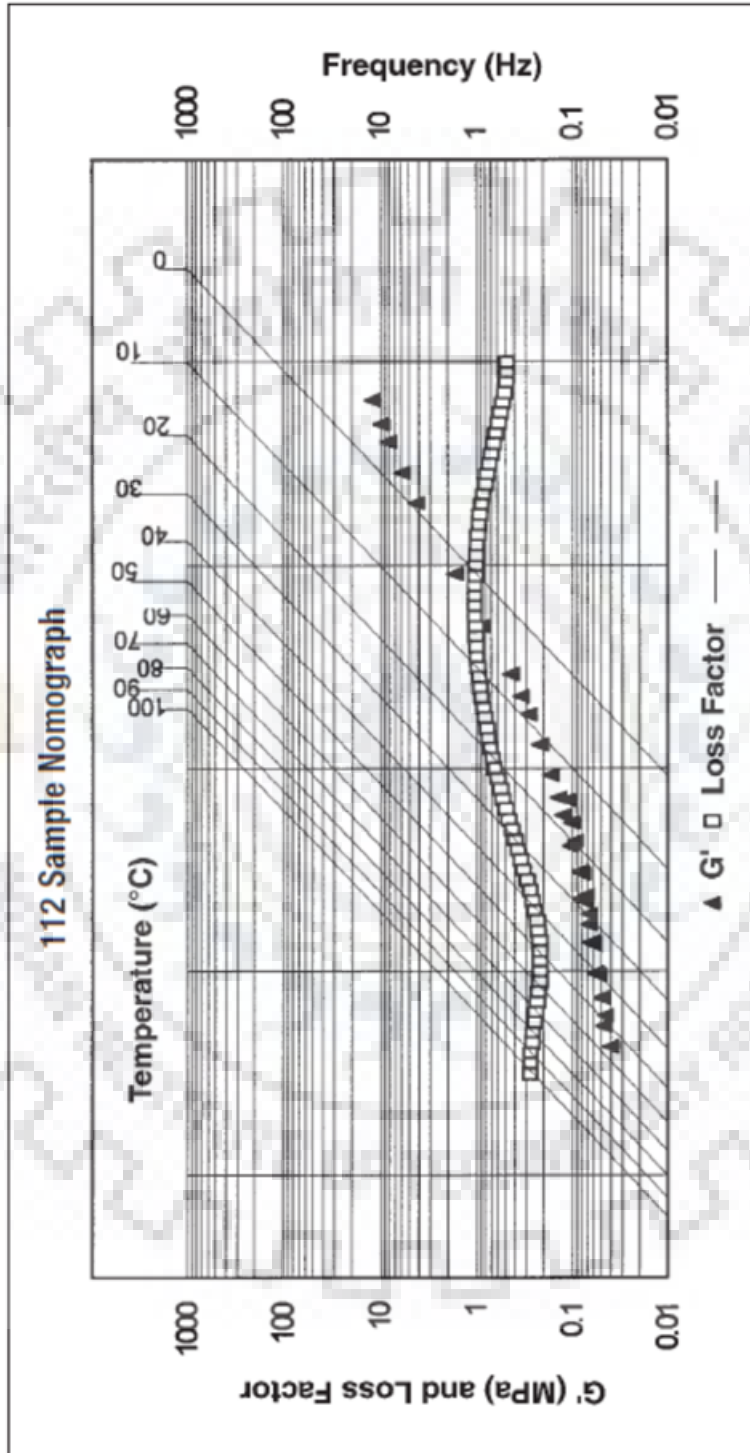
Figure 6.7: Sample nomograph for 112 series viscoelastic damping polymer (Technical Data, 3M Products [39])

Now for observing the trend of load reduction for increasing thickness (t) of pad we will present the stiffness calculation in a tabular form (Table 6.2). For this purpose, the shape factor is obtained from eq: (4.35) as:

$$S = \frac{BH}{2t\,(B+H)} \tag{6.6}$$

From Table 4.2 we get the Young's modulus (E_0) and Elastomer compression coefficient (ϕ) using the shear modulus (G).

Now, we get the effective compression modulus (E_c) using eq: (4.32):

$$E_c = E_0 \left(1 + 2\phi S^2\right) \tag{6.7}$$

Finally, we calculate the compression or bearing stiffness of the pad using eq: (4.36)

$$k_c = \frac{E_c A}{t} = \frac{E_c\,(BH)}{t} \tag{6.8}$$

Up to this point (calculation of compression or bearing stiffness of pad) is enlisted in Table 6.2 for pad thickness of 100 mm to 600 mm at an interval of 100 mm.

Table 6.2: Stiffness calculation table for different thickness of elastomer

Shear Modulus (G) (MPa)	Young's Modulus (E_0) (MPa)	Elastomer Compression coefficient (ϕ)	Thickness (t) (mm)	Shape Factor (S)	Effective Compression Modulus (E_c) (Pa)	Bearing or Compression Stiffness (k_c) (N/m)
0.8486	3.442	0.624	100	45.10	8.742×10^9	22.03×10^{12}
0.8486	3.442	0.624	200	22.55	2.190×10^9	2.76×10^{12}
0.8486	3.442	0.624	300	15.03	0.974×10^9	0.819×10^{12}
0.8486	3.442	0.624	400	11.28	0.550×10^9	0.346×10^{12}
0.8486	3.442	0.624	500	9.03	0.353×10^9	0.178×10^{12}
0.8486	3.442	0.624	600	7.52	0.246×10^9	0.103×10^{12}

Note– This bearing stiffness is for the whole damping pad. In order to make a uniformly distributed stiffness we have to equally divide this stiffness at each nodes of the Finite Element Model.

Now, since the stiffness is known we can calculate the damping coefficient for the whole pad using the theory given in section 4.3 and ultimately using eq: (4.30):

$$C_{eq} \approx \frac{\eta k}{\omega_n} \tag{6.9}$$

From the above equation (eq: (6.9)) we already know the value of loss factor ($\eta = 1.0$) from the nomograph and we have calculated the bearing stiffness (k) for different thicknesses of the damping pad. Only unknown remains is the natural frequency (ω_n) of the system.

We know that all the springs are in parallel and hence we can use the total stiffness and idealise the system to be a single degree of freedom system to get the natural frequency of the system. Hence, the natural frequency becomes:

$$\omega_n = \sqrt{\frac{k_c}{m}} \qquad (6.10)$$

Where k_c is the bearing stiffness of the whole pad obtained from Table 6.2 and m is the effective mass of the system. Now we have a considerable mass of the spring in terms of the rubber pad which we cannot neglect. Hence we have to use the effective mass which consists of the mass of the steel plate as well as a part of the mass of the spring and we can calculate it using the given equation:

$$m = m_{plate} + 0.33\, m_{pad} \qquad (6.11)$$

Where m_{plate} and m_{pad} are the mass of outer steel plate and the elastomer pad respectively. We will consider a standard value of density of steel (7850 kg/m^3). And density of elastomer pad for 3M 112 series is found to be 1000 kg/m^3 from the catalogue. Using these we can obtain the natural frequencies for different thickness of pad and get the damping coefficients and these are tabulated in Table 6.3.

Table 6.3: Damping coefficient calculation for different thickness of damping pad

Thickness (t) (mm)	Bearing stiffness (K_c) (N/m) (from Table 6.2)	Mass of damping pad (for thickness = t)(m_{pad}) (kg)	Mass of steel plate (for thickness = 50 mm) (m_{plate}) (kg)	Effective mass (m) (using eq: (6.11)) (kg)	Damping Coefficient of the pad (C_{eq}) (N.s/m)
100	22.03×10^{12}	37346	122154	134478	1.721×10^9
200	2.76×10^{12}	74693	122154	146803	6.36×10^8
300	0.819×10^{12}	112039	122154	159127	3.61×10^8
400	0.346×10^{12}	149385	122154	171451	2.44×10^8
500	0.178×10^{12}	186732	122154	183776	1.81×10^8
600	0.103×10^{12}	224078	122154	196100	1.42×10^8

Note–

1. Steel Plate has been kept of same thickness for all cases.

2. This damping coefficient is for the whole pad, hence we have to distribute it equally at each node of Finite Element model in order to get uniformly distributed dashpots.

This is how we have found out all the input parameters for the analytical model built in a software. In the next section we will discuss about the modelling in Finite Element software.

6.4. Modelling and Discussion of the Finite Element Model

ABAQUS/Explicit, a general-purpose finite element computer program software for finite element modelling, is used for our problem. A brief discussion of the model is given below.

The outer steel plate is modelled as 3D shell elements of four nodes (S4R element and the dimension of the plate is the same as the wall dimension with a thickness of $50\,\text{mm}$ ($24.7\,\text{m} \times 12.6\,\text{m} \times 0.05\,\text{m}$). The support is modelled as shell elements of same dimension but the material is made many times stiffer in order to make it a fixed support.

Then the meshing is done using S4R (4 node 3D Shell elements) with square elements of $0.5\,\text{m} \times 0.5\,\text{m}$ for both the outer plate as well as the support. Then the nodes of the support and the outer steel plate are connected by springs and dashpots using 'SpringA' connectors exclusively used for ABAQUS/Explicit. The total stiffness and damping coefficient is distributed equally among these springs and dashpots. The constitutive relation of E250 (Indian Standard) steel is modelled as an elastic- perfectly plastic behaviour (up to $0.87 \times 250 = 218$ MPa it is elastic and after that its perfectly plastic up to a plastic strain of 0.2). Now, as a boundary condition, the other face (other than the face at which springs and dashpots are connected) of the support (modelled as highly stiff shell element) is fixed. Finally, a compressive blast pressure of profile given in Figure 6.5 is applied on the outer steel plate and an explicit analysis is run. Figure 6.8 and Figure 6.9 shows the meshed Finite element model with springs and dampers.

After the analysis, the transferred pressure to the support is calculated from the recorded nodal forces. This transferred pressure is the load on the actual blast wall against which it has to be designed. The variation of transferred pressure for pad thicknesses of 100 mm to 600 mm is shown in Figure 6.10. It can be seen that the transferred pressure decreases with increasing pad thickness and the time history plot gets flattened.

Detailed closer view
is shown in Figure 6.9
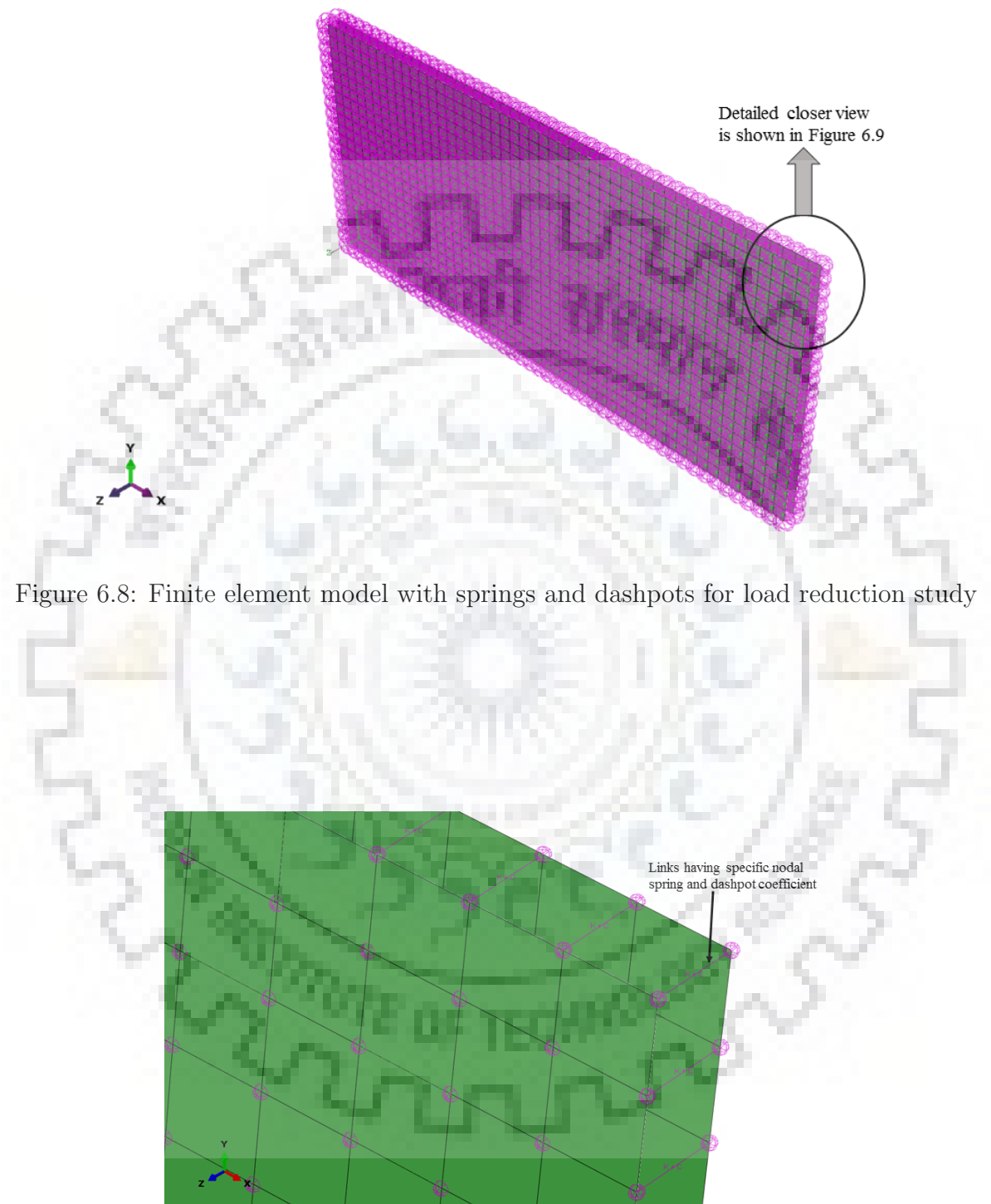
Figure 6.8: Finite element model with springs and dashpots for load reduction study

Links having specific nodal
spring and dashpot coefficient

Figure 6.9: Closer view of the spring and dashpot links between nodal points of base
and outer plate

6.5.   Results and Discussions of Load Reduction Study

After the analysis the transferred pressure to the support is calculated from the recorded nodal forces. This transferred pressure will be the blast load on the actual blast wall against which it has to be designed. The variation of transferred pressure for pad thickness of 100 mm to 600 mm is shown in Figure 6.10. It can be seen that the transferred pressure decreases with increasing pad thickness which is quite expected. We have also recorded the peak pressure that is getting transferred to the wall for different thickness of the elastomer pad and it is enlisted in Table 6.4.

Table 6.4: Peak pressure transferred to the blast wall

Elastomer Pad Thickness (mm)	Peak Transferred Pressure (MPa)
100	6.646
200	5.540
300	4.634
400	3.917
500	3.369
600	2.937

Discussions: We can see that when we use 600 mm thick pad the peak pressure is getting reduced by more than 50 % from that of the 100 mm pad. For the time being we will use 600 mm pad for further design purpose. The blast resistant wall system will be designed against transferred pressure time history that is noted from the output database of the ABAQUS/Explicit program. After preliminary design we will do a rigorous analysis of the wall in ABAQUS/Explicit again to check against the permissible stresses of materials. If failure occurs, we may redesign the section or we can also increase the pad thickness.
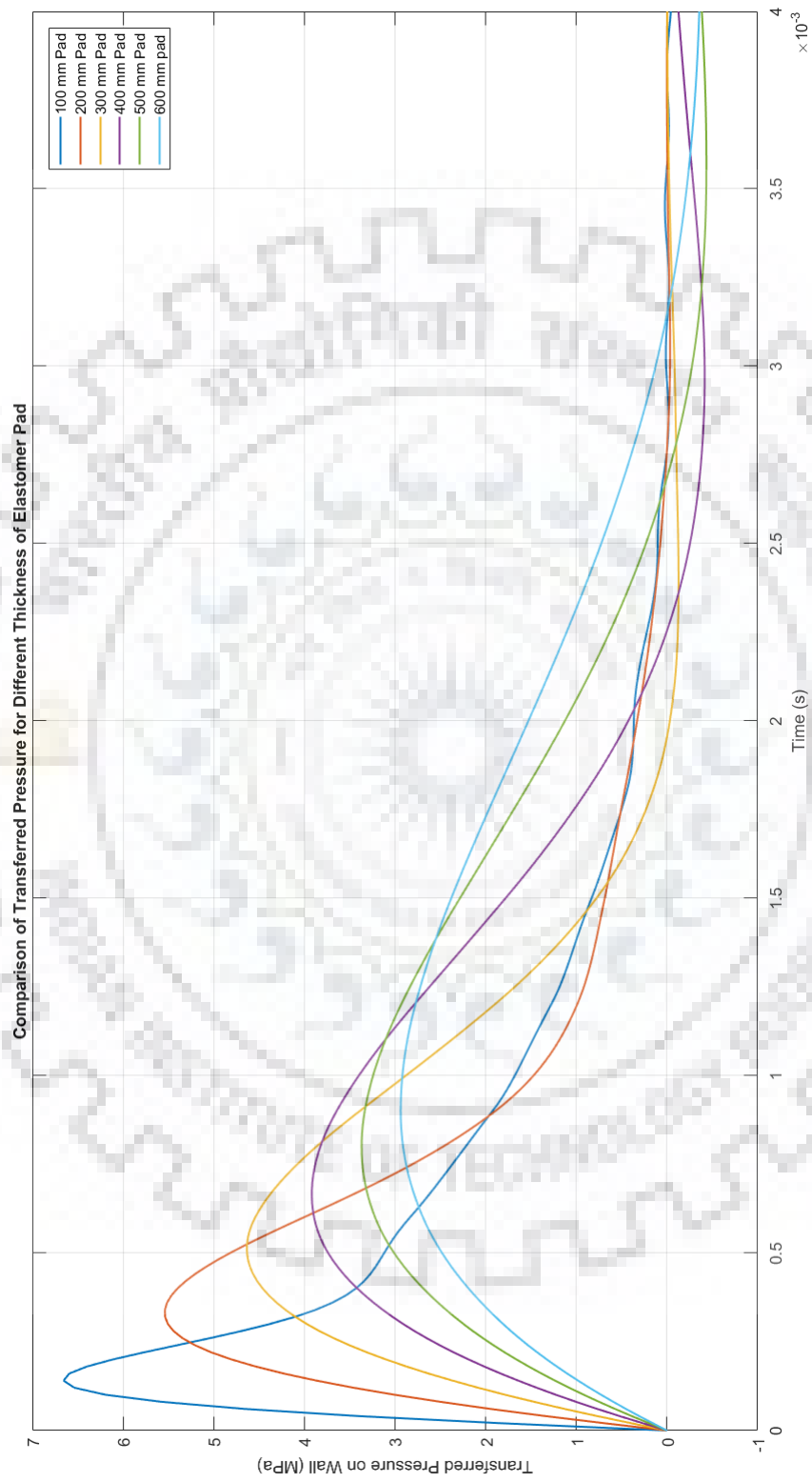
Figure 6.10: Comparison of transferred blast pressure for different thickness of damping pad

Chapter 7

Preliminary Analysis and Design

After getting the reduced transferred load to the wall the next job remains is to design the blast resistant reinforced concrete front wall system for the building. In this regard to start with an initial dimension and reinforcements we have to get some estimate of the bending moments and shear force and subsequent estimate of steel reinforcement. For this purpose, we will model some structures in SAP2000 software with some pre-assumed dimension of the wall system and will see if it is able to withstand or not. We will also have an estimate of steel reinforcement at different portions and faces of wall. Accordingly, we will set the section properties with reinforcement detailing based on the design and analysis data from SAP2000. All these analysis and design will be for transferred blast pressure through 600 mm thick elastomer damping pad. Later we will model the trial section obtained from preliminary design in ABAQUS/Explicit to check for the permissible stresses and damage. If severe damage or failure occurs or some stress exceeds permissible value, we will increase the pad thickness or redesign the section.

7.1. Analysis in SAP2000 Using Different Load Resisting Configuration

We have used different load resisting configurations in SAP2000 using one front wall under out plane action and several supporting shear walls. All the walls and the roof are modelled in SAP2000 using shell elements (thick or thin depending on span/depth ratio). Concrete of M40 and reinforcement of Fe 500 is used from the material library itself. **For design purpose LSM of IS:4991 [17] is adopted which has an in-built**

scheme in SAP2000. Factor of safety of 1.5 is assumed on dead load and 1.0 is assumed on blast load (since already we have taken factor of safety on the mass of the charge). A time history of blast pressure is given and the analysis is run under this environment.

It has been seen that the most critical portion of blast wall is at the portion of its support (at ground level) behind which no shear wall is situated. It happens because the structure is subjected to impact type of load and under this load the local flexibility is utilised rather than its integrated action (just like when a bullet hits a glass it only creates a hole). This thing will be more evident from Table 7.1 in which the maximum shear force and maximum tension steel required at the unsupported portion of wall base (the portion behind which no shear wall is there) for 1 m width of the wall for different configurations subjected to blast pressure is shown. This table shows results of analysis in which all wall thicknesses are considered as 1 m and roof slab of 450 mm thickness is given.

Table 7.1: Preliminary analysis results for different configuration (1m thick wall)

Configuration	Maximum amount of tension steel at outer face of wall along the height of the wall (mm^2/m width of wall)	Maximum shear force at the base of the front face (kN/m width of wall)	Maximum shear stress at the base of the front wall (MPa)
Straight Cantilever wall	14000	4700	4.7
Straight front wall supported by two shear wall at the edges	12740	4700	4.7
Curved face (convex) in plan (with middle portion at 4m away from the edges)	15000	4700	4.7
Curved face (convex) in plan (with middle portion at 4m away from the edges) with two shear walls at the edges	15000	4500	4.5

Again we can see that the maximum appearing shear stress is almost the same for all the cases. It happens because of this impact load where local flexibility is first tested rather than the integrated action. Same thing can be seen for tension steel requirement at the middle portion of the base where no shear wall is given. However, if we use more number of shear walls (from 2 to 5) the extent of area subjected to high shear stress and high requirement of tension steel reduces (in case of cantilever wall the whole base is subjected to high shear stress and high requirement of tension steel). So we have to choose the configuration wisely for optimum design.

7.2.   Preliminary Design based on SAP2000 Output

We are proceeding to the design of wall system choosing the straight wall with 2 numbers of shear wall at the edges. The outer face wall and shear walls are given thickness of 1 metre. The reinforcement has been designed as per the reinforcement output from SAP2000 according to LSM and with load combination of $1.5DL + BL$ (BL = blast load and DL = dead load).

Again it is seen that the maximum shear stress at the base for this configuration is 4.7 MPa which is greater than the maximum allowable permissible shear stress at any case ($\tau_{c,max}$) which is equal to 4 MPa in M40 or higher grade concrete (IS:456 [16]). Hence instead of using a RC section we will use a Steel – Concrete composite section up to a certain height (from shear stress contours) from the base. Here we will use a series of I – sections at the core of the concrete such that the flange will be sufficient for taking up the requirements of the tension and compression steel and the web will be able to take up the shear stress. The details of I section and the cross sections of the wall will be given in the figures under this section.

The details of the reinforcement and the configuration of the wall system are given in all the figures in this section. Again it has to be remembered that this is only a trial section which will be rigorously checked against the results of ABAQUS/Explicit after modelling all the walls and the reinforcements.
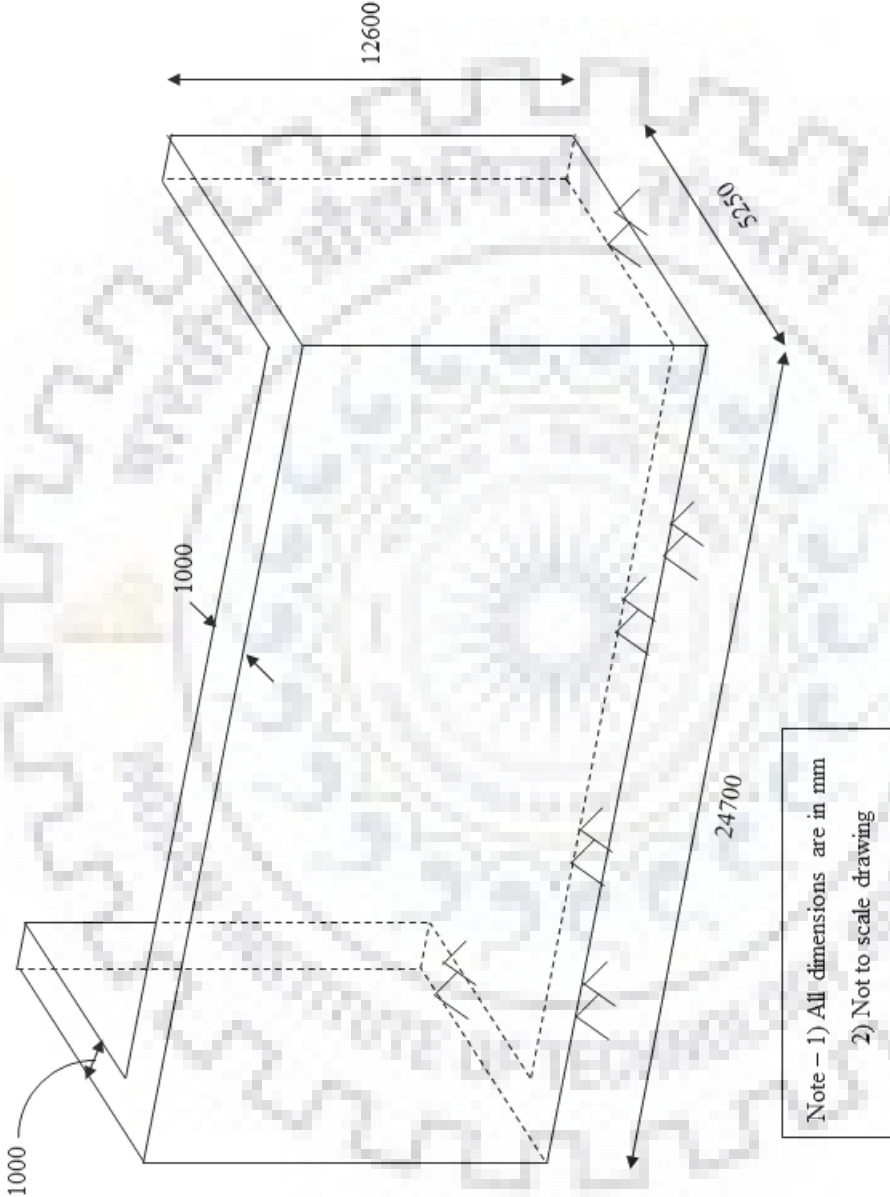
Figure 7.1: Integrated wall system (front wall and two shear walls)

7.2.1 Detailing of Blast Resistant Front Wall
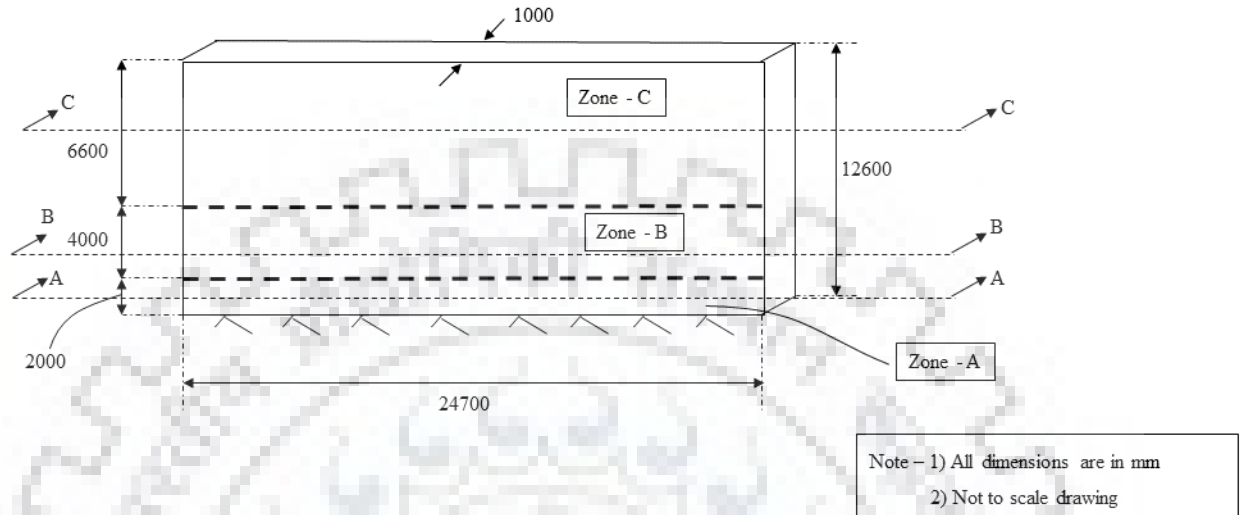
Figure 7.2: Schematic diagram of front wall with section marking
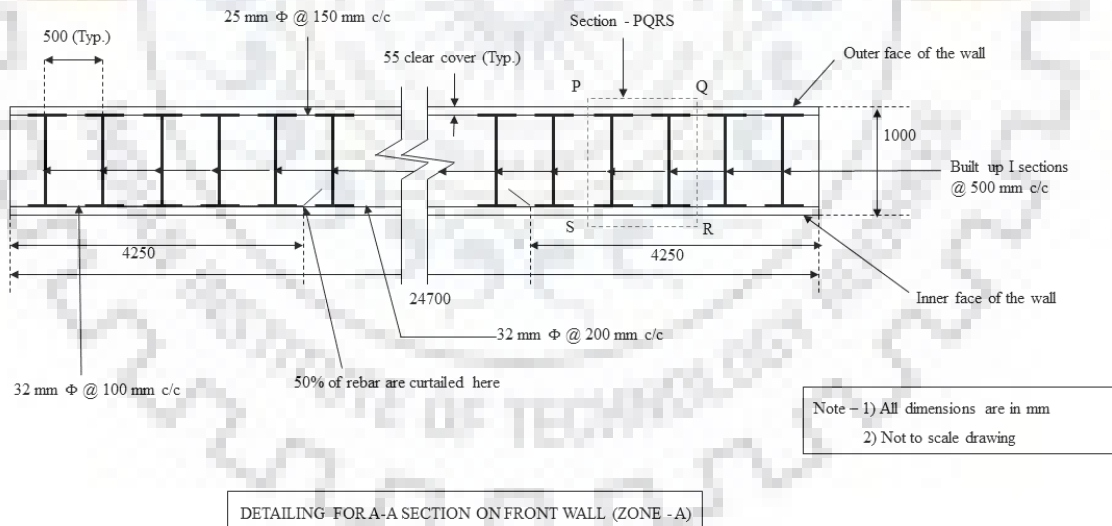
Figure 7.3: Detailing of Section A–A of front wall for zone – A
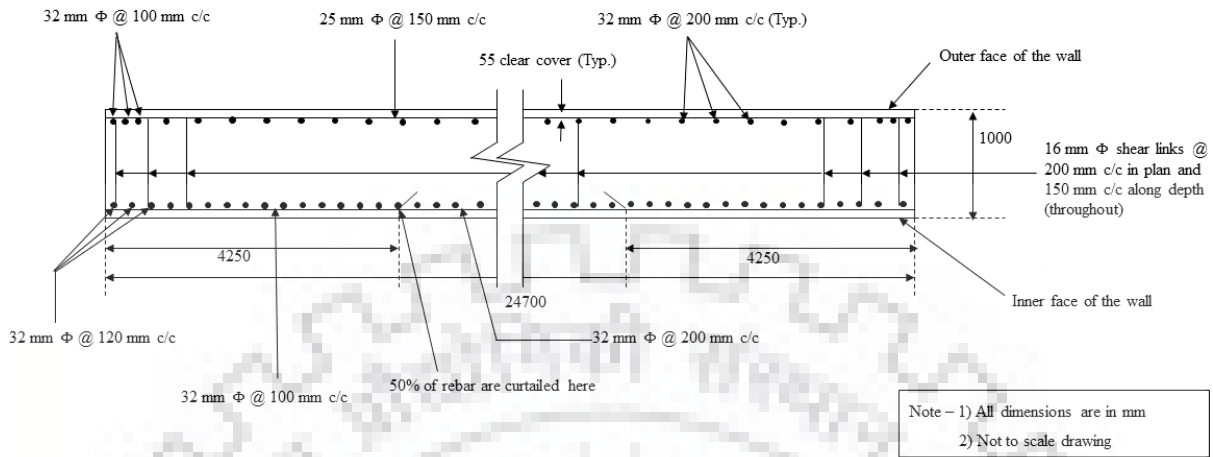
Figure 7.4: Detailing of Section B–B of front wall for zone – B
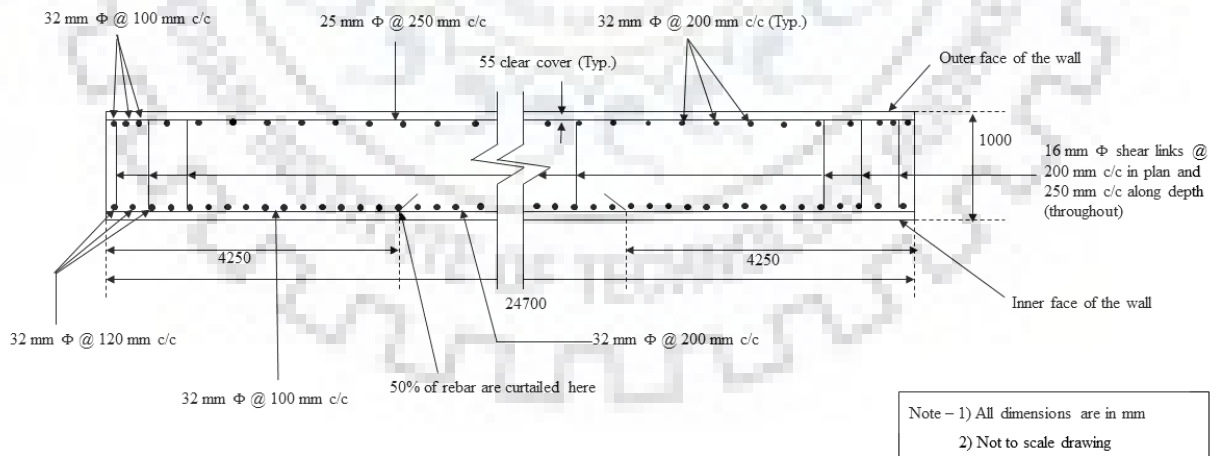
Figure 7.5: Detailing of Section C–C of front wall for zone – C
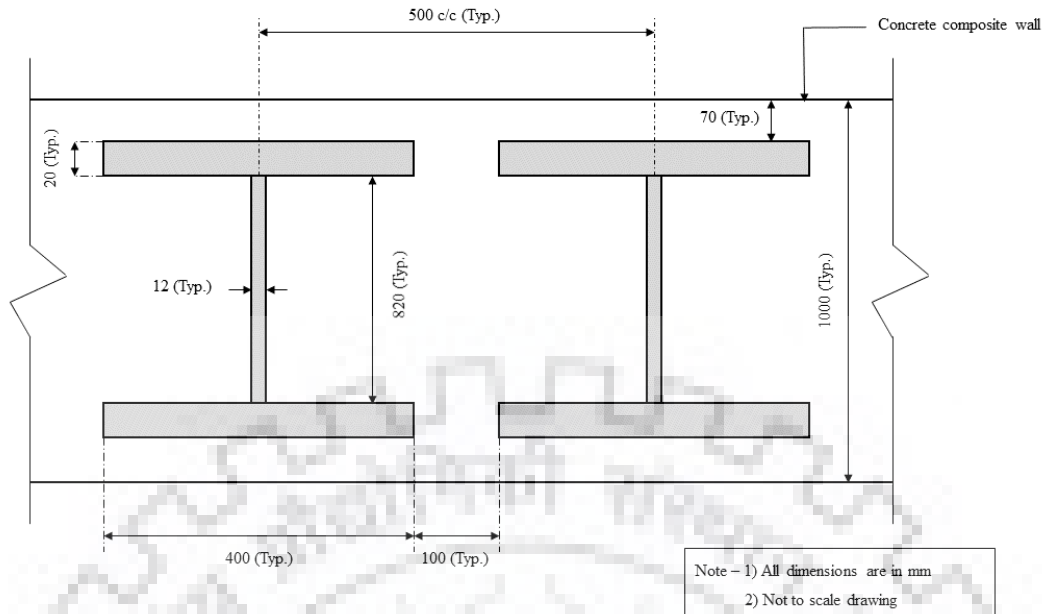
Figure 7.6: Detailing of section PQRS of front wall

7.2.2 Detailing of Supporting Shear Wall
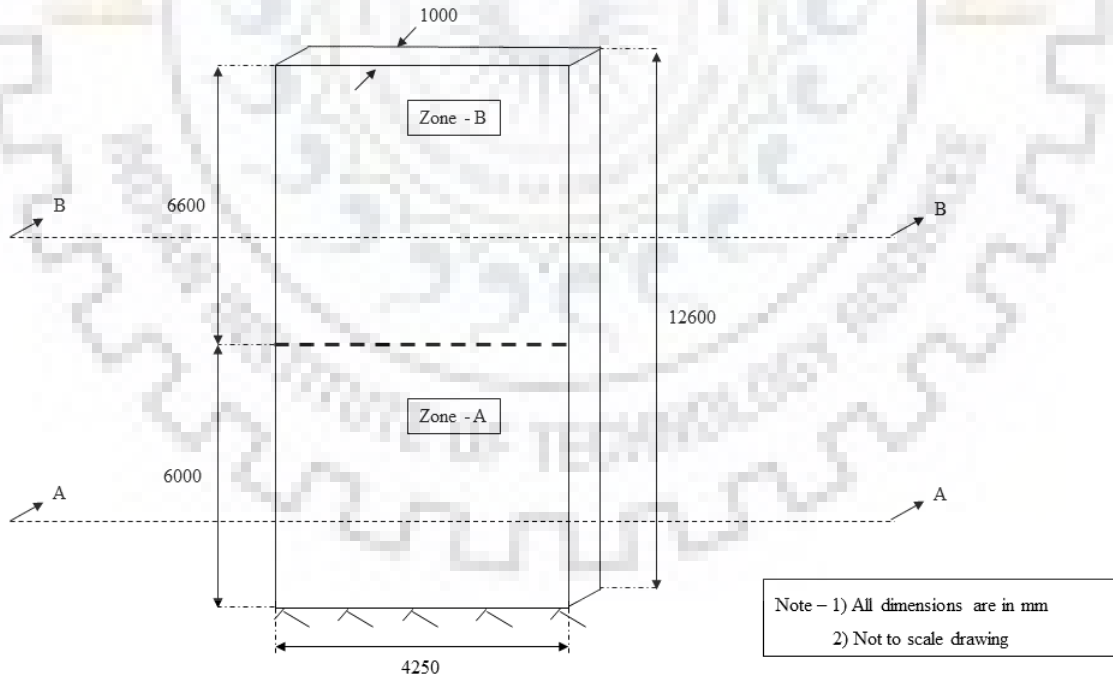
Figure 7.7: Schematic diagram of Shear wall with section marking
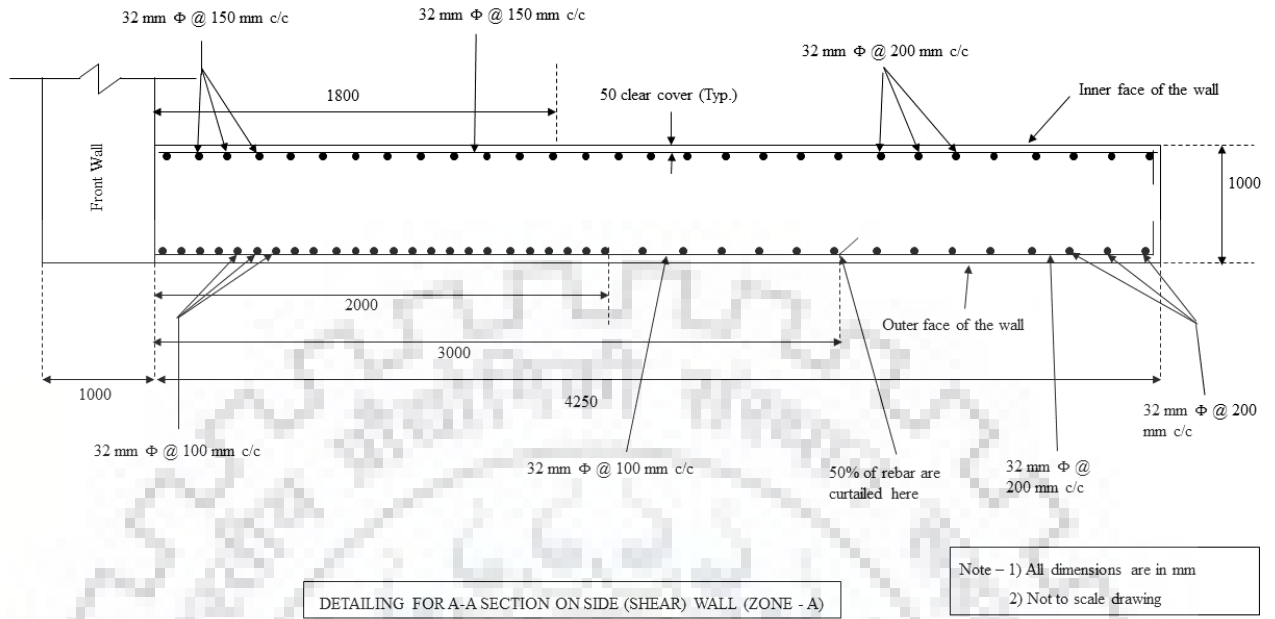
Figure 7.8: Detailing of Section A–A of shear wall for zone – A
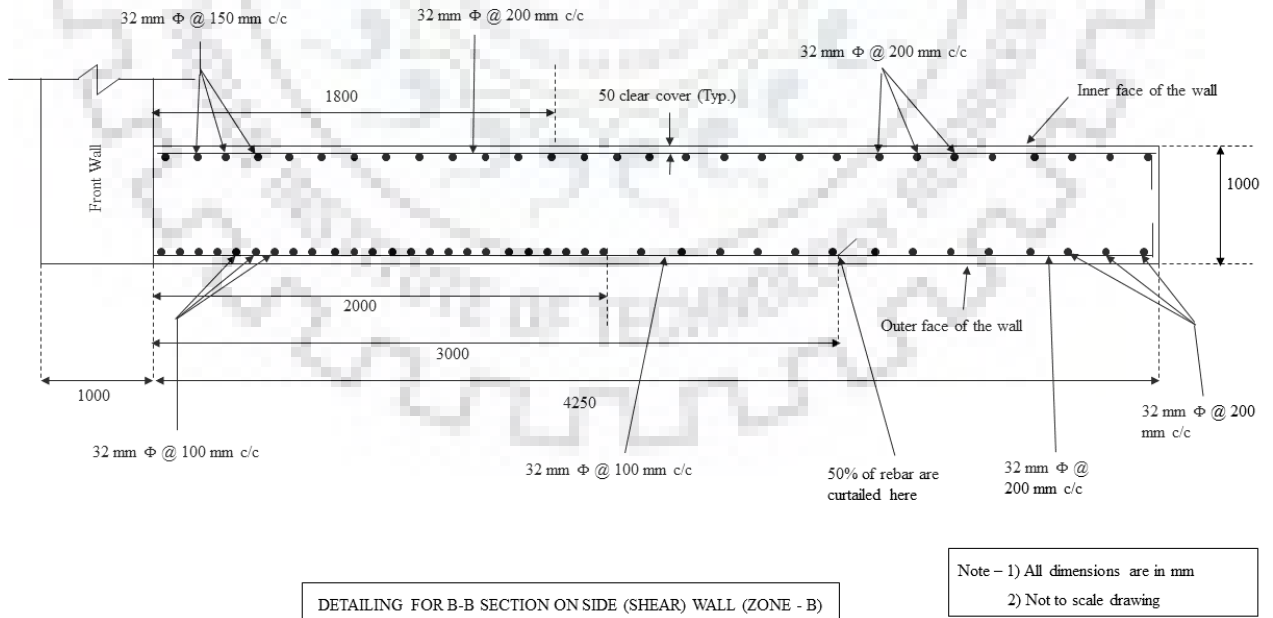
Figure 7.9: Detailing of Section B–B of shear wall for zone – B

7.2.3   Detailing of Roof Slab
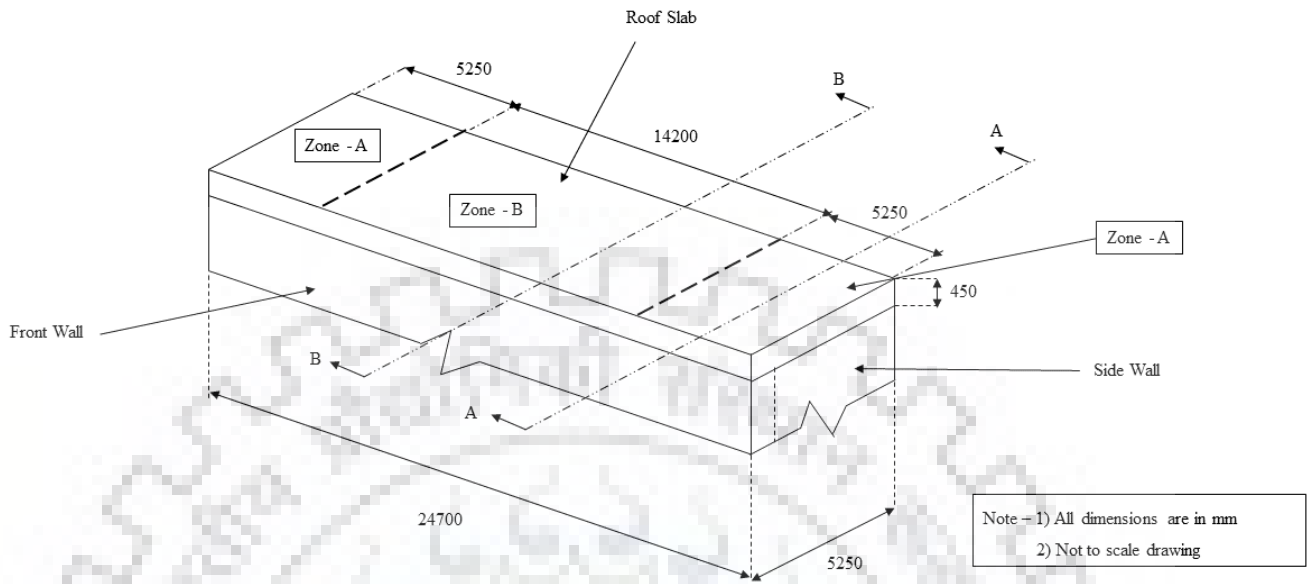
Figure 7.10: Schematic diagram of roof slab with section marking
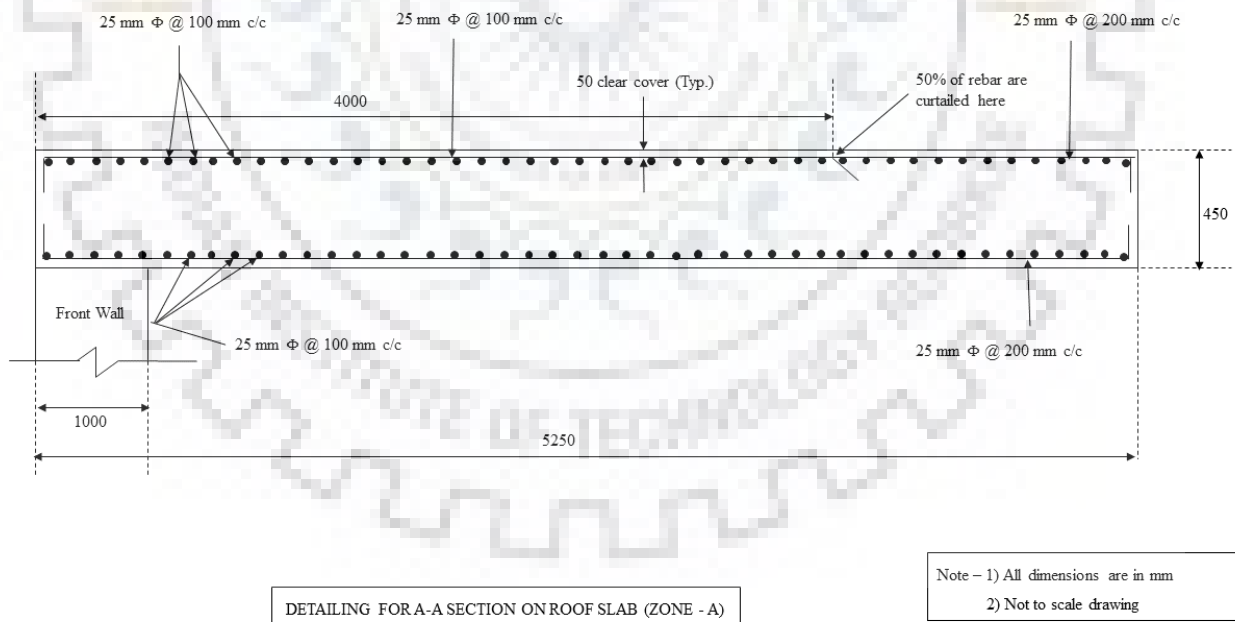
Figure 7.11: Detailing of Section A-A of roof slab for zone – A
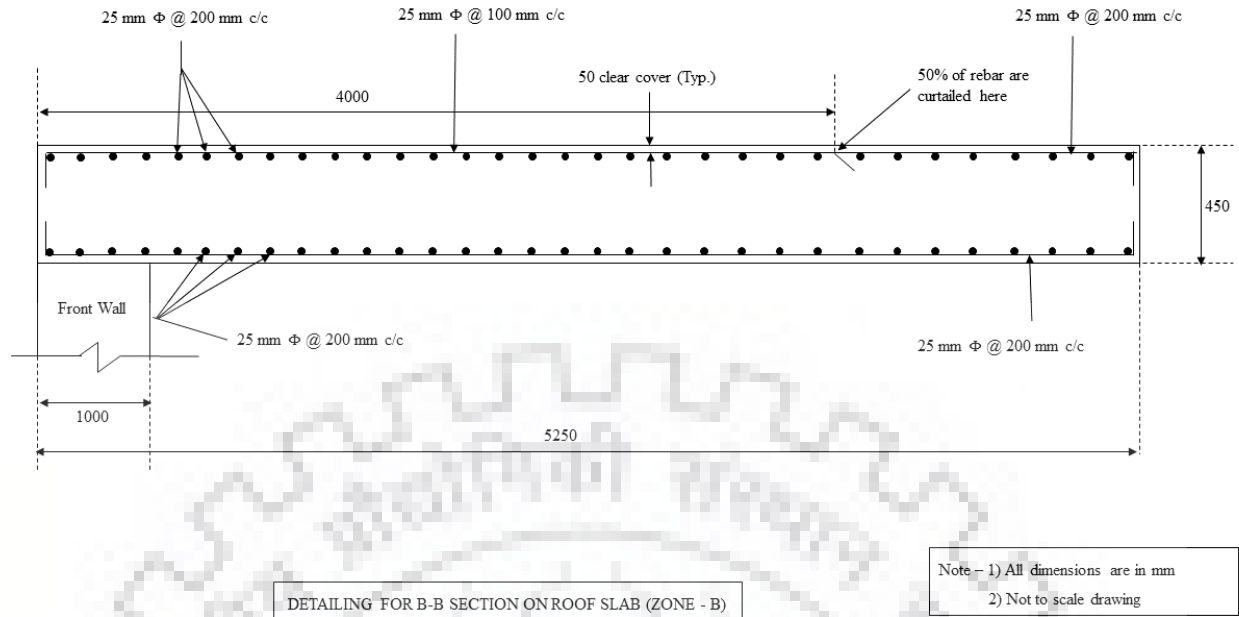
Figure 7.12: Detailing of Section B-B of roof slab for zone – B

These are the engineering drawings for the blast resistant wall system drawn not to scale to show the reinforcements properly. Now according to these drawings we will prepare a model in ABAQUS and check if any failure or damage is coming up or not.

Chapter 8

Detailed Modelling of Designed Wall System and Analysis

We have already had some section based on the preliminary design and the details are given in chapter 7. In this section we will try to rigorously model the whole blast resistant wall system that will be subjected to the transferred blast pressure through 600 mm thick elastomer pad. This rigorous modelling majorly includes proper constitutive modelling and FEM modelling in ABAQUS. Finally, it will be checked if at any section stress is exceeding the permissible value or not i.e. if there is any damage occurring (in concrete section we can allow tension cracks but we cannot allow crushing of material under compression).

8.1. Constitutive Models of Used Engineering Materials

We will be using the software ABAQUS/Explicit for entire modelling. But it has to be remembered that it is a common purpose finite element software which hardly has any material library. Hence every material has to be design with an appropriate constitutive model. Our blast resistant wall system consists of a small part of steel – concrete composite and mostly reinforced concrete section. Hence, we have to model structural steel, rebar steel and concrete. The modelling of these materials will be discussed under this section.

8.1.1 Structural Steel Model

For structural steel we will use E 250 grade of steel that will be used for I – section inside the composite. The material is modelled as an elastic – perfectly plastic material (i.e. equivalent bilinear assumption). The peak value of the stress (yield stress itself) has been lowered down by a factor of safety of 1.15 as per IS:800 [19]. Hence the peak stress becomes:

$$f_y = \frac{250}{1.15} = 217.4 \quad \text{MPa} \tag{8.1}$$

The elastic modulus is considered as $200\,\text{GPa}$ or $2 \times 10^5\,\text{MPa}$. Strain at yield becomes:

$$\epsilon_y = \frac{217.4}{2 \times 10^5} = 0.00109 \tag{8.2}$$

The density is considered to be $7850\,\text{kg/m}^3$ and the Poisson's ratio is 0.15. The plastic strain at ultimate is considered as 0.2 for mild steel.

The stress strain curve for this steel model is given in Figure 8.1.
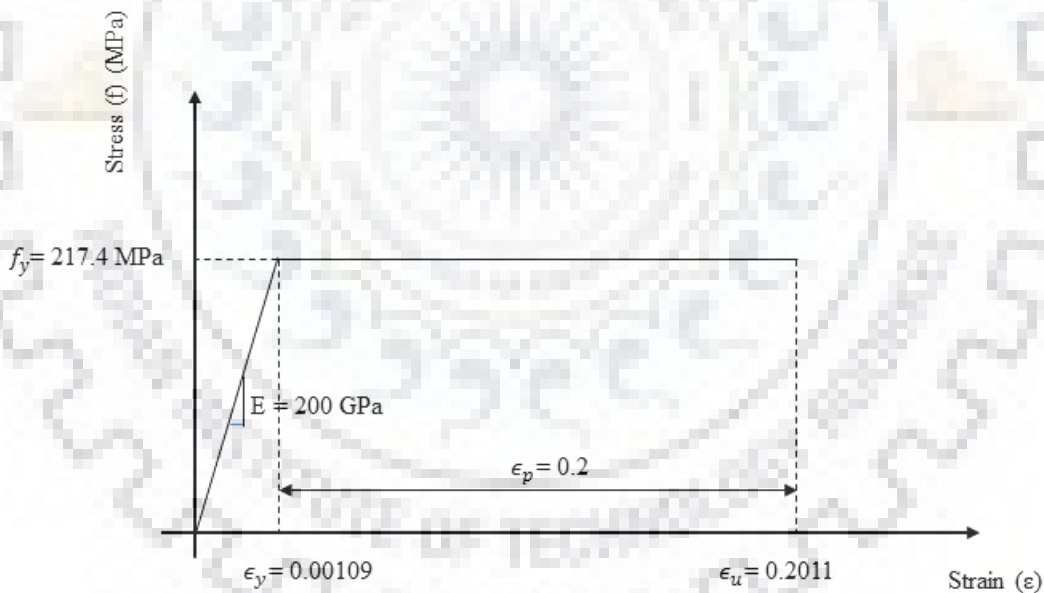
Figure 8.1: Stress – strain relation of structural steel of grade E 250

8.1.2 Flexural Rebar (Reinforcement) Steel Model

This steel is also similarly modelled with an idealised stress strain plot using equivalent bilinearisation of the plot given in IS:456 [16]. Fe 500 is used for the flexural reinforcement

for our model. In this case also a material factor of safety of 1.15 is used as specified in IS:456 [16]. Hence peak stress becomes:

$$f_y = \frac{500}{1.15} = 435 \quad \text{MPa} \tag{8.3}$$

The elastic modulus is considered as $200\,\text{GPa}$ or $2 \times 10^5\,\text{MPa}$. Strain at yield becomes:

$$\epsilon_y = \frac{435}{2 \times 10^5} = 0.002175 \tag{8.4}$$

The density is considered to be $7850\,\text{kg/m}^3$ and the Poisson's ratio is 0.15. The ultimate strain is considered as 0.145 for TMT bars. The stress strain curve for flexural rebar is given in Figure 8.2.

Figure 8.2: Stress – strain relation Fe 500 grade of reinforcing steel

8.1.3 Shear Reinforcement Steel Model

For this purpose, similar model is used, but Fe 415 is used (as specified by IS:456 [16]). The peak of idealised plot becomes:

$$f_y = \frac{415}{1.15} = 361 \quad \text{MPa} \tag{8.5}$$

The elastic modulus is considered as $200\,\text{GPa}$ or $2 \times 10^5\,\text{MPa}$. Strain at yield becomes:

$$\epsilon_y = \frac{361}{2 \times 10^5} = 0.001805 \tag{8.6}$$

The density is considered to be $7850\,\text{kg/m}^3$ and the Poisson's ratio is 0.15. The ultimate strain is considered as 0.145 for TMT bars. The stress strain curve for flexural rebar is given in Figure 8.3.

Figure 8.3: Stress – strain relation Fe 415 grade of reinforcing steel

Note – This type of idealised bilinear curve is used because most of the cases we see the concrete fails. However, the tension steel gets yielded and goes to plastic zone but does not reach failure point except some highly over reinforced sections.

8.1.4   Concrete Material Model

Modelling of constitutive behaviour is a real complex thing in any environment. Unlike SAP2000, ABAQUS does not have any library of commercial concrete material. Hence we have to model it in the ABAQUS by giving input of every parameters of **Concrete Damaged Plasticity (CDP)** Model that is supported in ABAQUS/Explicit. The reason behind such complexity is the uncertainty in concrete behaviour, non – homogeneity, and most importantly different behaviour under compression and tension. Moreover, the linear elastic range of concrete is almost negligible and this causes so many numerical issues in ABAQUS. We will calibrate the M 40 concrete by conducting some cube test in ABAQUS and see whether it is matching with the theoretical curve or not. Before that we will discuss the theory of different parameters in CDP modelling.

8.1.4.1 Concrete Damaged Plasticity Model – an Introduction

ABAQUS provides a field called CDP where we can fit the concrete behaviour, but it is not by simply giving the stress – strain relations. It has to be designed through a three stage data entry – behaviour under compressive stress, behaviour under tension and plasticity parameters related to failure criteria. We will discuss each and every of these in details in this section.

This CDP model is a plasticity based damage model for concrete. In this model the two main failure mechanisms are tensile cracking and compressive crushing. The yield or failure surface is controlled by two hardening variables – compressive plastic strain ($\tilde{\epsilon}_c^{pl}$) and tensile plastic strain ($\tilde{\epsilon}_t^{pl}$) corresponding to failure mechanisms under compressive and tensile loading respectively.

i. **Behaviour of Concrete Under Compression**

We all know that the concrete material is good under compression but it fails quickly under tension. However, unlike steel or such elastic materials concrete shows nonlinearity in its stress – strain plot from the very onset of the curve. For this reason, we cannot model concrete as an elastoplastic material model. And also during the unloading of the material some permanent set will be there in concrete due to its nonlinearity from the beginning and its lack of elastic response. Again, after peak stress is attained the stress decreases with rapid increase of strain until failure. Hence post peak behaviour includes damage in the concrete material which makes the modelling far more complex especially for cyclic type of loading or response of structure. To encounter this changing stiffness with damage and even without damage we will model it using yield stress vs inelastic strain (and plastic strain) behaviour instead of only stress strain behaviour. Typical stress – strain behaviour of concrete under uniaxial compression with different strain components is given in Figure 8.4.

In the CDP model uniaxial stress strain curve is converted to stress vs plastic strain curves which is done automatically by ABAQUS from the user defined input of stress vs inelastic strain data. We can define the stress strain behaviour of concrete in uniaxial compression even outside the elastic range. The compressive stress data are provided as a tabular function of inelastic strain ($\tilde{\epsilon}_c^{in}$) or plastic strain ($\tilde{\epsilon}_c^{pl}$) and if desired also as function of plastic strain rate ($\dot{\tilde{\epsilon}}_c^{pl}$), temperature ($\theta$) and a number of field variables
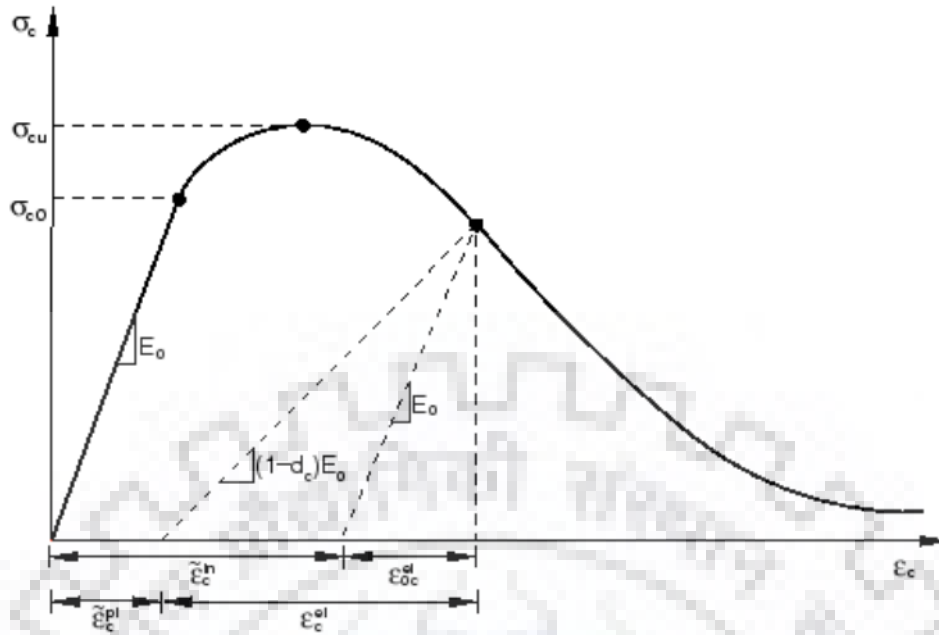
Figure 8.4: Stress – Strain behaviour of concrete under compression (ABAQUS Documentation [1])

(f_i) $(i = 1, 2, \dots)$ (subscript c stands for compression). Hence compressive stress is given by:

$$\sigma_c = \sigma_c\left(\tilde{\epsilon}_c^{pl}, \dot{\tilde{\epsilon}}_c^{pl}, \theta, f_i\right) \tag{8.7}$$

Now if we look into Figure 8.4 we will see different strain components related to the nonlinear stress strain diagram of concrete under compression. The initial portion of the curve is assumed to be linear with elastic modulus E_0 despite the fact that it hardly shows any linearity in the curve. We can find the inelastic or crushing strain for input using the following relation obtained by analysing the stress strain plot:

$$\tilde{\epsilon}_c^{in} = \epsilon_c - \epsilon_{0c}^{el} \tag{8.8}$$

Where ϵ_{0c}^{el} is the elastic strain corresponding to the undamaged material:

$$\epsilon_{0c}^{el} = \frac{\sigma_c}{E_0} \tag{8.9}$$

Thus the stress strain relation is obtained from any constitutive model of concrete and the inelastic strain is calculated which is given as input in a tabular form.

The unloading data are provided in ABAQUS in terms of compression damage (d_c) (when strain reaches post peak portion of the curve). ABAQUS automatically calcu-

lates the plastic strain components from the input inelastic strain and damage parameter:

$$\tilde{\epsilon}_c^{pl} = \tilde{\epsilon}_c^{in} - \frac{d_c}{1 - d_c} \cdot \frac{\sigma_c}{E_0} \tag{8.10}$$

If the unloading happens before the peak is attained, the damage parameter dc becomes zero and hence the plastic and inelastic strain becomes equal. Detailed discussion of damage variable (d_t and d_c) will be given in later sections.

Note – the dependency on plastic strain rate, temperature and field variables has not been considered due to lack of data.

Again Kmiecik and Kamiński [21] has noted that the CDP model can show numerical issues leading to failure in solver if we use nonlinear curve right from the beginning of the stress strain curve which is a typical case of any concrete. Hence, the first entry for stress with zero inelastic strain has to have a considerable value to avoid the numerical failure. According to Majewski [27], this linear elasticity limit increases with concrete strength and it can be assumed by an empirical relation rather than going for experiments. He calculated it as a percentage of stress to concrete strength:

$$e_{lim} = 1 - \exp\left(-\frac{f_c}{80}\right) \tag{8.11}$$

Where, f_c is the compressive strength of concrete in MPa.

However, Eurocode-2 [9] defines the modulus of elasticity of concrete as the secant modulus in the range of 0–0.4f_{cm} (f_{cm} is the peak compressive strength). Hence this ceiling of linear elasticity can be arbitrarily assumed to be up to 0.4f_{cm}. This leads to better convergence of the ABAQUS program with lessened numerical issues.

ii. **Behaviour of Concrete Under Tension**

For tension also, concrete behaviour is expressed in term of tabular data of tensile stress vs plastic strain which can be calculated by ABAQUS itself from the user defined inelastic or cracking strain data:

$$\sigma_t = \sigma_t\left(\tilde{\epsilon}_t^{pl}, \dot{\tilde{\epsilon}}_t^{pl}, \theta, f_i\right) \tag{8.12}$$

Where all the parameters are defined earlier in compression behaviour, with only difference in the subscript t which stands for tension.

Now in general the peak tensile strength is much lesser than the peak compressive strength and that is why a linear approximation of the tension stress – strain curve

gives a reasonable model in until the peak tensile stress is attained. Now the peak strength in tension is approximated from some empirical relations obtained from indirect tension tests (splitting tension, flexural tension etc.) since direct uniaxial tension tests lead to failure in solver due to large rate of deformation once the peak is achieved. Eurocode-2 [9] gives a reasonable approximation of the peak tensile strength (f_{ctm}) which is a function of the peak cube compressive strength (f_{ck}):

$$f_{ctm} = 0.3\, f_{ck}^{2/3} \tag{8.13}$$

The post peak behaviour is modelled with 'tension stiffening' which allows us to define strain softening behaviour of cracked concrete. It also allows for the effect of the reinforcements in the concrete in a simplified manner (Reinforcements are modelled by one dimensional elements which is embedded in the concrete with proper orientation. For this reason, effects associated with rebar such as bond slip and dowel action are modelled approximately by introducing some tension stiffening in the concrete). This tension stiffening is defined in two manners – post failure stress strain relation or fracture energy cracking criterion. However, we will only focus on the post failure stress strain relation.

ABAQUS Documentation [1] says to assume a linear degradation in the post failure stress starting from the strain at peak tensile strength (f_{ctm}) to a strain that is 10 times the strain at the f_{ctm}. However, for accurate modelling we have to use some calibrated relation as mentioned by Kmiecik and Kamiński [21]. They also referred to a proper tensile stress – strain relation proposed by Wang and Hsu [41]:

$$\sigma_t = \begin{cases} E_c \epsilon_t & \text{if } \epsilon_t \leq \epsilon_{cr} \\ f_{ctm}\, \frac{\epsilon_{cr}}{\epsilon_t} & \text{if } \epsilon_t > \epsilon_{cr} \end{cases} \tag{8.14}$$

Where f_{ctm} is the peak tensile strength and ϵ_{cr} is the strain at peak at which cracking appears in the concrete. Using these, stress – strain behaviour with different strain components is given in Figure 8.5.

In tension behaviour inelastic strain or cracking strain ($\tilde{\epsilon}_t^{ck}$) is used to define the 'tension stiffening using the post failure stress strain relation'. The cracking strain ($\tilde{\epsilon}_t^{ck}$) is defined by the difference between total strain and elastic strain corresponding to undamaged material:

$$\tilde{\epsilon}_t^{ck} = \epsilon_t - \epsilon_{0t}^{el} \tag{8.15}$$
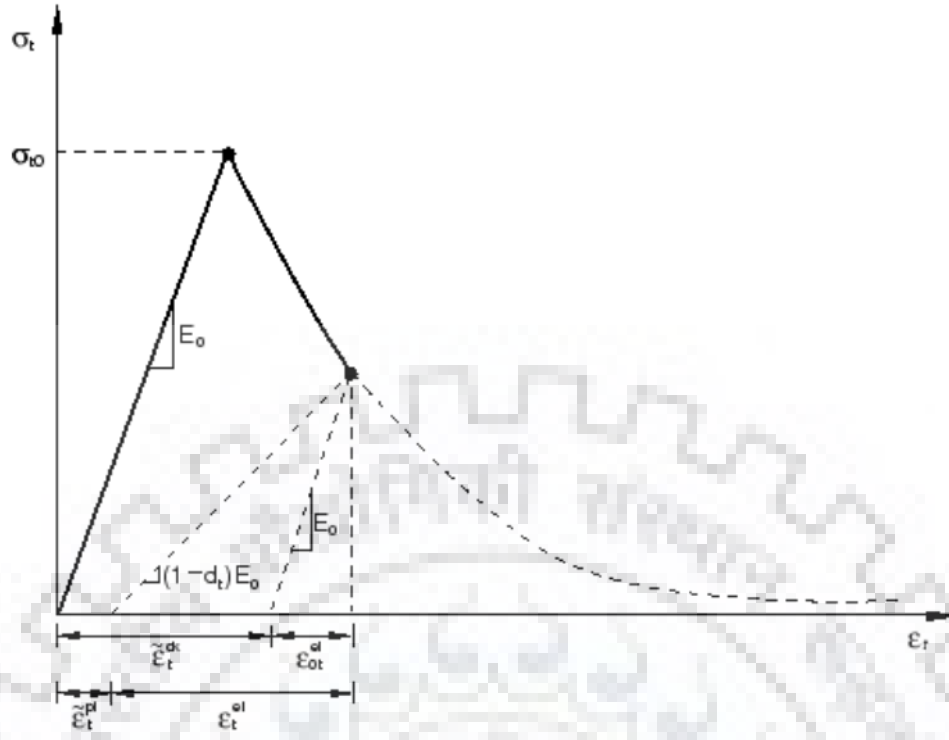
Figure 8.5: Stress – Strain behaviour of concrete under tension (ABAQUS Documentation [1])

Where ϵ_{0t}^{el} is the elastic strain corresponding to undamaged material:

$$\epsilon_{0t}^{el} = \frac{\sigma_t}{E_0} \tag{8.16}$$

Hence, tension stiffening can be given by $\tilde{\epsilon}_t^{ck}$ and when unloading data are available (or approximated using eq: (8.14)) ABAQUS converts the cracking strain to plastic strain using cracking strain ($\tilde{\epsilon}_t^{ck}$) and damage variable (d_t):

$$\tilde{\epsilon}_t^{pl} = \tilde{\epsilon}_t^{ck} - \frac{d_t}{1 - d_t} \cdot \frac{\sigma_t}{E_0} \tag{8.17}$$

Naturally, if peak strength is not achieved there will be no damage and cracking strain will be same as plastic strain.

Note – In case of less or no reinforcement mesh sensitivity is induced in the model and the results get diverged even after mesh refinement since it leads to 'narrower crack band'. It typically occurs in case of localised cracking and hence proper amount of reinforcement has to be provided to avoid divergence in Finite Element Analysis.

iii. **Damage in Concrete and Stiffness Recovery in Cyclic Loading Condition**

We have already seen that plastic strain after unloading depends on the extent of

damage for both tension and compression. It can be seen in Figure 8.4 and 8.5 that if the specimen is unloaded from any post failure point i.e. point of strain softening branch, the unloading response is weakened i.e. the elastic stiffness is appeared to be damaged. The damage or degradation variables d_c and d_t are functions of plastic strain, temperature and other field variables although we will neglect the effects of latter two.

$$\left.\begin{array}{ll} d_c = d_c\left(\tilde{\epsilon}_c^{pl}, \theta, f_i\right) & \text{and} \quad 0 \leq d_c \leq 1 \\ d_t = d_t\left(\tilde{\epsilon}_t^{pl}, \theta, f_i\right) & \text{and} \quad 0 \leq d_t \leq 1 \end{array}\right\} \tag{8.18}$$

A value of zero for degradation variable means no damage and a value of one means complete loss of strength.

Now in uniaxial cyclic loading conditions the mechanism is quite complex. Experimentally it is observed that some amount of degraded stiffness is recovered as load changes its sign. This is known as stiffness recovery or 'unilateral effect'. This effect is more prominent in case when load changes from tension to compression causing all the cracks to be closed providing a load transfer through cracked area too.

The damage variable values have to be given as input in CDP model in a tabular form of crushing or cracking strain vs damage variable. The damage variable is calculated from ratio of stress in strain softening branch to the peak stress of concrete and subtracting from unity:

$$d_c \text{ or } d_t = 1 - \frac{\text{stress in the declining part of the stress vs strain curve}}{\text{stress at the peak}} \tag{8.19}$$

Now in case of cyclic loading or cyclic behaviour of structure, the CDP model assumes the degradation of stiffness or elastic modulus in terms of damage variable d as:

$$E = E_0\left(1 - d\right) \tag{8.20}$$

Where E_0 is the elastic stiffness at zero strain for the concrete. Now, the degradation variable d includes components of both compressive and tensile damage variables (d_c and d_t). Also, this expression holds for both uniaxial tension ($\sigma_{11} > 0$) and compression ($\sigma_{11} < 0$). Hence for uniaxial cyclic conditions ABAQUS assumes that:

$$(1 - d) = (1 - s_t d_c)(1 - s_c d_t) \tag{8.21}$$

Where s_c and s_t are functions of stress state introduced for stiffness recovery. They are defined as:

$$s_t = 1 - w_t r^* (\sigma_{11}) \quad 0 \leq w_t \leq 1 \tag{8.22}$$

$$s_c = 1 - w_c r^* ((\sigma_{11})) \quad 0 \leq w_c \leq 1 \tag{8.23}$$

Where:

$$r^* (\sigma_{11}) = H (\sigma_{11}) = \begin{cases} 1 & \text{if } \sigma_{11} > 0 \ (tension) \\ 0 & \text{if } \sigma_{11} < 0 \ (compression) \end{cases} \tag{8.24}$$

The weight factors control tension or compression stiffness recovery under load reversals. For example, if $w_c = 1$ that means full stiffness recovery upon reversal of load from tension to compression. Similarly, if $w_c = 0$ it means no stiffness recovery in the material when load is reversed from tension to compression. Figure 8.6 illustrates stiffness recovery for load reversal from tension and compression for concrete which has no previous compression damage. In general, we consider $w_c = 1$ (ABAQUS de-
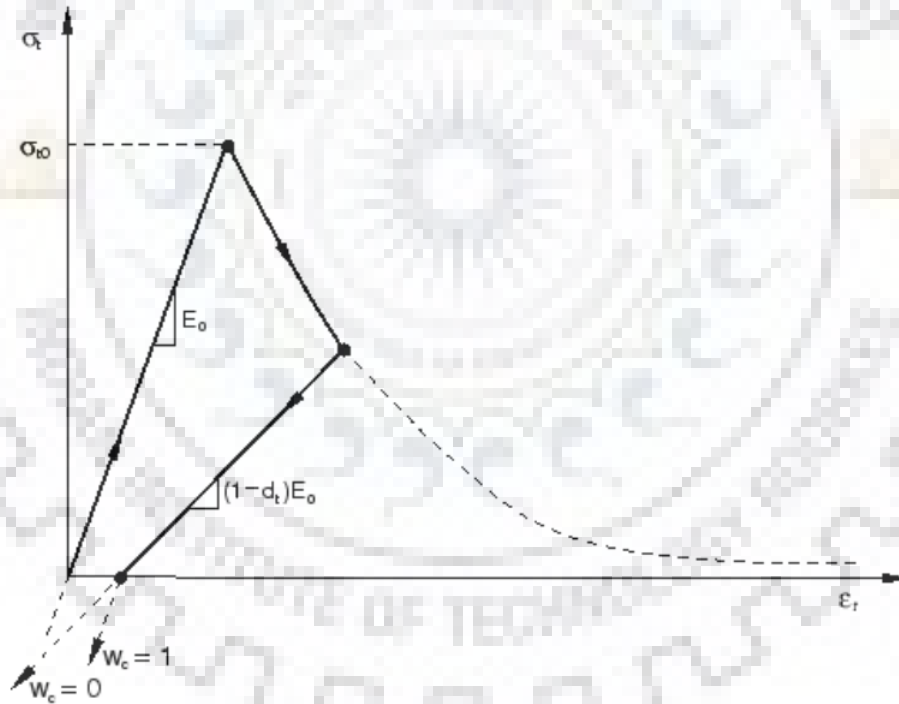
Figure 8.6: Illustration of compressive stiffness recovery parameter w_c (ABAQUS Documentation [1])

fault) because the tension cracks get closed under compression and hence full stiffness is recovered. In the other hand $w_t = 0$ because after crushing of concrete no stiffness is recovered under load reversal.The behaviour of concrete in a uniaxial load cycle for $w_t = 0$ and $w_c = 1$ is shown in Figure 8.7.
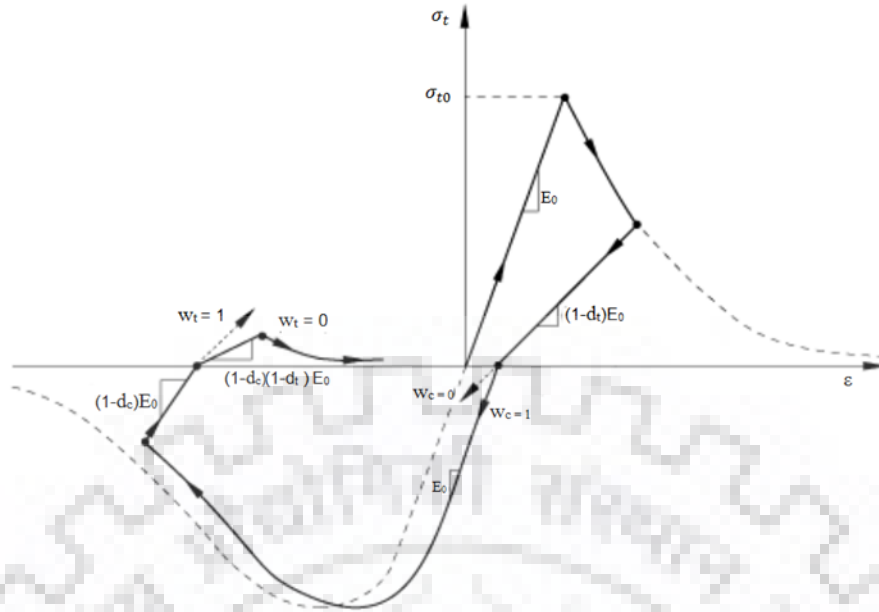
Figure 8.7: Uniaxial load cycle (tension-compression-tension) assuming default values for the stiffness recovery factors: $w_t = 0$ and $w_c = 1$ (ABAQUS Documentation [1])

iv. **Plasticity Parameters Related to CDP**

A commonly used hypothesis for granular materials (like concrete) is the Drucker Prager Hypothesis (1952) in which failure is determined by non-dilatational strain energy and in stress space the failure or yield surface assumes a shape of a cone. But for concrete it's not completely consistent with its behaviour. However, the advantage is the smoothness of the surface which reduces many numerical complications inside the solver. For a concrete sample the tension and compression capacity is different. Hence, two different cones are found if we fit concrete behaviour in Drucker Prager failure criterion. Figure 8.8 shows two different cones for tensile and compressive behaviour of concrete (showing compression and tension meridian).

The Concrete Damaged Plasticity (CDP) model in ABAQUS uses a modified Drucker Prager criteria. CDP uses yield function given by Lubliner et al. [26] with further modifications made by Lee and Fenves [25] for different strength of concrete under tension and compression. According to these modifications the deviatoric cross section of the failure surface is not necessarily a circle (Figure 8.9) and for concrete it is governed by a parameter K_c.
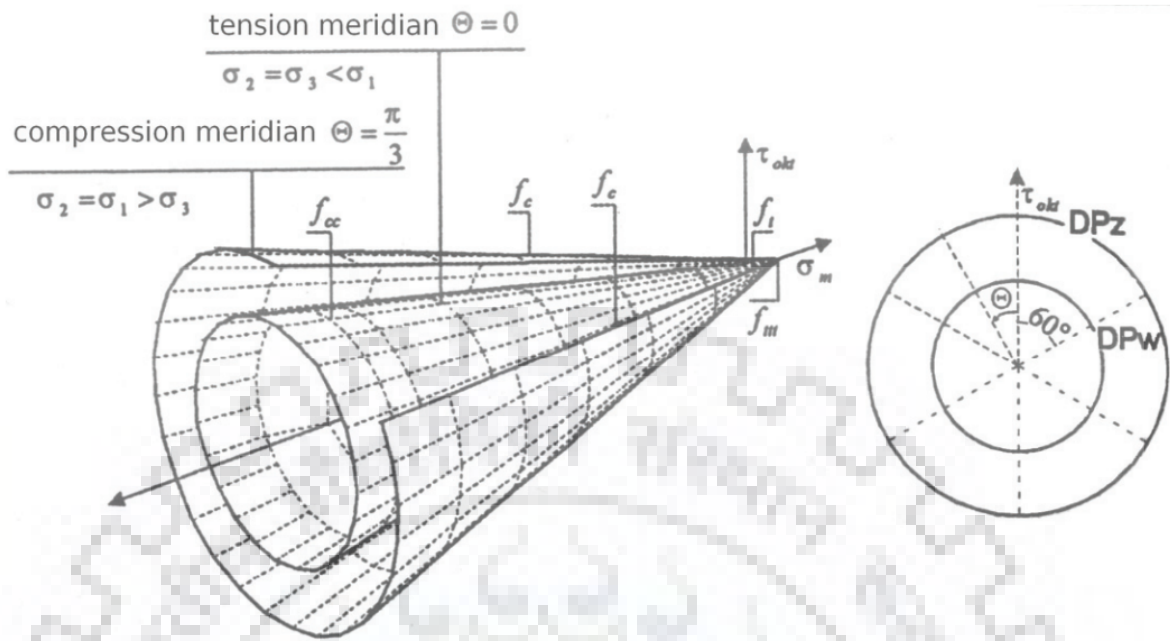
Figure 8.8: Drucker Prager boundary surface view and deviatoric cross section (Kmiecik and Kamiński [21])
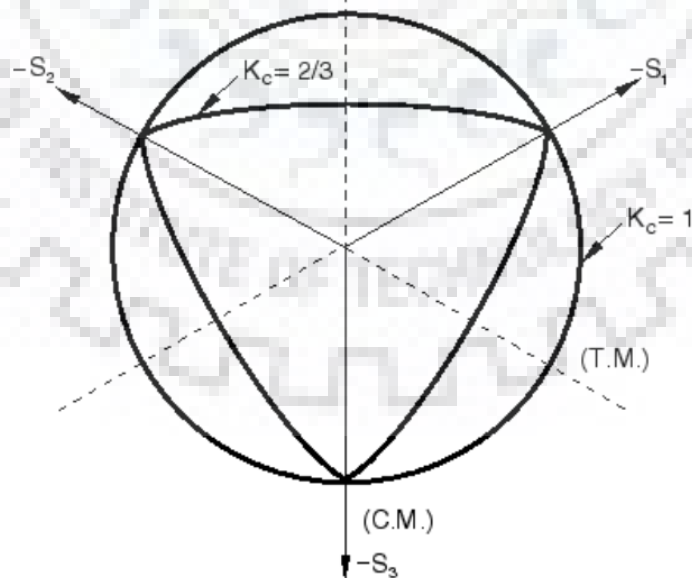
Figure 8.9: Uniaxial load cycle (Deviatoric cross section of failure surface for CDP model (ABAQUS Documentation [1])

The parameter K_c is defined by the ratio of distance between hydrostatic axis and tension meridian to distance between hydrostatic axis and compression meridian in deviatoric cross section. It is always greater than 0.5 and can take a maximum value of 1. When its value becomes 1 the deviatoric cross section of failure surface becomes a circle and it becomes the same as Drucker Prager criterion.

Now the shape of meridians also changes in stress space. Experimental results reveal that the meridians are curves. In CDP model the plastic potential surface in meridional plane is a hyperbola. It comes from the hyperbolic flow potential function (G) from Drucker Prager Hypothesis:

$$G = \sqrt{\left(\epsilon\, \sigma_{t0}\, \tan\psi\right)^2 + \bar{q}^2} - \bar{p}\tan\psi \tag{8.25}$$

Where hydrostatic pressure is $\bar{p} = -\frac{1}{3}\,trace\,(\bar{\sigma})$, and $\bar{\sigma}$ is the effective stress tensor. The Mises equivalent effective stress is $\bar{q} = \sqrt{\frac{3}{2}\bar{S}\cdot\bar{S}}$, where $\bar{S}$ is the effective deviatoric stress defined as $\bar{S} = \bar{\sigma} + \bar{p}I$. Again ψ (sometimes termed as β) is the dilation angle measured in $p-q$ plane at high confining pressure. It is the inclination of failure surface at meridional plane towards the hydrostatic axis. As per Kmiecik and Kamiński [21] it can be interpreted as internal angle of friction for concrete. Usually it varies from $36\,^{\circ}$ to $40\,^{\circ}$.

Other parameter σ_{t0} is the uniaxial tensile stress at failure which is directly extracted from the tension stiffening data provided by the users. The last parameter ϵ is known as eccentricity which defines the rate at which the function approaches to asymptote (if eccentricity tends to zero the flow potential tends to be a straight line or the failure surface in meridional plane becomes a straight line). Physically it is measured as the length along the hydrostatic axis from the vertex of the hyperbola to the point of the intersection of asymptote with hydrostatic axis. Recommended value of ϵ is 0.1. Figure 8.10 gives us an idea of plastic potential surface in meridional plane.

Finally, the CDP model uses the yield function stated by Lubliner et al. [26] with further modifications made by Lee and Fenves [25] and it is given by:

$$F = \frac{1}{1-\alpha}\left(\bar{q} - 3\alpha\bar{p} + \beta\left(\tilde{\epsilon}^{pl}\right)\langle\hat{\bar{\sigma}}_{max}\rangle - \gamma\langle-\hat{\bar{\sigma}}_{max}\rangle\right) - \bar{\sigma}_c\left(\tilde{\epsilon}^{pl}_c\right) = 0 \tag{8.26}$$
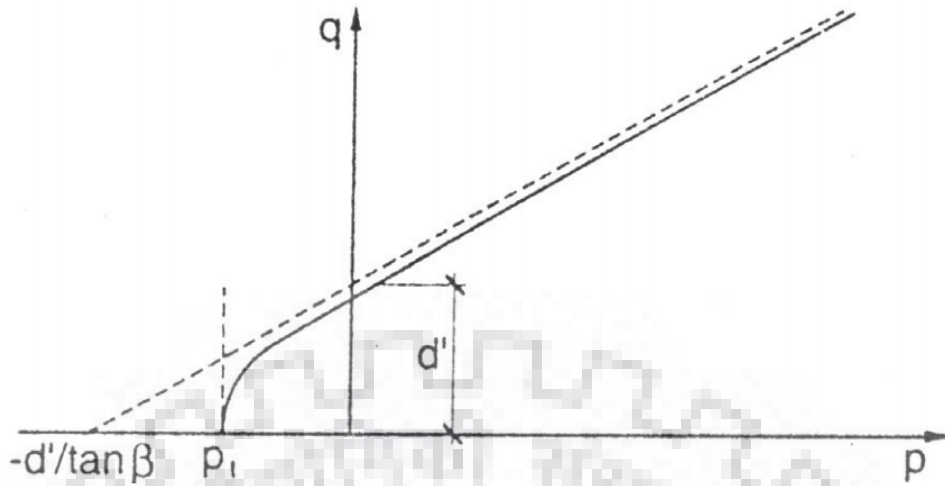
Figure 8.10: Hyperbolic surface of plastic potential in meridional plane (Kmiecik and Kamiński [21])

Lubliner et al. [26] have defined all the parameters as the following:

$$\alpha = \frac{(\sigma_{b0}/\sigma_{c0}) - 1}{2(\sigma_{b0}/\sigma_{c0}) - 1} \quad \text{where,} \ 0 \leq \alpha \leq 0.5 \tag{8.27}$$

$$\beta = \frac{\bar{\sigma}_c\left(\tilde{\epsilon}_c^{pl}\right)}{\bar{\sigma}_t\left(\tilde{\epsilon}_t^{pl}\right)}(1 - \alpha) - (1 + \alpha) \tag{8.28}$$

$$\gamma = \frac{3(1 - k_c)}{2k_c - 1} \tag{8.29}$$

Here,

$\hat{\bar{\sigma}}_{max}$ is the maximum principal effective stress.

Macaulay bracket $\langle . \rangle$ is defined by $\langle x \rangle = \frac{1}{2}(|x| + x)$

K_c is the same as defined earlier (corresponding to Figure 8.9).

$\bar{\sigma}_c\left(\tilde{\epsilon}_c^{pl}\right)$ and $\bar{\sigma}_t\left(\tilde{\epsilon}_t^{pl}\right)$ are the effective compressive and tensile cohesion stress respectively and is defined by the expressions:

$$\bar{\sigma}_c\left(\tilde{\epsilon}_c^{pl}\right) = \frac{\sigma_c}{1 - d_c} = E_0\left(\epsilon_c - \tilde{\epsilon}_c^{pl}\right) \tag{8.30}$$

$$\bar{\sigma}_t\left(\tilde{\epsilon}_t^{pl}\right) = \frac{\sigma_t}{1 - d_t} = E_0\left(\epsilon_t - \tilde{\epsilon}_t^{pl}\right) \tag{8.31}$$

All the parameters of eq: (8.30) and (8.31) are described in this section earlier while discussing about property of concrete under tension and compression. These two parameters are evaluated automatically by ABAQUS from the user defined compression and tension data.

Now remaining things to define the yield function completely is α, β and γ. Among these γ can be determined by ABAQUS from the user input K_c value. β is evaluated from α and effective compressive and tensile stress obtained from user defined compression and tension data. But to determine α the main thing that is required is the ratio $(\sigma_{b0}/\sigma_{c0}$) i.e. the ratio between initial equibiaxial compressive yield stress (σ_{b0}) to initial uniaxial compressive yield stress (σ_{c0}) of concrete. The most reliable and most commonly used data to find this ratio is the experimental results reported by Kupfer et al. [24] in which they have reported results for behaviour of B50 class of concrete under biaxial state of stress. Figure 8.11 shows the plot for results of biaxial test result for B50 class of concrete. After their elliptical approximation of scattered
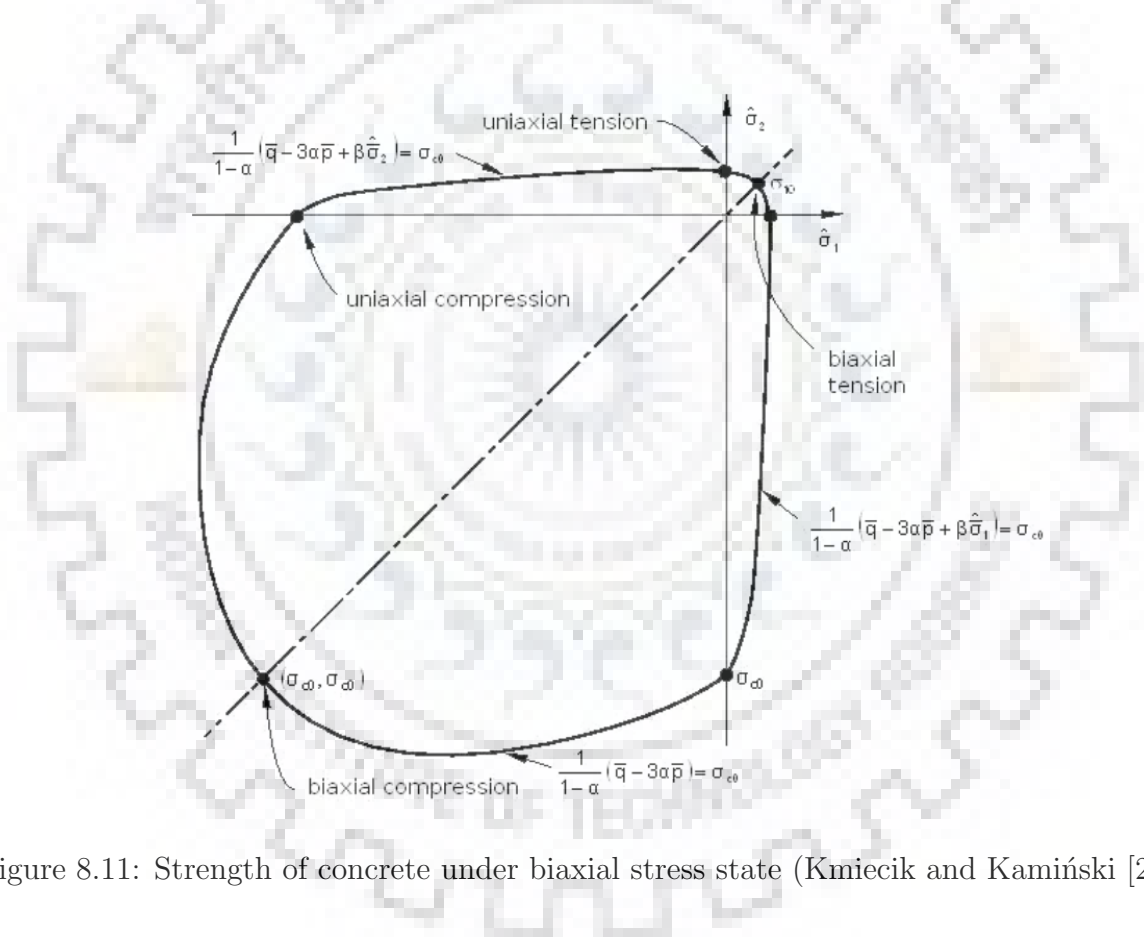
Figure 8.11: Strength of concrete under biaxial stress state (Kmiecik and Kamiński [21])

plot as shown in the Figure 8.11, they found the ratio of biaxial compressive strength to the uniaxial compressive strength as σ_{b0}/σ_{c0} =1.16248 and hence CDP model in ABAQUS uses the ratio of 1.16 by default.

The last input required to define the plasticity of concrete is the viscosity parameter used for viscoplastic regularisation to overcome numerical issues regarding convergence difficulties for stiffness degradation and softening behaviour especially in small problem

steps. Though ABAQUS by default chooses zero viscosity, an adjustment of viscosity $\mu > 0$ is recommended such that the ratio of problem step to viscosity ratio approaches infinity (Kmiecik and Kamiński [21]).

8.1.4.2 Modelling Input Parameters of Concrete of Grade M40

We will now fit the M40 grade of concrete in the CDP model. Now compressive stress behaviour of concrete in IS:456 [16] gives an idealised plot in which there is a flat peak portion which cannot be used properly in CDP since it would not take any damage. Hence we will use stress strain model given by Mander et al. [29] which was actually for confined concrete but we have used it for unconfined strength of concrete. It is defined as following:

$$f_c = \frac{f_{c0}\, xr}{r - 1 + x^r} \tag{8.32}$$

Where, f_c is stress at any point, f_{c0} is the compressive strength of concrete and $x = \epsilon_c/\epsilon_{c0}$ where ϵ_c is the compressive strain at any point and ϵ_{c0} is the compressive strain at peak stress (generally $\epsilon_c = 0.002$ is assumed). Finally, $r = \frac{E_c}{E_c - E_{sec}}$, where E_c is the tangent modulus of elasticity of concrete (assumed to be $E_c = 5000\sqrt{f_{ck}}$ as per IS:456 [16]) and Esec is the secant modulus at the peak stress ($E_{sec} = f_{c0}/\epsilon_{c0}$). The peak compressive stress as per IS:456 [16] for M40 is given by $f_{c0} = 0.446 f_{ck} = 0.446 \times 40 = 17.84$ MPa. The strain at peak stress is considered to be 0.002 and the ultimate compressive strain is considered to be 0.004 (though in IS:456 [16] it is 0.0035, since we are modelling declining portion instead of flat peak we can consider it to be 0.004).

For tensile stress we will use the empirical relation given by Wang and Hsu [41] which is given in eq: (8.14). Now we will fit M40 in these relations. The peak tensile strength as per Eurocode-2 [9] is given by eq: (8.13) : $f_{ctm} = 0.3 f_{ck}^{2/3} = 3.51$ MPa.
Figure 8.12 shows the assumed stress strain curve in compression and Figure 8.13 shows the assumed stress strain curve in tension for M40 grade of concrete.

Now for modelling the M40 in CDP we have used the concepts of section 8.1.4.1. First of all, the compression data is given in Table 8.1 using the crushing strain from eq: (8.8) and damage using eq: (8.19). Similarly, the tension data has been tabulated in Table 8.2 using cracking strain from eq: (8.15) and damage using eq: (8.19).
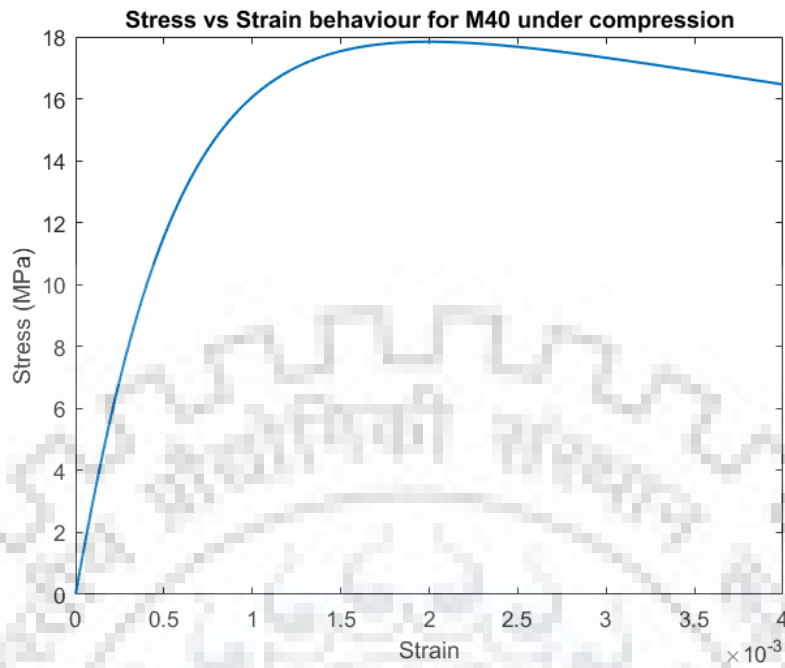
Figure 8.12: Stress vs Strain curve under compression for M40 concrete following Mander et al. [29]
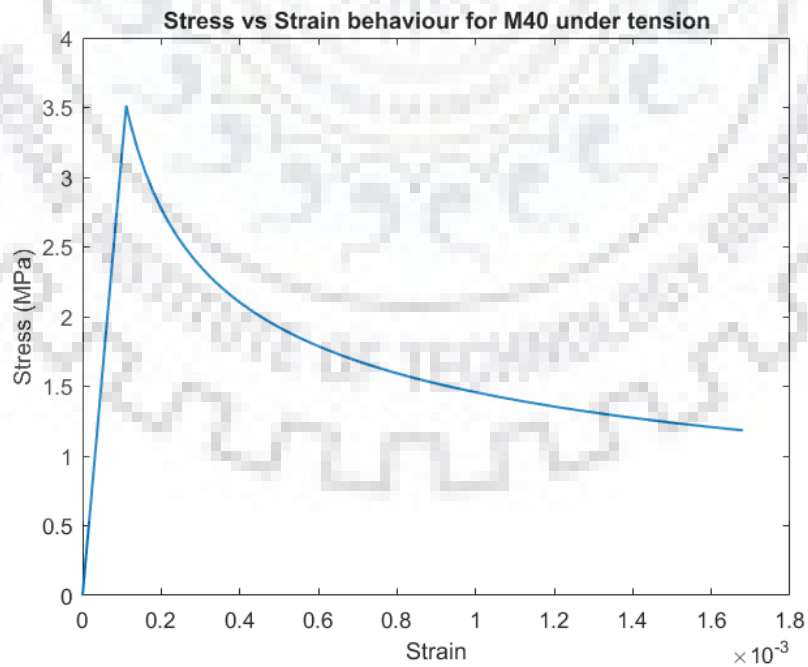
Figure 8.13: Stress vs Strain curve under tension for M40 concrete following Wang and Hsu [41]

Table 8.1: CDP input for M40 under compression

Yield Stress (MPa)	Crushing Strain	Damage Parameter	Crushing Strain
7.383219969	0	0	0
9.956436014	3.33345×10^{-05}	0	3.33345×10^{-05}
14.79240547	0.00025524	0	0.00025524
16.87065543	0.000578705	0	0.000578705
17.65968023	0.000949647	0	0.000949647
17.84087582	0.001342974	0	0.001342974
17.72919473	0.001747087	0.006211	0.001747087
17.47613269	0.002156407	0.020396	0.002156407
17.15764822	0.002568136	0.038248	0.002568136
16.81307326	0.002980825	0.057563	0.002980825
16.46316102	0.003393711	0.077177	0.003393711

Table 8.2: CDP input for M40 under tension

Yield Stress (MPa)	Cracking Strain	Damage Parameter	Cracking Strain
3.511098	0	0	0
3.112835971	3.62×10^{-05}	0.113989009	3.62×10^{-05}
2.774474527	9.85×10^{-05}	0.210297315	9.85×10^{-05}
2.218020329	0.000269	0.368681675	0.000269
1.923112711	0.00043	0.452621656	0.00043
1.8511758	0.000482	0.473097163	0.000482
1.78785478	0.000535	0.491120316	0.000535
1.680945079	0.000639	0.521550178	0.000639
1.593517162	0.000742	0.546434912	0.000742
1.555339386	0.000793	0.557301508	0.000793

It can be noted that the compression curve is assumed to be linear up to around $0.4 f_{cm} = 7.136$ MPa where f_{cm} is the peak compressive strength (following Eurocode-2 [9] as specified in eq: (8.13)). Now the plasticity parameters are mostly used as given in ABAQUS default and there are given in Table 8.3.

Table 8.3: CDP input for M40 under tension

Parameter Name	Value
Dilation Angle	$36\,^{\circ}$
Eccentricity	0.1
f_{b0}/f_{c0}	1.162
K_c	0.667
Viscosity Parameter	10^{-12}

Again the modulus of elasticity used is the secant modulus at $0.4f_{ck}$ which is 27345 MPa and the Poisson's ratio is considered to be 0.2. The density of concrete is 2500 kg/m^3. Now we will conduct a cube test in ABAQUS and will try to validate the stress strain plot in compression with the actual stress strain plot predicted in Mander's model.

8.1.4.3   Finite Element Modelling of Standard Concrete Cube Under Compressive Quasi Static Strain Controlled Load (For Validation Purpose)

Now we will model a concrete cube of $150\,\mathrm{mm} \times 150\,\mathrm{mm} \times 150\,\mathrm{mm}$ in ABAQUS/Standard with the same input parameters as discussed in the previous section. This cube is meshed with quadratic brick elements known as C3D20R having a uniform size of 15 mm $\times$15 mm $\times$15 mm. The step is modelled as a quasi-static implicit analysis scheme. A quasi static displacement controlled compressive load is applied. Since it is displacement controlled we have provided compressive displacement at the supports (top and bottom face) instead of applying load. The maximum compressive displacement is given such a way that the maximum compressive strain is 0.004 in the specimen. The schematic meshed model with displacement controlled load is given in Figure 8.14. The analysis scheme used is an implicit analysis scheme. After analysis we will compile the stress and strain at different point of time and plot the stress strain curve and verify whether it is coming out to be the same as theoretical stress vs strain curve be Mander et al. [29] or not.
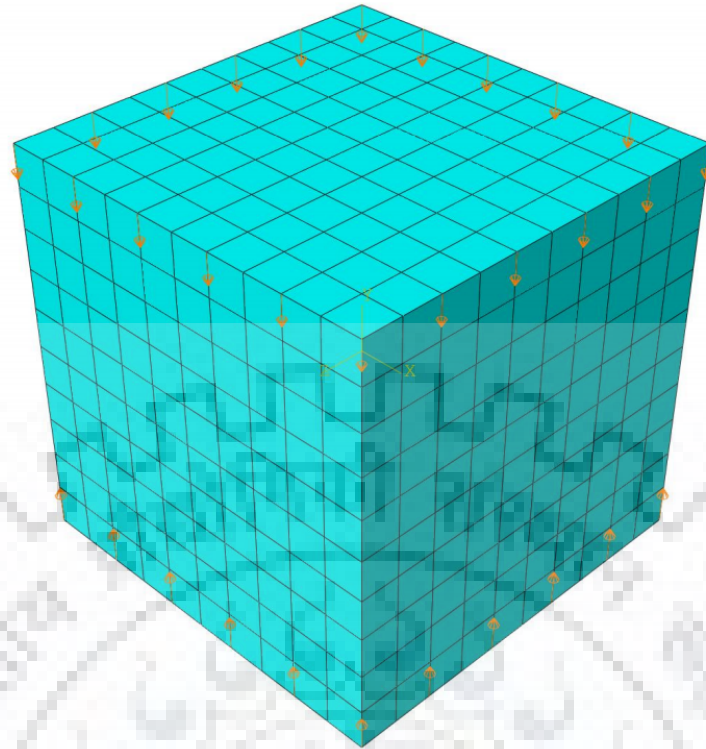
Figure 8.14: Finite element meshing of concrete cube in ABAQUS with displacement controlled loading

8.1.4.4   Results for Stress Vs Strain in Cube Test in ABAQUS Using CDP and Validation Against Actual Stress Vs Strain Plot for Mander's Model

After the quasi-static loading is applied it is seen that the entire cube is subjected to uniform compressive stress and uniform ultimate compressive strain of 0.004. However, it is to be noted that in actual experiment for cube testing, there are two rigid plates used for pressure application on the cube. Due to the rigidity of the end supports, an end friction is generated working against the lateral bulging of concrete. Hence at the ends any small element would be subjected to triaxial compression. However, at the mid height of the specimen no such end friction effect is mobilised and hence it is prone to lateral bulging due to Poisson's effect and any small element would be subjected to uniaxial compression and biaxial tension. For this reason, in cube test the strength of concrete comes out to be higher than the actual strength.

However, we have not modelled the end friction effect in our problem because we have already reduced the peak strength from the cube strength considering all these parameters

using IS:456 [16]. The peak strength in our case is $f_{cm} = 0.446 \times 40 = 17.84$ MPa, while the cube strength is 40 MPa. Now we have observed the stress strain behaviour at different time frame and plotted the curve. We have also superimposed the actual stress vs strain plot using Mander's model in Figure 8.15.
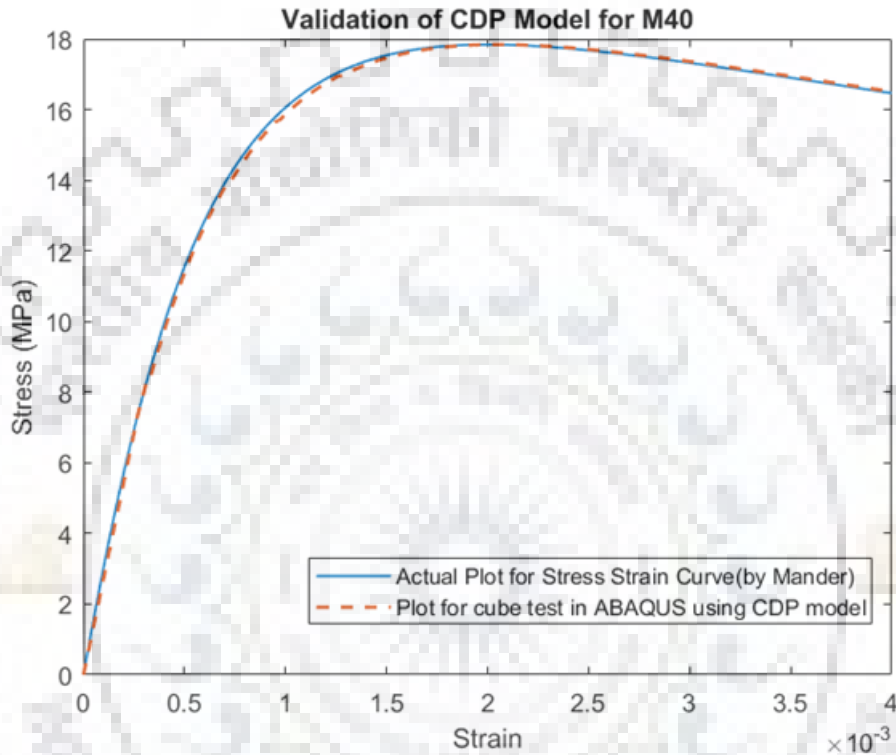
Figure 8.15: Validation of CDP modelling for M40 observing the stress vs strain Curve

Hence from the Figure 8.15 it is quite evident that our modelling is correct for CDP modelling for M40. From this point forward we will use the above mentioned input data for concrete in order to model the reinforced concrete blast resistant wall system and analyse the results in the next sections. Thus, the constitutive modelling is done for the ABAQUS/Explicit model for actual blast wall system.

Note – Slight changes of the plasticity parameters do not hamper the result much but it can help to converge a solution more quickly. Hence, since CDP is a numerically sensitive model it is recommended to change the plasticity data slightly if the solution does not converge for numerical issues.

8.1.4.5 Finite Element Modelling of a Notched Bar for Direct Tension Test (For Validation Purpose)

Now, a 2 dimensional 6 units long notched concrete bar is modelled in ABAQUS/Standard which has maximum width of 2 units and minimum width at the notch of 1 unit. An approximate size of mesh is considered as 0.05 unit. Two dimensional 4 noded plane stress element CPS4R is used for the meshing purpose. Now one end of the bar is restrained against movement in the axial direction. A displacement controlled tensile loading is applied on the other edge of the bar. In this case we expect an unstable situation within a very few steps due to huge plastic deformation at an elevated rate. Therefore in stead of explicit scheme, Rik's Arc Length Method is used as the analysis scheme. The meshed bar is shown in Figure 8.16.
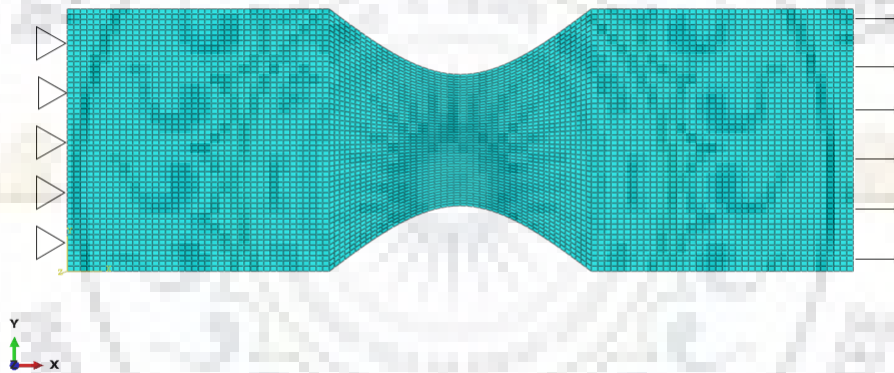
Figure 8.16: Meshed bar with notch for direct tension

8.1.4.6 Results of Direct Tension Test and Validation against Wang and Hsu's Model

After the displacement controlled loading is applied the stress vs strain diagram is plotted from stress and strain time history. If we look into the tension damage we can see that upto a point the tension crack is uniformly propagating in the notched area (Figure 8.17). After this the damage starts accumulating at a point due to the numerical issues (Figure 8.18). Hence this point onwards the stress strain diagram gets disoriented but this is only due to numerical issues after a certain point. Hence we have plotted the validated result upto the point when instability begins. The validated curve is given in Figure 8.19.
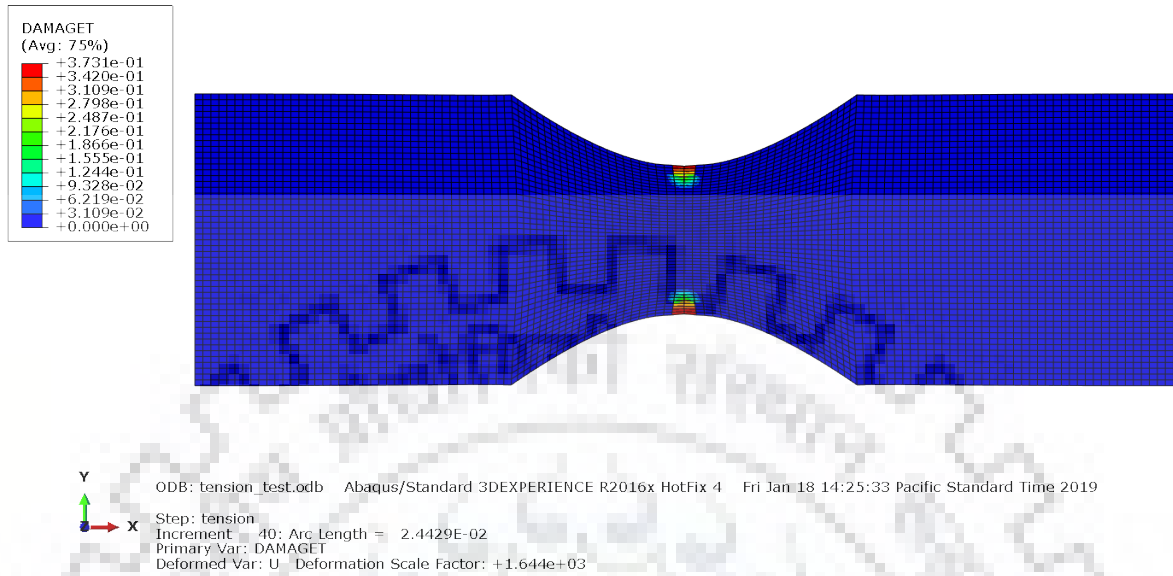
Figure 8.17: Uniform crack propagation in the bar

Figure 8.18: Localized crack propagation in the bar
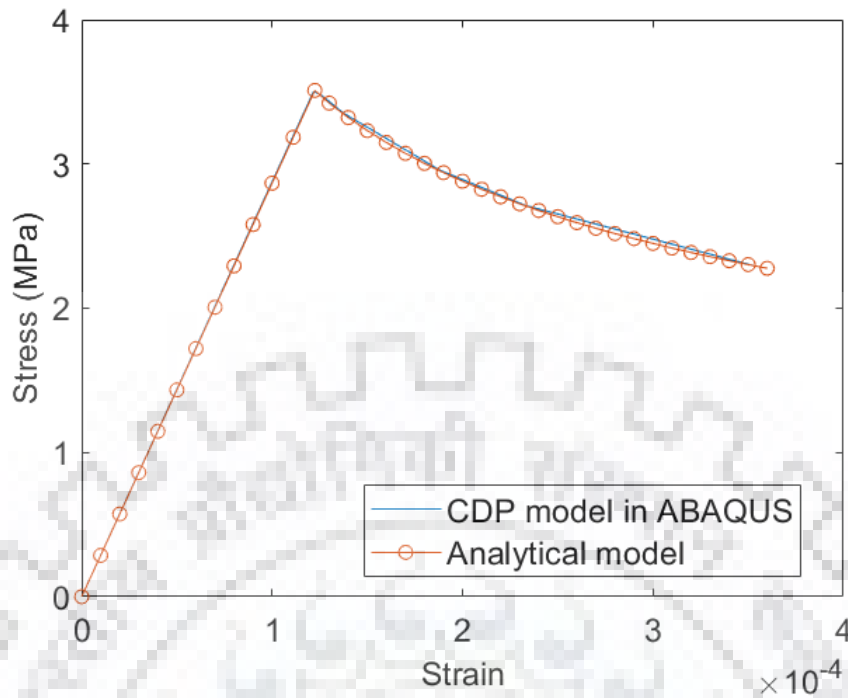
Figure 8.19: Validation of CDP model with Wang and Hsu's model

8.2.   Finite Element Modelling of the Blast Resistant System

We can already incorporate material properties used in blast wall model in ABAQUS using the constitutive models discussed earlier and assign these material properties to different constituents of the designed structure (section 7.2). Now next important thing is the meshing. Since for a short term heavy impact load is generated by the blasting, we will use an explicit solution scheme and model it in ABAQUS/Explicit. We used an explicit scheme compatible linear brick element C3D8R with approximate element size of $0.5\,\mathrm{m} \times 0.5\,\mathrm{m} \times 0.5\,\mathrm{m}$ to model the concrete wall. To model rebar, we have used linear 3D truss element T3D2 and to model I section in the composite we have used quadratic beam element B32. The mesh size of rebars and I sections is 0.5 m. The reason behind these mesh size is given in the upcoming section. All the reinforcements and I sections are embedded in concrete. At the ground level support all the points have been fixed including the I section (assuming that the raft foundation gives sufficient rigidity at support). Figure 8.20 and 8.21 shows the meshed model of the blast resistant wall system.

Figure 8.20: View of meshed wall-roof system from outer side

Figure 8.21: View of meshed wall-roof system from inner side

Now, the last thing that is remained before load application is the viscous damping introduction. This will be discussed in the next section.

8.3. Modelling of Viscous Damping Present in the Structure

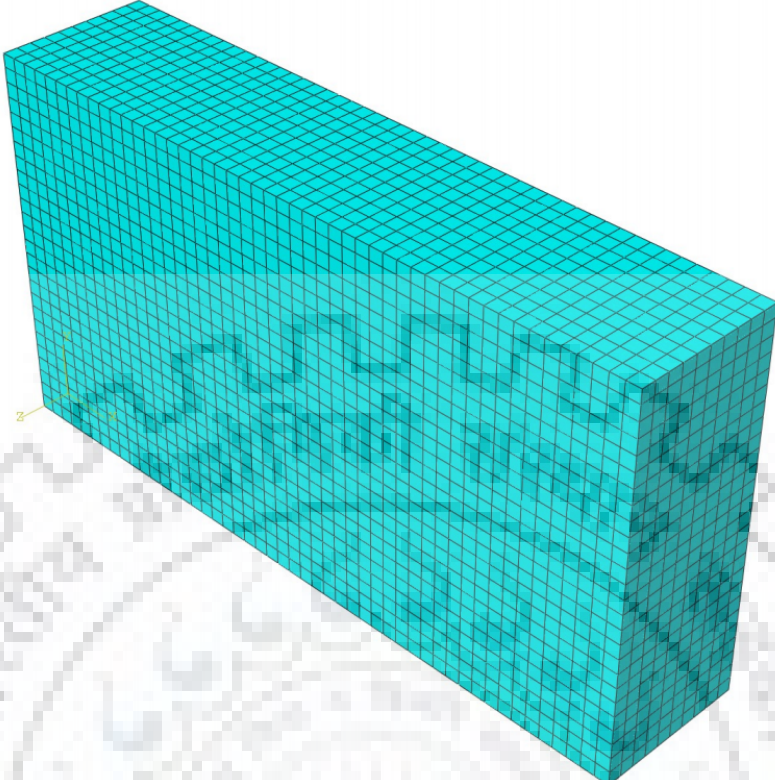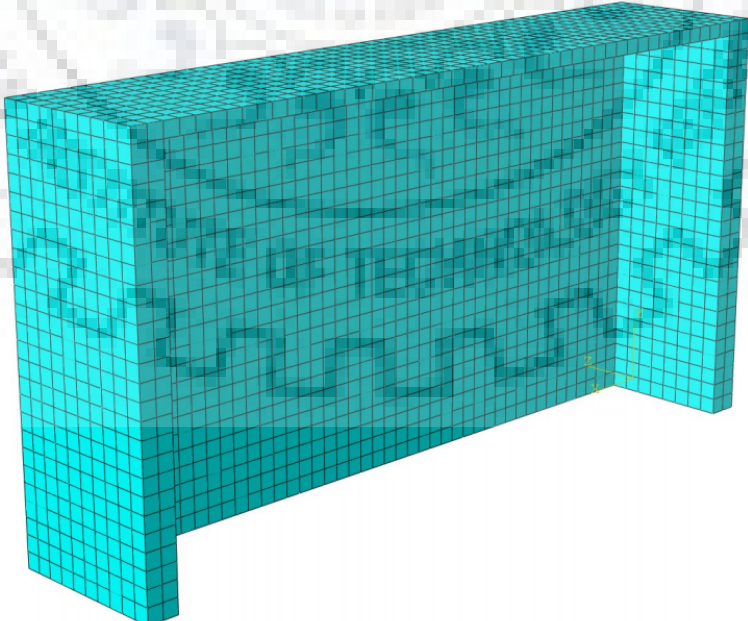We will use Rayleigh damping in this model. To model the Rayleigh damping a frequency analysis is necessary which is done in ABAQUS using the above model with proper boundary condition (fixed support at ground surface). The Rayleigh damping coefficient matrix is defined by:

$$[C] = \alpha [M] + \beta [K] \tag{8.33}$$

Where M and K are mass and stiffness matrices respectively, α and β are two coefficients which are calculated as:

$$\alpha = \frac{2\omega_i\omega_j}{\omega_j^2 - \omega_i^2} \left(\omega_j\xi_i - \omega_i\xi_j \right) \tag{8.34}$$

$$\beta = \frac{2}{\omega_j^2 - \omega_i^2} \left(\omega_j\xi_j - \omega_i\xi_i \right) \tag{8.35}$$

Now in all our analysis we consider a single value of damping ratio, in case of concrete which is $\xi = 5\%$. Hence eq: (8.34) and (8.35) becomes:

$$\alpha = \frac{2\omega_i\omega_j}{\omega_j + \omega_i}\xi \tag{8.36}$$

$$\beta = \frac{2}{\omega_j + \omega_i}\xi \tag{8.37}$$

And damping ratio becomes:

$$\xi = \frac{\alpha}{2\omega} + \frac{\beta\omega}{2} \tag{8.38}$$

Where ω_i is the fundamental natural frequency and ω_j is the natural frequency of the structure at which mass participation exceeds 90 % (as per IS:1893 (Part I) [15]). A schematic plot of natural frequency (ω) vs damping ratio (ξ) for Rayleigh Damping is given in Figure 8.22.

Now we have run an analysis to generate a large number of frequencies using Frequency analysis in ABAQUS and we have also extracted the effective mass at each mode. We have only considered the translational vibration along 'Z' direction i.e. the direction of the blast loading. Thereafter we have calculated the frequency corresponding to 90 %
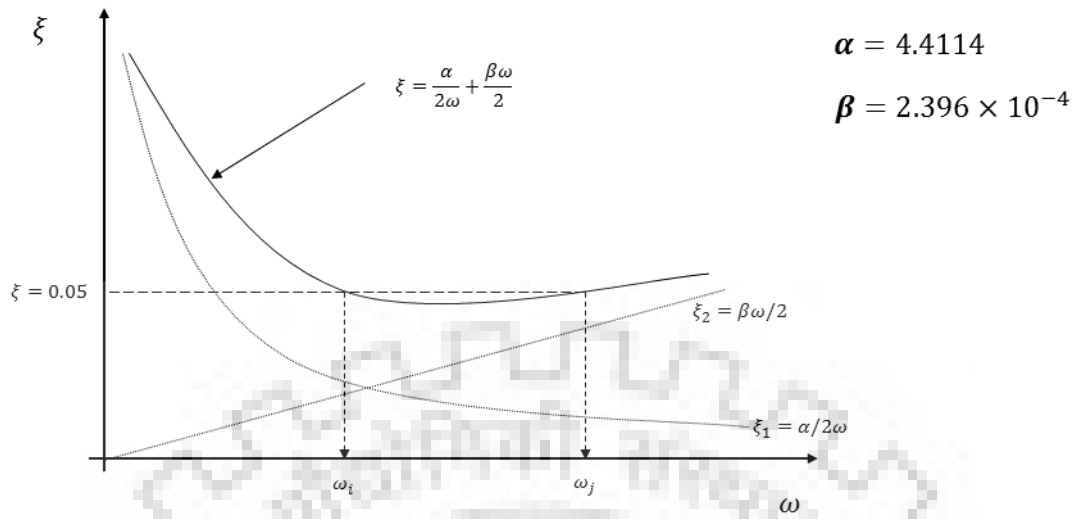
Figure 8.22: Schematic representation of Rayleigh damping parameters for concrete in our model

mass participation (ω_j) and we already know that the fundamental frequency(ω_i) will be the minimum one for the specified direction. Our result is:

$$\omega_i = 50.136 \quad \text{rad/s} \quad \text{and} \quad \omega_j = 367.28 \quad \text{rad/s}$$

Hence using eq: (8.36) and (8.37) we can find out the mass proportional damping (α) and stiffness proportional damping (ξ) for damping ratio of $\xi = 0.05$:

$$\alpha = 4.4114 \quad \text{and} \quad \beta = 2.396 \times 10^{-4}$$

Hence we can assign these two parameters as a damping input in material property of concrete. Now we can provide load in the structure and find out the response.

8.4.   Final Load Application and Results

So far we have meshed the whole model with different parts and applied viscous damping of 5 % in form of Rayleigh damping. Finally, we are all set to apply load and analyse the response of structure. We have used a tabular function for time history of transferred load in form of pressure that is coming through 600 mm thick pad in the inward direction on the front wall. We can get the time history of transferred blast pressure has already been discussed in Section 6.5 and shown in Figure 6.10. After applying the load (self-weight

and blast pressure) an explicit integration scheme is opted which is best suited for blast loading with automatic stable time increment. After the analysis is complete, we will look into the damage contour in concrete. Before that we have to ensure if the mesh size is sufficient or not.

8.4.1   Mesh Convergence Study

Before analysing results we will have to verify if the mesh size is consistent or not. For this we have performed a mesh convergence study in which we will start with a coarse mesh size and will go on reducing the mesh size. We will plot the stress contour (since it contains first derivative of primary variable, we have to consider stress to verify mesh size) at a particular point and observe if they are converging for decreasing mesh size or not. In our case we have considered a point at the fixed support on ground surface on the inner side of the front face of the building and will check the stress in concrete along the height of the wall (along 'Y' axis) which depicts the bending stress in that portion. The reason behind this selection is that the compressive stress is maximum at this point for the front wall because the local flexibility is mobilised in high impact load like blast (however in supporting shear wall the stress can be higher because it can act as a web of a channel section in uniaxial bending in the integrated action of wall system). It was also confirmed in the preliminary analysis results in SAP2000 that bending moments and stresses are maximum near the ground support behind which no supporting shear wall is present. The choice behind inner face of front wall is that it is subjected to high compressive stress in a very short time. A series of cube element mesh size from 0.7 m, 0.6 m, 0.5 m to 0.4 m is used. Figure 8.23 shows the nodal stress time history along 'Y' axis (representing bending stress) at that specified location for different mesh sizes.

In Figure 8.23, the positive value of stress represents tensile stress and negative value of stress represents tensile stress and positive value represents the compressive stress (can be visualised from the axes system in Figure 8.20 and 8.21). It is noted that the time history plot for mesh size of 0.6 m, 0.5 m and 0.4 m has almost merged with each other (with a very little deviation) and this convergence is more prominent at the portion when high compressive stress is developed about which we are most interested in. Hence our initial assumption of mesh size of 0.5 m is quite reasonable and we will follow the output for the 0.5 m mesh size model only.
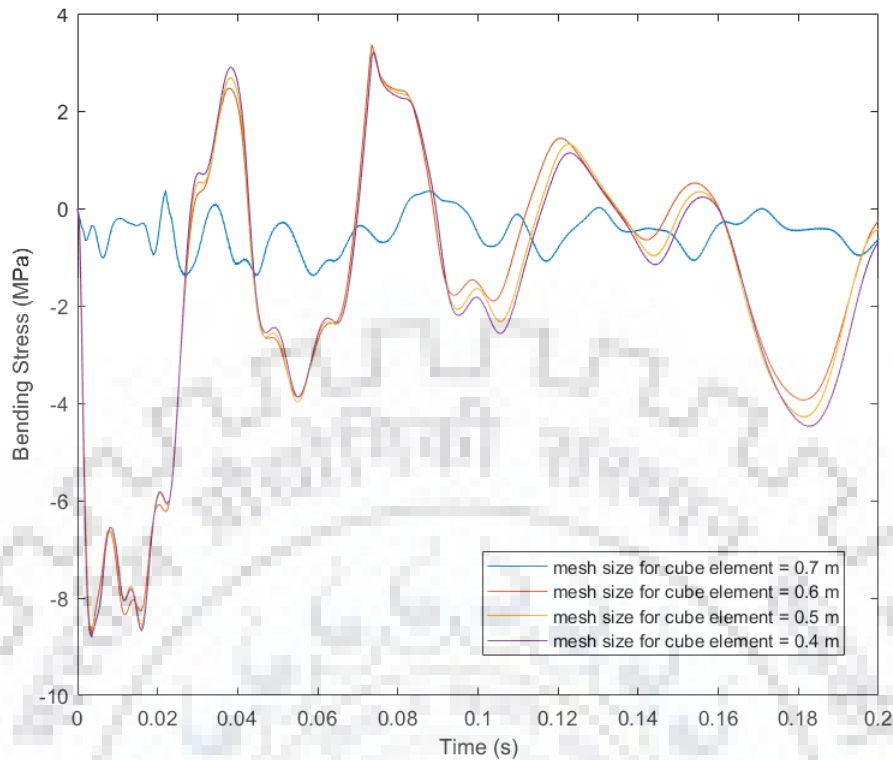
Figure 8.23: Mesh convergence study for bending stress at backside of the front wall

Note- It is also seen that the maximum compressive stress is well within the permissible peak stress (which is 17.84 MPa) and tensile stress also does not exceed the value of 3.51 MPa. Hence our modelling is correct and the front wall at least is not failing in compressive stress. More idea can be achieved from damage contour.

8.4.2   Damage Contour from Analysis Output

Now we have simulated our analysis for 0.5 m mesh size only. We know that in a reinforced concrete structure there will definitely be some tension cracks but we cannot allow crushing of concrete material i.e. compression damage inside the concrete. Hence in terms of ABAQUS results we can expect some tension damage but we should not get the compression damage in order to make the structure safe. Figure 8.24 and 8.25 depicts the tension and Figure 8.26 and 8.27 depicts the compression damage contour respectively at the end of the analysis.
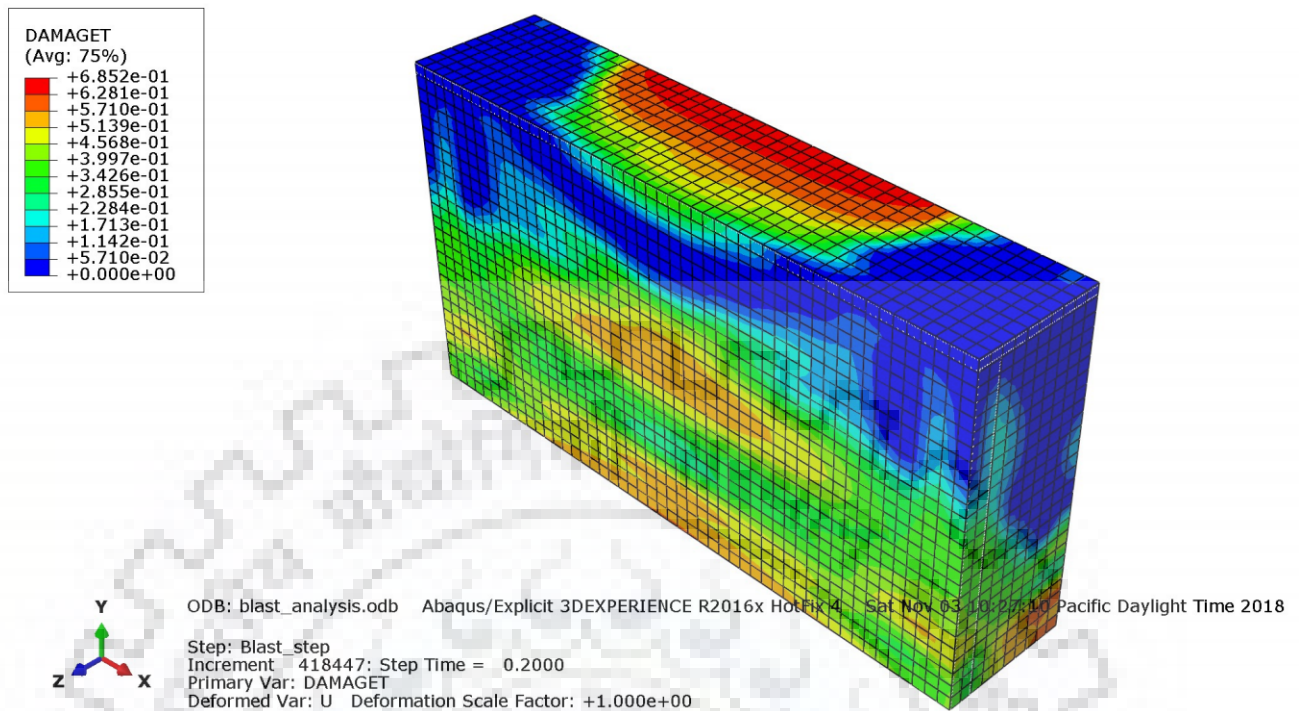
Figure 8.24: Tensile damage contour on the blast resisting wall system (view from outer side)
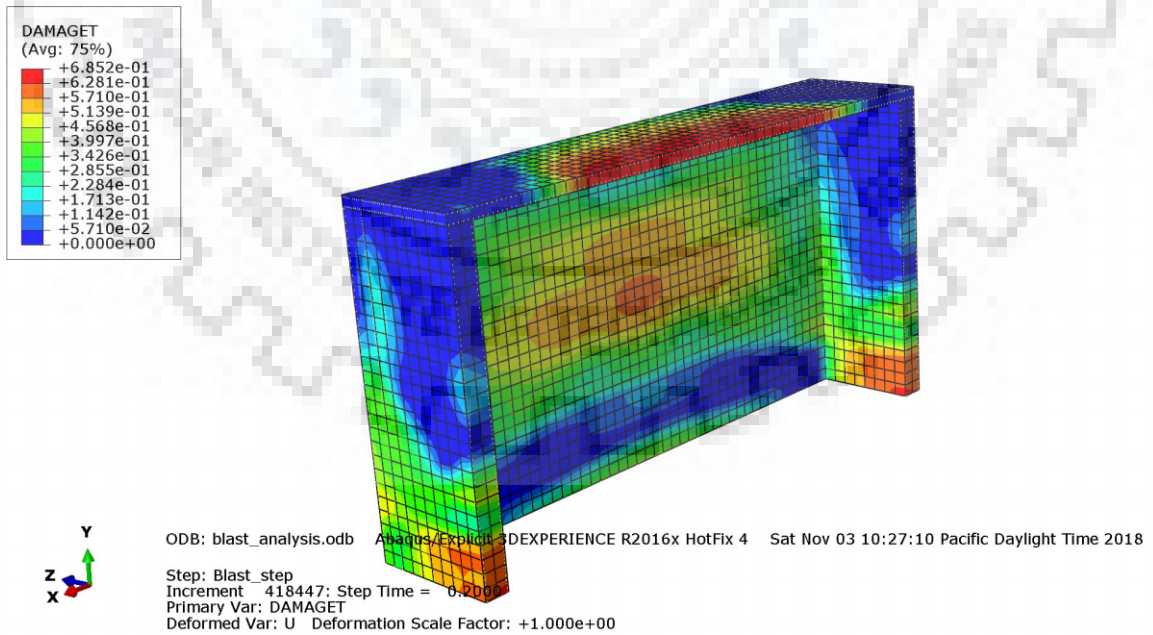
Figure 8.25: Tensile damage contour on the blast resisting wall system (view from inner side)
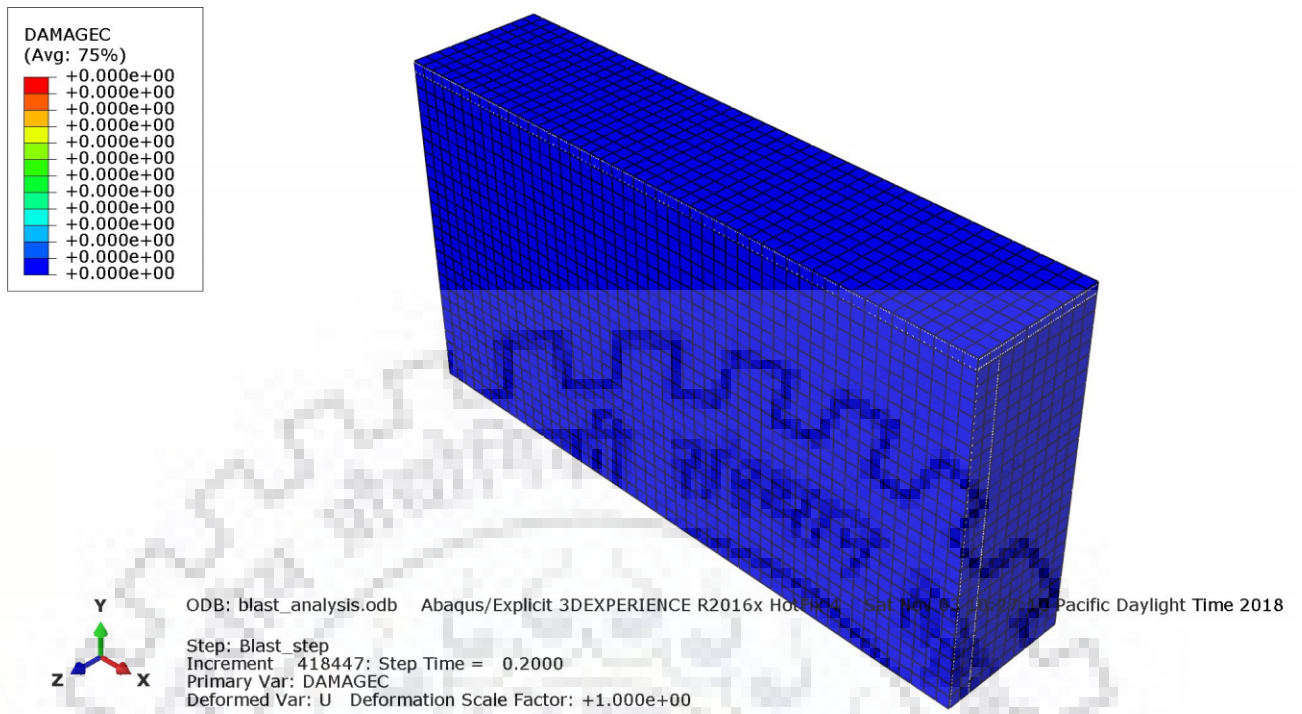
Figure 8.26: Compressive damage contour on the blast resisting wall system (view from outer side)
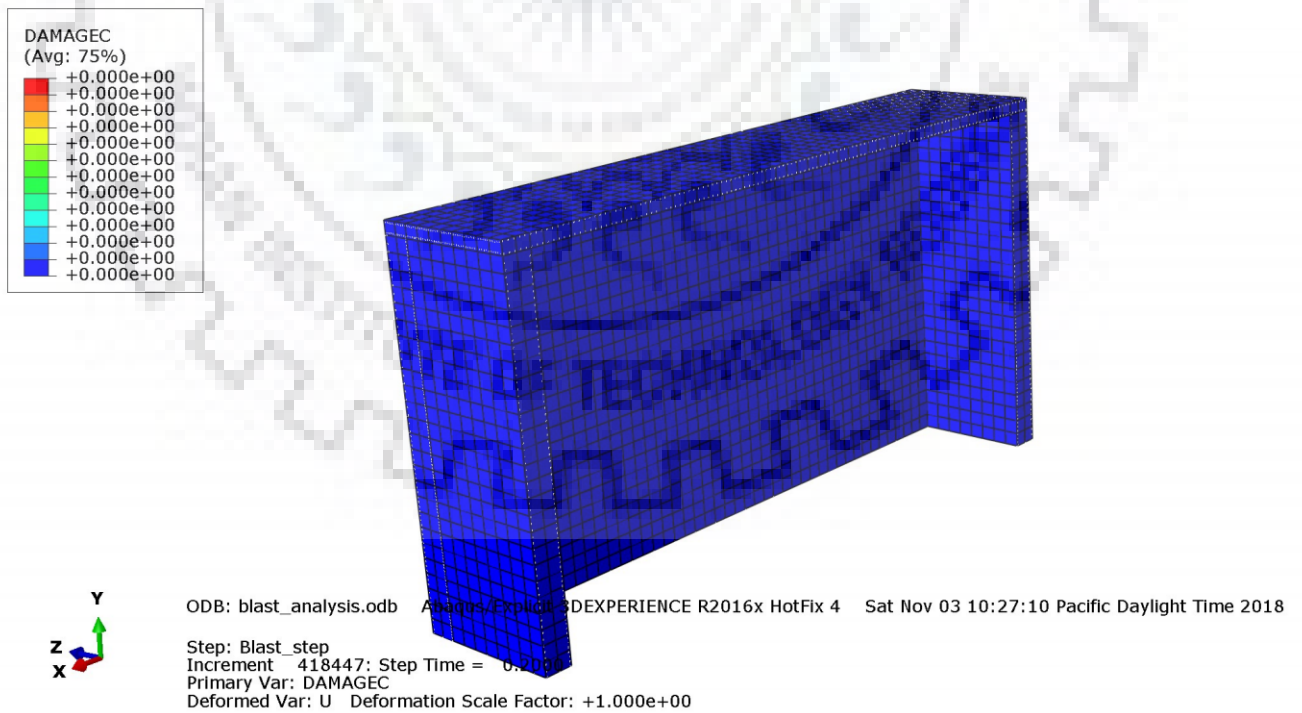
Figure 8.27: Compressive damage contour on the blast resisting wall system (view from inner side)

We can see that there will be tension cracks in the wall but there will not be any crushing or compression failure in the wall system because the damage contour gives zero value at every point for compression damage.

8.4.3 Shear Stress and Adequecy of Shear Links

ABAQUS does not directly show any failure under shear for concrete material. For this we have to check time history of shear stress at potential points of high shear stress concentration. Observing the time histories at several points we can tabulate the maximum appearing shear stress at different locations.

Table 8.4 gives us the maximum shear stress results at different locations and hence we will check the adequacy of the shear links. Figure 8.28 and 8.29 shows different locations at which shear stress are recorded.
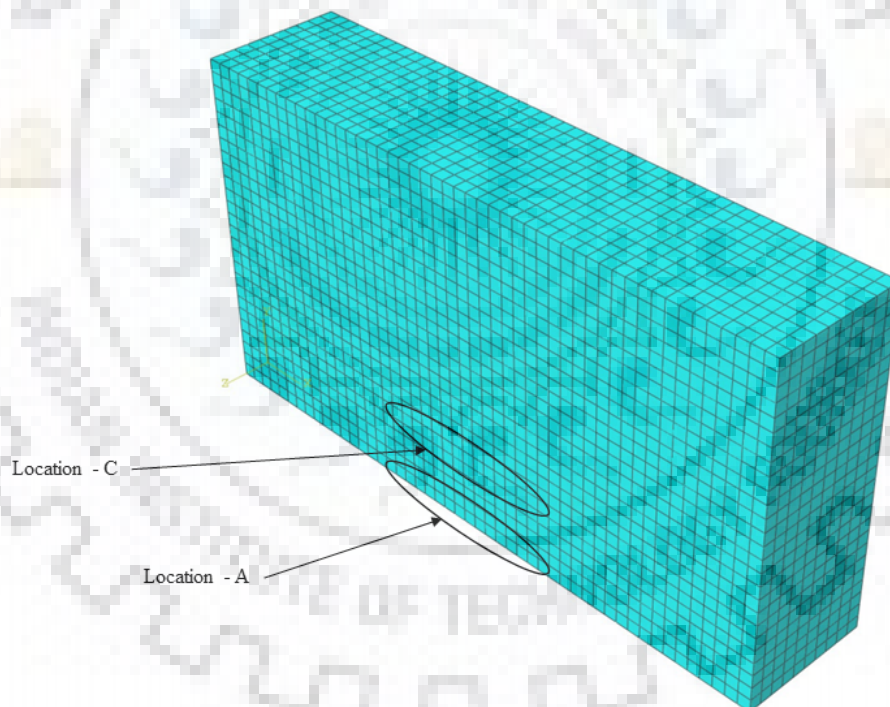
Figure 8.28: Location Markers (outer view)
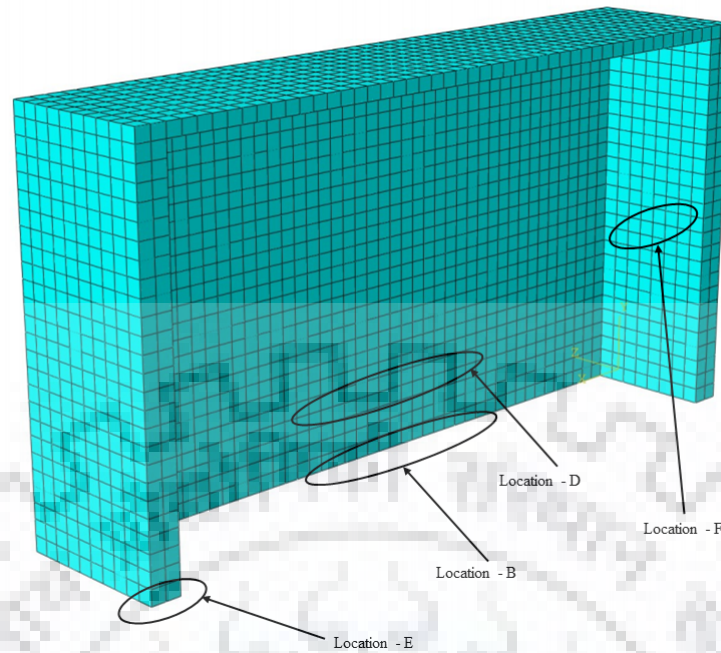
Figure 8.29: Location Markers (inner view)

Table 8.4: Maximum developed shear stress concentration at different locations

Location	Maximum Shear Stress (MPa)
At fixed support of the front wall at ground level in the outer face (location - A)	2.23 MPa
At fixed support of the front wall at ground level in the inner face (location - B)	4.33 MPa
At 2 m height (point of curtailment of I section) of the front wall on the outer face (location - C)	1.98 MPa
At 2 m height (point of curtailment of I section) of the front wall on the inner face (location - D)	2.57 MPa
At the fixed support of the shear (side) wall at ground level (location - E)	2.78 MPa
At the mid height and mid span portion of shear (side) wall (location - F)	2.83 MPa

We know that the maximum nominal shear stress that can be allowed in concrete section in flexure for M40 is $\tau_{c,max} = 4.0$ MPa (as per IS:456 [16]). However at location

'B' i.e. at fixed ground support in the inner face of the front wall, it is exceeding just the way it is predicted by SAP2000 in the preliminary design and hence inclusion of I section composite near ground in front wall was required (in blast loading the structure's local flexibility initially matters more than the integrated action). The I sections prevents the structure from shear failure. However the maximum stress 4.33 MPa is a concentrated stress (not the nominal shear stress) and in the other face (outer) of the front wall at ground level the maximum shear stress is only 2.23 MPa. So in reality the nominal shear stress should lie below 4 MPa at the support too. However, we have used I sections near ground level to prevent the shear failure even if the nominal shear stress exceeds the permissible value of 4 MPa.

Now there are 2 no.s of I sections per metre width ($b=$ 1 m) of the front wall. Hence shear area of each I section (having web thickness t_w = 12 mm) for 2 metre height is $A_{sv} = h \times t_w = (2000 \times 12) \times 2 = 48000\,\text{mm}^2$. Now centre to centre distance (spacing) of I section is s_v = 600 mm. Effective depth (d) of wall = 920 mm. The material used in I section is E250. Now neglecting the capacity of concrete in shear, approximate shear force that the composite section (I section + concrete) can withstand is:

$$V_{us} = \frac{0.87 f_y A_{sv} d}{s_v} = \frac{0.87 \times 250 \times 48000 \times 920}{600} = 16008 \times 10^3 \quad \text{N per m width}$$

Hence maximum shear force allowed in the composite is V_{us} = 16008 kN per metre width of the wall. Hence maximum allowable shear stress in the composite:

$$\tau_{all} = \frac{V_{us}}{db} = \frac{16008 \times 10^3}{920 \times 1000} = 17.4 \quad \text{MPa}$$

Therefore developed shear stress of 4.33 MPa is well within the allowable limit at the front wall near the ground. However it is majorly due to the I section in the composite. Hence we have to check if the shear links are sufficient at the locations where no I section is given.

We will check at location C and D at height of 2 m at front wall because the I sections are curtailed at this location. Now at this location the maximum shear stress concentration is around 2.57 MPa. Now at this location the shear links of 16 mm diameter (Fe415) are spaced evenly by 200 mm along width and 150 mm along height. Now lets consider unit width of front wall at that location (b = 1000 mm). The effective depth (d) is 920 mm (approximately). Along height the spacing is s_v= 150 mm. There are $1000/200 + 1 = 6$ shear links in 1 metre width. At any level the total shear reinforcement

area– $A_{sv} = 6 \times \left(\frac{\pi \times 16^2}{4}\right) = 1206.4\,\text{mm}^2$. Now, neglecting contribution of concrete in shear capacity the maximum shear force (V_u) per m width at location C and D (2 m height) is:

$$V_{us} = \frac{0.87 f_y A_{sv} d}{s_v} = \frac{0.87 \times 415 \times 1206.4 \times 920}{150} = 2672 \times 10^3 \quad \text{N per m width}$$

Hence the allowable shear stress at this location:

$$\tau_{all} = \frac{V_{us}}{db} = \frac{2672 \times 10^3}{920 \times 1000} = 2.904 \quad \text{MPa}$$

We can see that the developed shear stress at this location is 2.57 MPa (maximum) and it is well within the limit 2.904 MPa.

Now for the shear walls also the maximum shear stress is less than the allowable maximum shear stress 4 MPa for M40 concrete. The maximum shear stress along the direction of the blast pressure is 2.83 MPa for the shear wall (more or less). Now longitudinal reinforcements in shear wall will be contributing to the major shear capacity. The longitudinal bars of full length (without curtailment) are considered for the shear capacity for ease of calculation and being on safer side. The bars are of 32 mm dia in both inner and outer face of the wall and the full length is 4.25 m. Hence here effective depth of side wall section will be d = 4250 mm. Now the width of the wall is 1 m and there are 2 bars at any level acting as shear reinforcement. Hence shear area– $A_{sv} = 2 \times \left(\frac{\pi \times 32^2}{4}\right) = 1608.5\,\text{mm}^2$. The maximum spacing along height is s_v= 200 mm. even if we have used Fe500 at this location still As per IS:456 [16] we have to consider f_y= 415 MPa. Hence maximum nominal shear force allowed in location E and F:

$$V_{us} = \frac{0.87 f_y A_{sv} d}{s_v} = \frac{0.87 \times 415 \times 1608.5 \times 4250}{200} = 12341 \times 10^3 \quad \text{N per m width}$$

Hence the allowable shear stress at this location:

$$\tau_{all} = \frac{V_{us}}{db} = \frac{12341 \times 10^3}{4250 \times 1000} = 2.904 \quad \text{MPa}$$

The maximum shear stress concentration at this location is 2.83 MPa and hence it is within limit. Moreover this number 2.83 MPa is for some concentrated stress. If we could calculate the nominal stress it would have been much lower (since stress concentration happens at certain locations). Also, the stress is appearing for a very short time. Hence even if the allowable and appearing shear stress is in close viscinity, then also the structure should be safe because all these checks are only against the nominal shear stress which is generally quite less for a section (stress that we have considered is at a location of high stress concentration).

8.4.4 Displacement Time History at Location of Potential Maximum Displacement

It is evident that the maximum displacement will be at roof and it was also found out from the ABAQUS analysis as well as initial SAP2000 analysis results. The displacement will be high for a very short time but it is important to decide the seperation joint width in order to avoid pounding with the rest of the structures which will not be designed against blast pressure. The roof displacement history is obtained from ABAQUS results and it is shown in Figure 8.30.
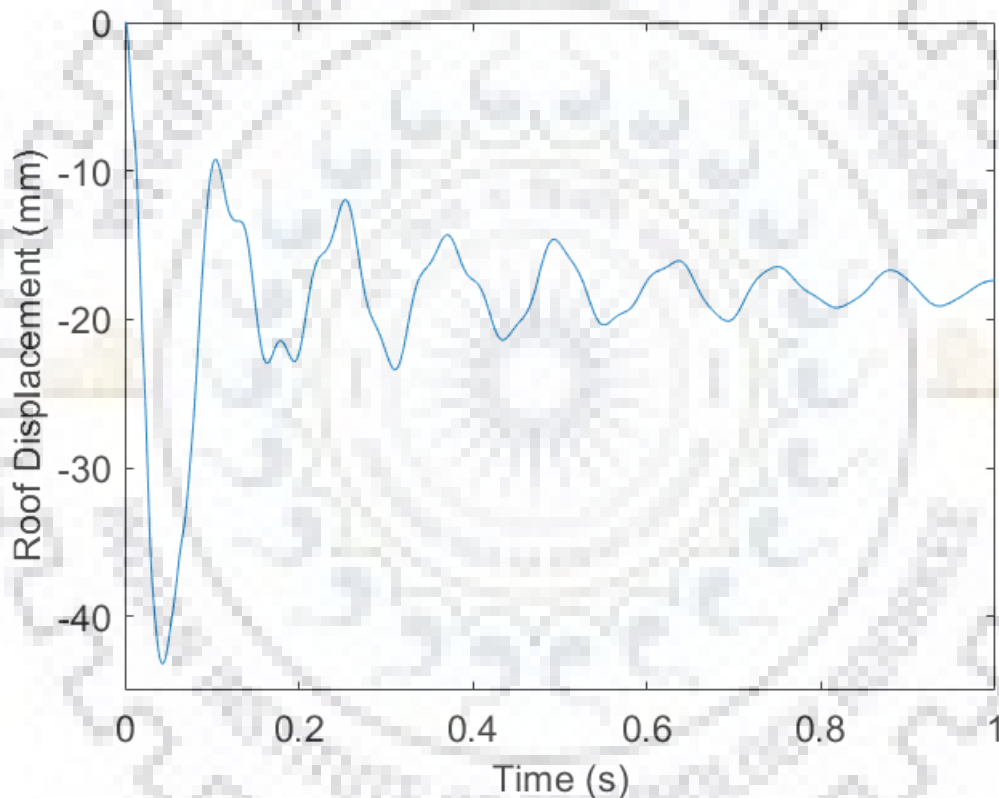
Figure 8.30: Time history of roof displacement in direction of blast load (Z axis)

It is seen that the maximum displacement is coming out to be around 44 mm. Hence we have to make sure that the separation joint is having a width of at least 100 mm (accommodating the static displacement of the inner framed structure as well). That joint can be covered by some material of low strength which will be preventing the blast wall from transferring the pressure on the inner structure which is mainly designed against gravity load.

Chapter 9

Design of the Rest Building Elements

We have managed to design a blast resistant wall so far. However the rest of the building has been designed against gravity loads only since this portion is separated by a separation joint from the blast resisting wall system. The proposed building system is given in Figure 9.1, 9.2 and 9.3. The next thing done is the design of the building components (beams and columns) using SAP2000. Figure 9.4, 9.5 and 9.6 show the details of gantry girder, typical beam section and a column section respectively. The gantry girder is designed using IS:800 [19] and the beam and column sections are designed using SAP2000 for load combinations as per IS:456 [16].
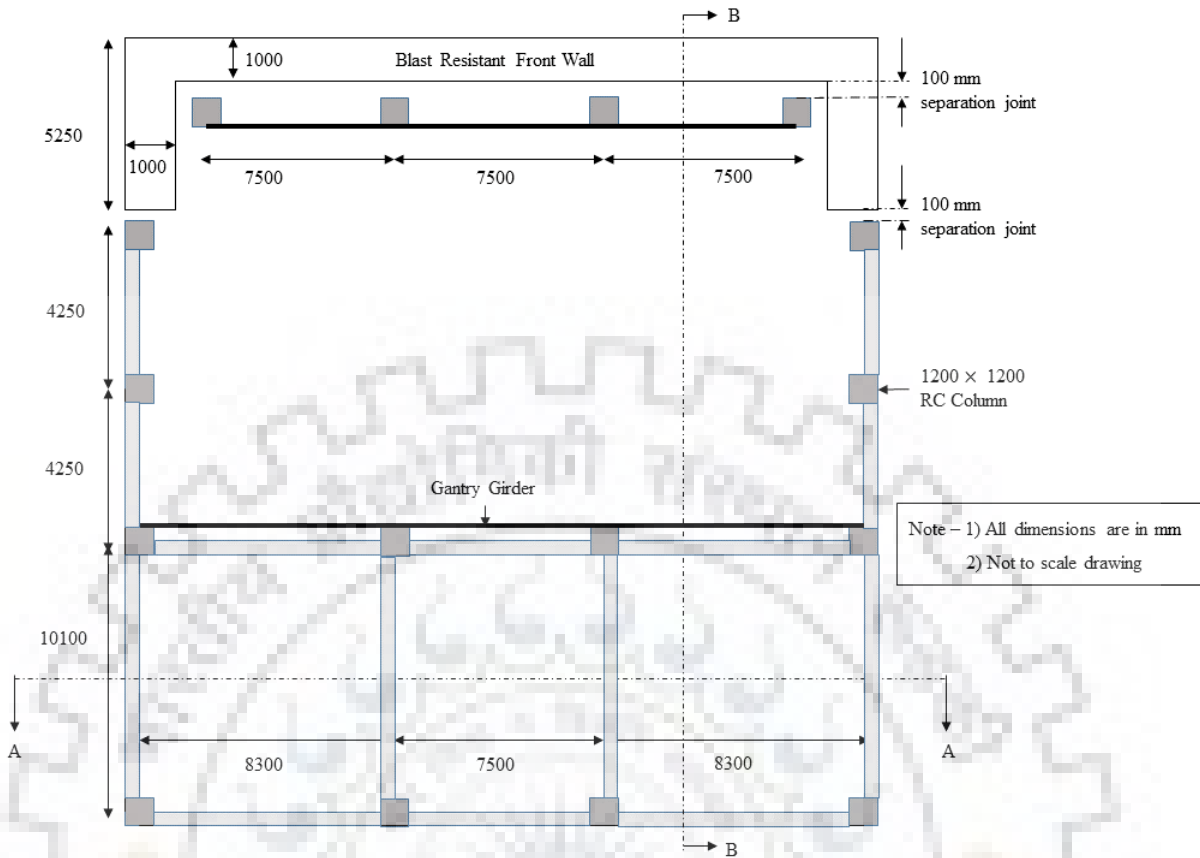
Figure 9.1: Proposed Building System
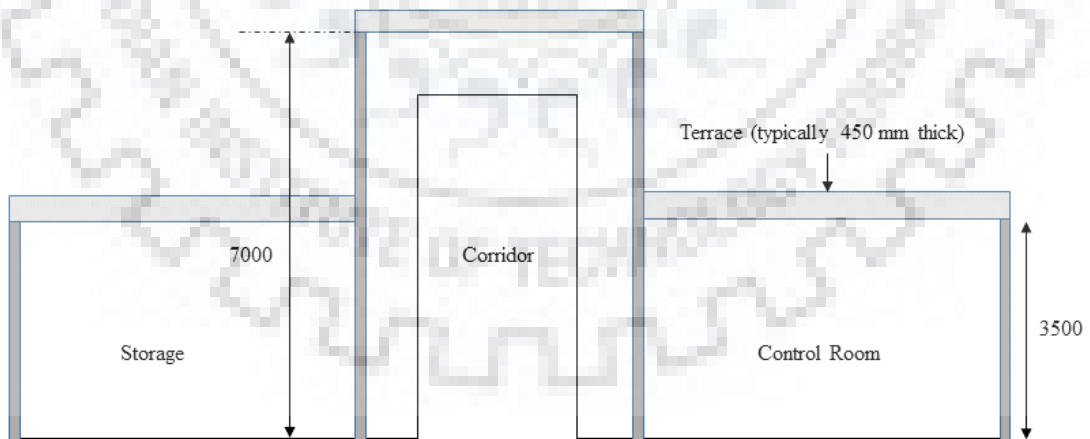
Section A-A

Figure 9.2: Sectional elevation of section A-A
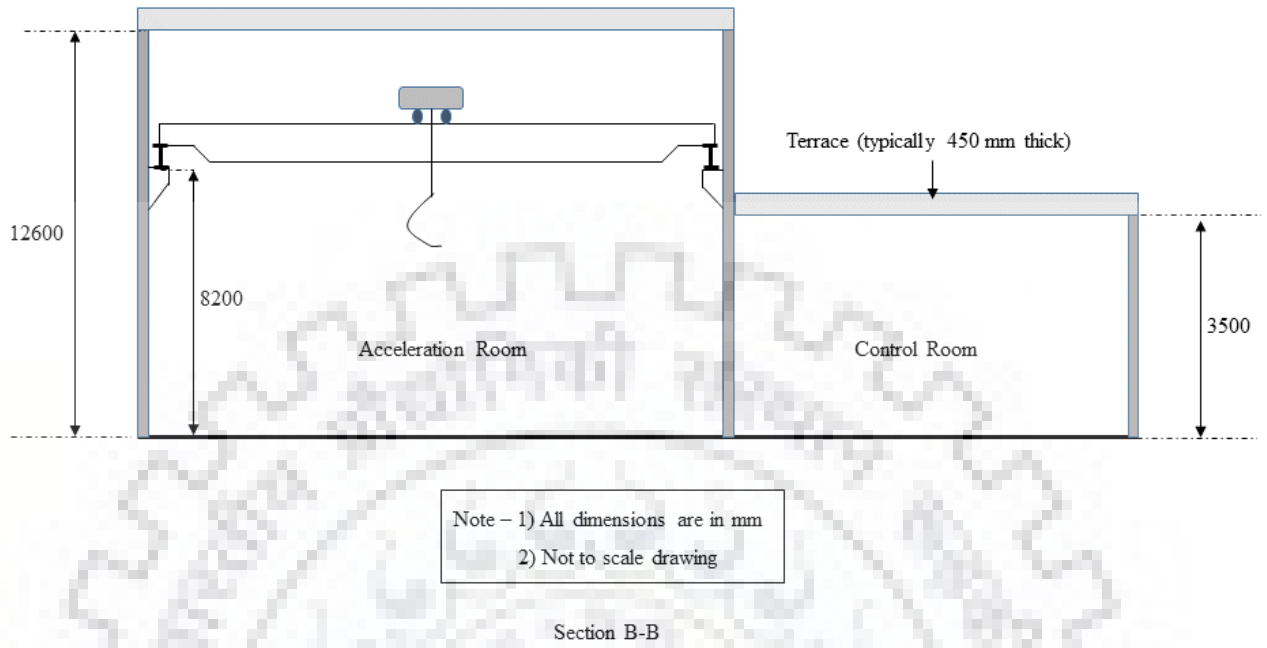
Figure 9.3: Sectional elevation of section B-B
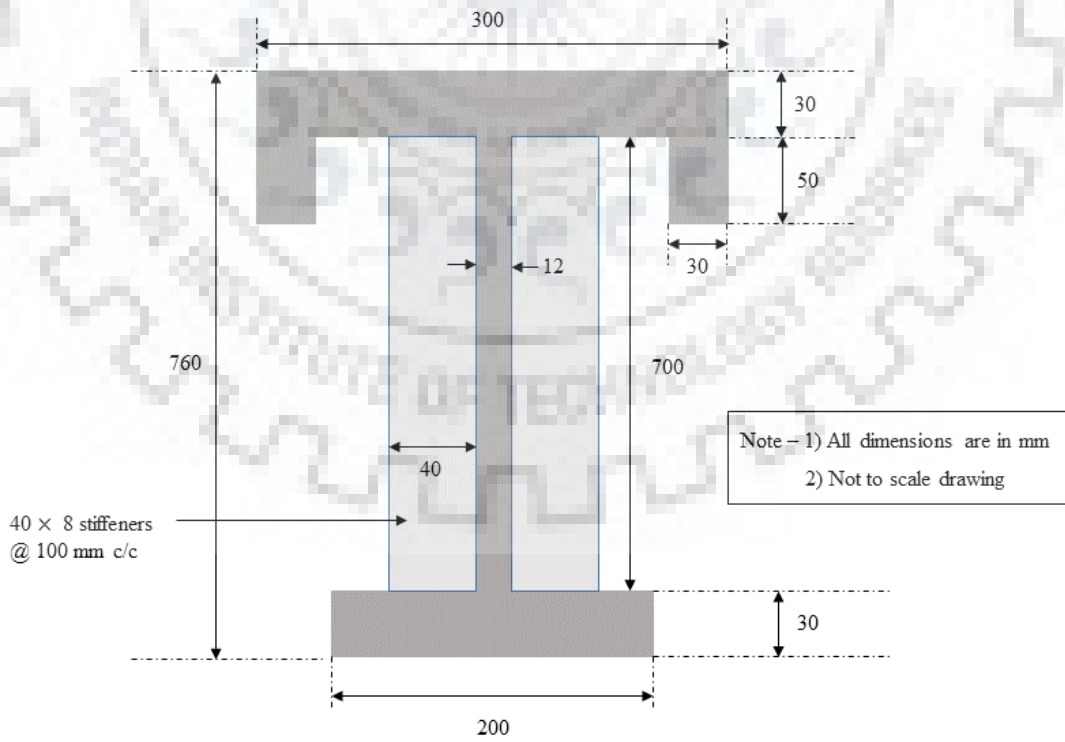
Figure 9.4: Details of the gantry girder section
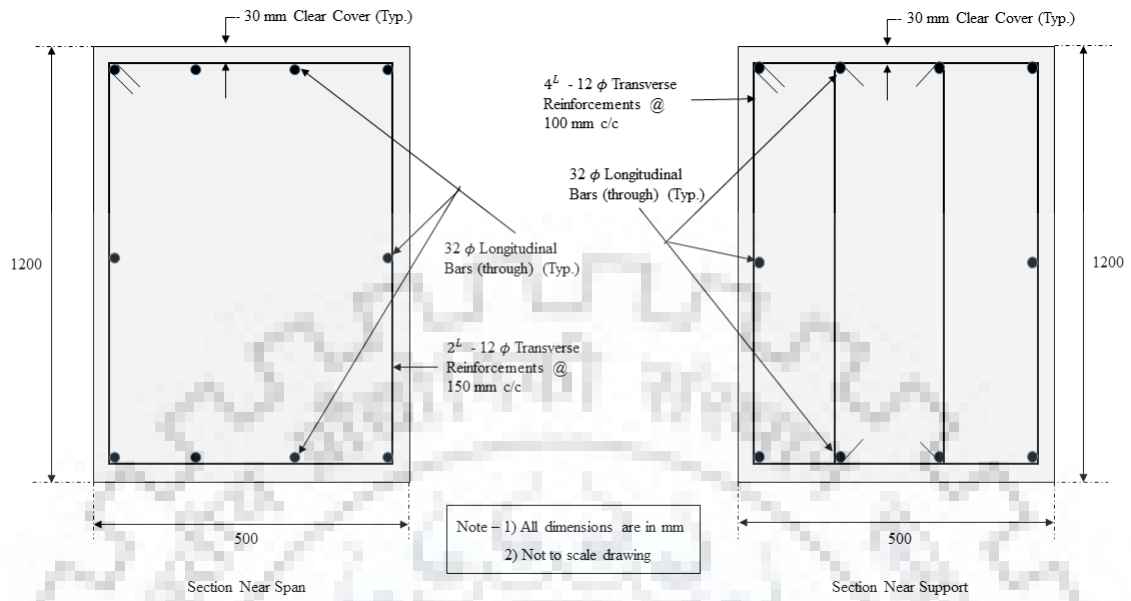
Figure 9.5: Details of a typical beam section
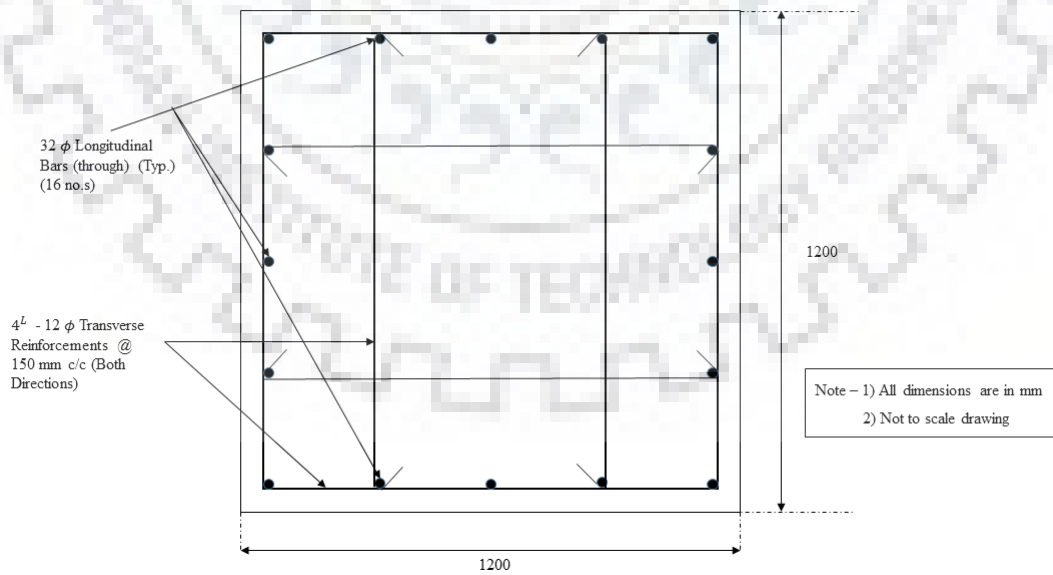
Figure 9.6: Details of a typical column section

Chapter 10

Reduction of Blast Induced Ground Vibration

10.1. Objective and Possible solution

So far we have managed to keep the blast pressure under a certain limit using the viscoelastic pad and designed the blast resistant wall system to withstand the reduced blast pressure. However elevated air pressure is not the only effect of a blast phenomenon. The other important and noticeable effect lies in the ground motion which is especially prominent in case of near ground or surface explosion. The blast pressure wave hits the ground the same way as it strikes the face of a structure. As a result, a shock wave is created due to impact in the ground surface which propagates as surface waves and body waves inside the earth. Therefore our objective lies in controlling this excessive shock type of ground motion so that proper foundation and maybe isolation system can be installed to mitigate this challenge.

To reduce the intensity of ground motion, a suitable trenching system is considered here lying almost at the midway between point of detonation and surface of the building. Depth of the trench is varied to look into the reduction in horizontal acceleration. Detailed procedures have been discussed in the later sections.

10.2. Site Soil Properties

This blast resistant building is to be built in a sandy site. It has to be remembered that proper soil improvement technique including compaction is required to enhance the properties to construct such a structure in reality. A three layer soil domain is used in this problem. We have considered the basic properties such as density (ρ), Poisson's ratio (ν), cohesion (c) and friction angle (ϕ) of an improved sand at each layer for the chosen site. We have found the standard penetration resistance (N value) from IS:6403 [18] and hence the shear wave velocity (V_s) at different layers using ASCE/SEI 7-16 [3]. Hereafter the shear modulus (G) and the elastic modulus (E) can be calculated using eq: (10.1) and eq: (10.2) respectively.

$$G = \rho \times V_s^2 \tag{10.1}$$

$$E = 2(1 + \nu) \times G \tag{10.2}$$

Now we can get the P-wave velocity (V_p) using eq: (10.3).

$$\frac{V_p^2}{2V_s^2} = \frac{1 - \nu}{1 - 2\nu} \tag{10.3}$$

The basic considered properties and the calculated properties are given in Table 10.1 and Table 10.2 respectively.

Table 10.1: Basic Properties of Sandy Soil at the Site

Layer Number	Density(ρ) (kg/m^3)	Poisson's Ratio (ν)	Friction Angle (ϕ)
1	1600	0.3	33 °
2	1800	0.3	36 °
3	2100	0.3	38 °

This way we are being able to create a Mohr-Coulomb's ($c - \phi$) constitutive model for different layers of soil. The schematic representation of the three layered soil domain is given in Figure 10.1.

Table 10.2: Obtained Properties of Sandy Soil at the Site

Layer Number	Standard Penetration Value (N) (blows/30 cm) (using IS:6403 [18])	Shear Wave Velocity (V_s) (m/s) (using ASCE/SEI 7-16 [3])	Shear Modulus ($G = \rho V_s^2$) (MPa)	Elastic Modulus (E) (MPa)	P-wave Velocity (V_p) (m/s)
1	20	209	70	182	391
2	30	261	123	320	488
3	40	313	206	536	586
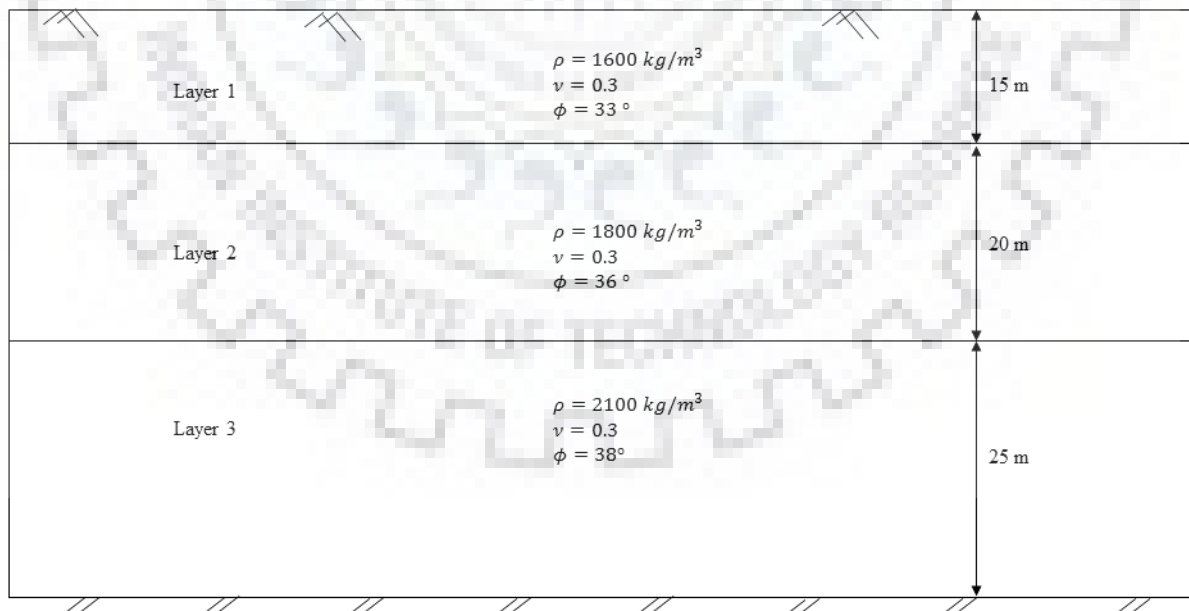
Figure 10.1: Sandy soil properties for the given site

10.3.   Model of Blast Load on Soil

We can get the blast profile using the theories and expressions available in Chapter 3. We will again use the same explosive which is 60 kg TNT equivalent with a 20% factor of safety on the charge weight as mentioned in UFC 3-340-02, 2008 [40]. However, the stand-off distance will be different in this case and it will be the height of explosion. The most detrimental effect can be found when the blast load is almost a point load due to explosion right at the surface of earth. We will however consider a minimum height of explosion 1 m and apply the blast pressure of a strip of 1 m width. For the sake of simplicity we will consider a linear decay profile of blast pressure acting on the ground 5 m away from the building surface. The trench will be cut around at the midway between point of detonation and surface of the blast wall. The applied blast pressure time history is given in Figure 10.2.
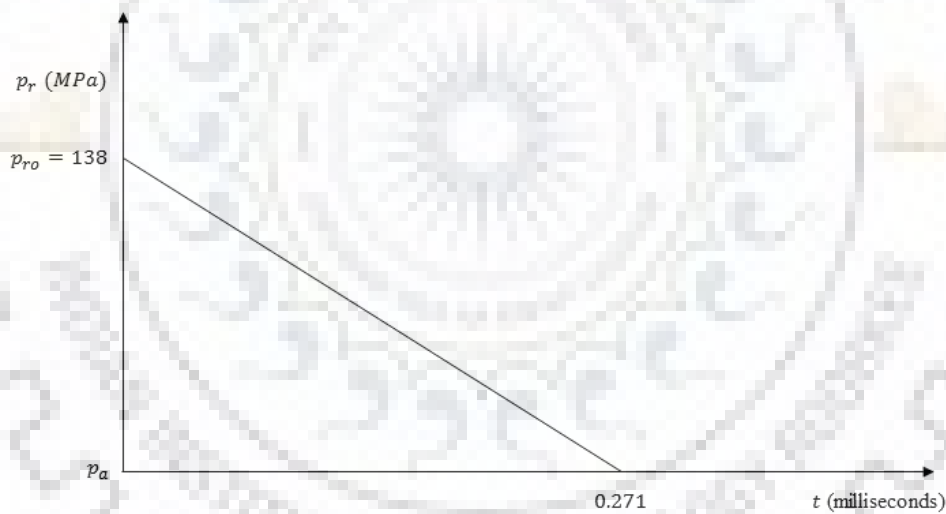
Figure 10.2: Time History of applied blast pressure at ground surface

10.4.   Finite Element Modelling of Soil Domain

The finite element modelling is done in ABAQUS/Explicit. The depth and width of the domain is considered such a way that no reflected wave comes back in the specified frame of time. The time of action for the blast pressure profile is only 0.272 milliseconds.

Therefore the time frame set in analysis is very low and in this problem we have considered it to be 0.1 seconds or 100 milliseconds. It is observed that all noticeable shocks come well within this time frame. The maximum shear wave and P-wave velocity are 313 m/s and 586 m/s respectively. We are modelling a 2-dimensional plane strain model of the soil domain. Hence minimum width of the model required in either side of the detonation point is $313 \times 0.1 = 31.3$ m while minimum depth of the model required is $586 \times 0.1 = 58.6$ m.Therefore we are considering 140 m wide and 60 m deep soil domain for finite element analysis in order to avoid the necessity to provide dampers at the boundaries. The trench is having a width of 0.5 m and with some flexible liner. It is installed almost in the halfway between the surface of the wall and the point of detonation. The significance of flexible liner is that it will only be retaining the soil for a short period of time and may get broken or damaged when the blast phenomenon occurs in order to get as much plastic deformation as possible to dissipate energy. Thereafter we have made the bottom boundary fixed because of the presence of rock. The lateral boundary is restrained against is lateral motion considering presence of huge soil mass on the both sides of the soil boundaries.

Now the whole model is meshed using plain strain elements. The size of the mesh is judiciously using commonly used eq: (10.4) for maximum mesh size (s_{max}) for wave propagation problem.

$$s_{max} = \frac{V_s}{a f_{max}} \tag{10.4}$$

Where f_{max} is the maximum frequency interest in a ground motion problem which is typically considered as 10 Hz for regular earthquakes and as high as 50 Hz for blast induced motion and a is a constant whose value is considered between 5 to 10. This equation basically suggests to accommodate at least 5 to 10 times the wavelength at the largest considered frequency of the ground motion. Hence maximum mesh size limit requirement in this problem is $209/(5 \times 50) = 0.836$ m. Hence, we have considered a mesh size of 0.5 m along the lateral dimension throughout the model while in the vertical direction it is 0.5 m at the top and middle layer and 0.8 m at the bottom layer. The chosen element type is CPE4R which is a 4 noded plain strain element with reduced integration.

Mohr-Coulomb's plasticity model is adopted for modelling properties of sand. It will itself include the damping due to plasticity or the hysteresis damping. An additional 5% viscous damping is applied in form of Rayleigh Damping ($\alpha = 1.0289$ and $\beta = 1.338 \times 10^{-3}$

using the frequency analysis results).

Finally the load is applied at a point which is 2.5 m away from the trench edge and thus 5 m away from the building surface. The pressure is applied over an area of 1 metre width to avoid any numerical failure in the solver. An explicit analysis is thereafter run for different trench depths. The typical model for Finite Element Analysis is shown in Figure 10.3.
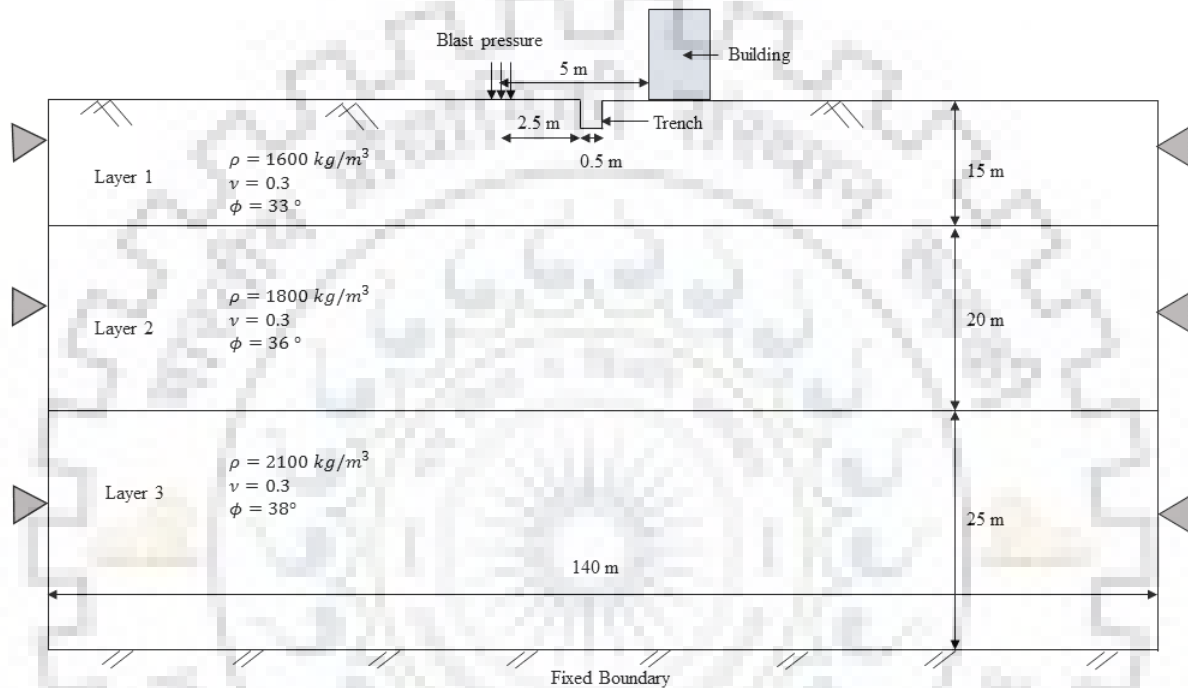
Figure 10.3: Soil domain model used for finite element analysis

10.5.   Results and Discussions

Analysis is run for trench depths of 0 m (no trench), 0.5 m, 1.0 m, 1.5 m and 2.0 m. Our interest is in horizontal acceleration at the front face of the building. Figure 10.4 shows the plotted the horizontal acceleration time history at that point. If we look into the trend we can observe that due to the impact on the ground surface only one major peak is coming in the acceleration history which exerts a shock type of load in form of ground motion. We can observe that for 0 m and 0.5 m trench depth there is no considerable decrease in the horizontal acceleration at the front face of the building. However as we further increase the trench depth it will intersect the stress dispersion path of the applied blast pressure.
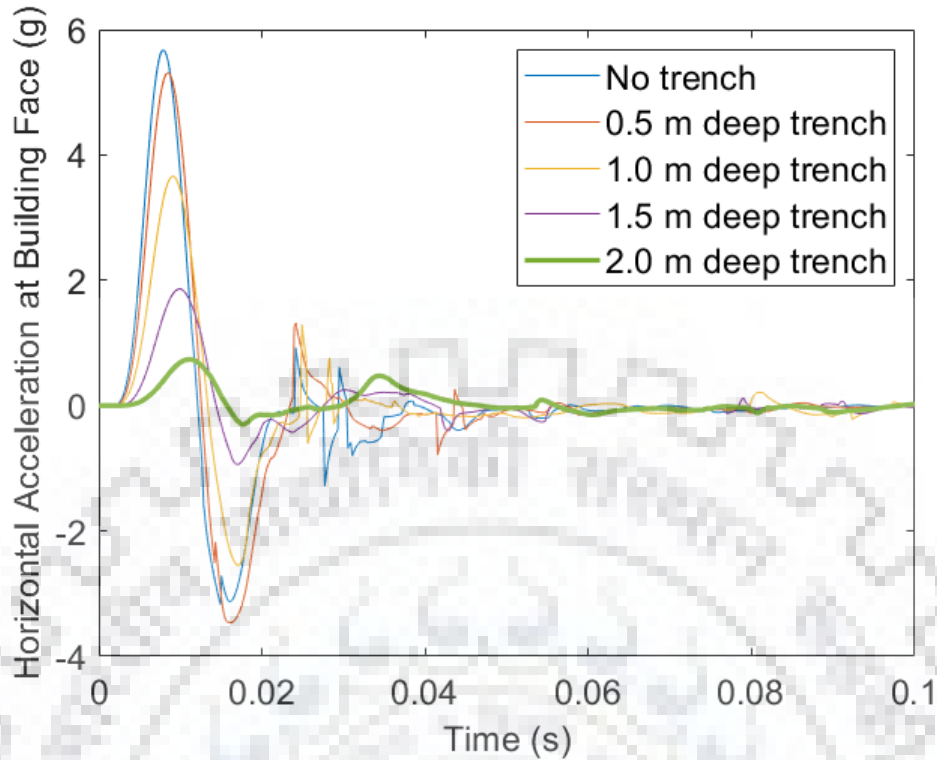
Figure 10.4: Comparison of horizontal ground acceleration at front face of building for diferent trench depths

This makes the trench more effective. As a result we can observe considerable decrease in the peak value of the shock ground acceleration at the mentioned point. We can see that at 2 m trench depth we are getting peak horizontal acceleration of less than 1g in the shock. In this very short period of time 1g ground acceleration is quite manageable and thus we conclude to build a 2 m deep sacrificial trench of 0.5 m width.

Now from the Figure 10.4 it can be seen that the damped period of the horizontal ground acceleration time history is roughly 0.02 second and hence the frequency is around 50 Hz. Now the blast resistant wall system is enough stiffened to withstand the blast pressure and hence it will easily be able to safeguard the blast wall against the attenuated blast induced ground motion as well. Again, the framed structure of the rest of the building which is designed against conventional method does have much higher period compared to the predominant 0.02 second period of blast induced ground motion. For an approximate estimate of fundamental natural period (T) we can use the formula for bare frame RC framed building using IS:1893 (Part I) [15]:

$$T = 0.075 \times h^{0.75} = 0.075 \times 12.6^{0.75} = 0.50 \, \text{second}$$

Hence it is clearly visible that the period of ground motion is different from that of the framed structure portion of the building by a huge margin. Hence, we can assure that blast induced ground motion will not be giving any detrimental effect on the framed structure which is designed against gravity loads only and hence our design assumption is correct. However if earthquake resistant design is required, standard protocol given in IS:1893 (Part I) [15] has to be followed.

Thus the complete system is predicted under the given circumstances. An isolation system may however be necessary to safeguard the machine foundations for sensitive equipments, which may have a higher natural frequency, from the attenuated ground motion. However in such small amount of shock load in such a short duration creating very small impulse the framed building will easily cater this ground motion because of the gap in period of horizontal acceleration and the fundamental natural period.

Chapter 11

Conclusions and Scope

The problem of design of a blast resistant wall for high impact explosions at short stand-off distance is considered. It is found that it is practically impossible to design a blast resistant wall system without any external energy dissipation mechanism when the explosion is in close range. Viscoelastic pads offer some promise in this context when the geometry and functional requirements do not allow use of an outer frame and energy dissipation systems.

Even after using the viscoelastic damping pad and getting more than 50% dissipation in peak pressure and using two shear walls to support the out of plane action on the front wall, the stresses are too high and require use of a composite section to provide adequate resistance and safety. The recommended design solution of using embedded I-sections in concrete wall is found to perform satisfactorily. However, it has to be ensured that proper raft foundation is built below the whole structure which can provide sufficient fixity to the blast wall as well as the columns. It is also required to make the lateral and vertical deflection of the whole structure under dynamic loading uniform. Base isolators can also be designed with supplemental passive dampers above the raft to ensure safety of the equipments and the rest portion of the building which is not designed against blast pressure.

The equipments inside the building have to be safeguarded using some isolation techniques. However again it is impractical to design these isolators or dampers against the whole shock ground motion due to surface blast phenomenon. Trenches are found out to be an effective solution to attenuate the ground acceleration lasting for very short duration. We can reduce the shock ground acceleration down to as low as a value of 1g using only 2.0 m deep trench. However, it has to be kept in mind that some flexible material has

to be used to create liners of the trench in order to incorporate some damage or plastic deformation in these liners thus dissipating more energy. The design should be based on the load and stresses appearing at the portion of the liners. The liners as well as the whole trench is a sacrificial one. Every time before the experiment such trench can be excavated with some flexible liners. Using of the trenches allows us to incorporate suitable dampers or isolators which can easily be installed to keep the equipments safe against this well reduced ground motion acting for a very short duration. The high frequency ground motion does not affect the RG framed structure part of the building with much lower fundamental frequency.

There are always scopes for further research in this or related topic. Some are discussed here. We have used some simplified models for blast load as well as the viscoelastic pad. This is sufficient for engineering problems like this. However if one has to look into the physics more rigorously, then more rigorous model has to be structured. For example, in this study, simplified rheological model is used for viscoelastic damping pad. For more precise study one must obtain proper non linear constitutive model for damping pad, maybe from creep test data (experimental). Likewise for the blast load too, we have considered uniform pressure as specified in IS:4991 [17]. However, if the behaviour of structure under close range blast has to be studied more extensively, then a proper distribution of pressure on the wall has to be incorporated. The best way to do so is to model the surrounding air as a fluid and accounting for a Computational Fluid Dynamics (CFD) problem. Thus it will become a fluid structure interaction problem due to the complex dynamics of blast wind and its effect on the blast resistant wall. Considering these factors would make this problem more complex which is unnecessary for this specific problem and therefore simplified model is considered. However, this is always a scope to partly or fully incorporate the actual model of damping pad or blast load to get a more precise result.

Bibliography

[1] ABAQUS Documentation (2016). *ABAQUS Analysis User's Manual*. Dassault Systems, Providence, RI, USA.

[2] Amadio, C. and Bedon, C. (2012). Blast analysis of laminated glass curtain walls equipped by viscoelastic dissipative devices. *Buildings*, 2(3):359–383.

[3] ASCE/SEI 7-16 (2016). *Minimum Design Loads and Associated Criteria for Buildings and Other Structures*. The American Society of Civil Engineers, USA.

[4] ASTM D 395-03 (2003). *Standard Test Methods for Rubber Property–Compression Set*. ASTM International, USA.

[5] Brode, H. L. (1955). Numerical solutions of spherical blast waves. *Journal of Applied Physics*, 26(6):766–775.

[6] Connor, J. J. (2003). *Introduction to Structural Motion Control*. Prentice Hall Pearson Education Upper Saddle River, New Jersey.

[7] Design Handbook, Lord (1971). *Lord Kinematics Design Handbook*. Lord Corporation, North Carolina, USA.

[8] Draganić, H. and Sigmund, V. (2012). Blast loading on structures. *Technical Gazette*, 19(3):643–652.

[9] Eurocode-2 (2008). *Eurocode 2 : Design of Concrete Structures: British standard*. British Standards Institution,London, UK.

[10] Fediuc, D. O., Budescu, M., Fediuc, V., and Venghiac, V.-M. (2013). Compression modulus of elastomers. *Buletinul Institutului Politehnic din lasi. Sectia Constructii, Arhitectura*, 59(2):157.

[11] Friedlander, F. G. (1946). The diffraction of sound pulses i. diffraction by a semi-infinite plane. *Proc. R. Soc. Lond. A*, 186(1006):322–344.

[12] Gent, A. N. (2012). *Engineering with Rubber: How to Design Rubber Components.* Carl Hanser Verlag GmbH Co KG, Munich, Germany.

[13] Genta, G. (2009). *Vibration Dynamics and Control.* Springer.

[14] Hamburger, R. and Whittaker, A. (2004). Design of steel structures for blast-related progressive collapse resistance. *Modern Steel Construction*, 44(3):45–51.

[15] IS:1893 (Part I) (2016). *Criteria for Earthquake Resistant Design of Structures.* Bureau of Indian Standards (BIS), New Delhi, India.

[16] IS:456 (2000). *Plain and reinforced Concrete – Code of Practice.* Bureau of Indian Standards (BIS), New Delhi, India.

[17] IS:4991 (1968). *Criteria for Blast Resistant Design of Structures for Explosions Above Ground.* Bureau of Indian Standards (BIS), New Delhi, India.

[18] IS:6403 (1981). *Code of Practice for Determination of Bearing Capacity of Shallow Foundations.* Bureau of Indian Standards (BIS), New Delhi, India.

[19] IS:800 (2007). *General Construction in Steel – Code of Practice.* Bureau of Indian Standards (BIS), New Delhi, India.

[20] Jankowiak, T. and Lodygowski, T. (2005). Identification of parameters of concrete damage plasticity constitutive model. *Foundations of Civil and Environmental Engineering*, 6(1):53–69.

[21] Kmiecik, P. and Kamiński, M. (2011). Modelling of reinforced concrete structures and composite structures with concrete strength degradation taken into consideration. *Archives of Civil and Mechanical Engineering*, 11(3):623–636.

[22] Kranzer, C., Gürke, G., and Mayrhofer, C. (2005). Testing of bomb resistant glazing systems. experimental investigation of the time dependent deflection of blast loaded 7.5 mm laminated glass. In *Glass Processing Days,* Tempére, Finland, 17–20 June.

[23] Krauthammer, T. and Altenberg, A. (2000). Negative phase blast effects on glass panels. *International Journal of Impact Engineering*, 24(1):1–17.

[24] Kupfer, H., Hilsdorf, H. K., and Rusch, H. (1969). Behavior of concrete under biaxial stresses. *ACI Journal*, 65(8):656–666.

[25] Lee, J. and Fenves, G. L. (1998). Plastic-damage model for cyclic loading of concrete structures. *Journal of Engineering Mechanics*, 124(8):892–900.

[26] Lubliner, J., Oliver, J., Oller, S., and Onate, E. (1989). A plastic-damage model for concrete. *International Journal of Solids and Structures*, 25(3):299–326.

[27] Majewski, S. (2003). The mechanics of structural concrete in terms of elasto-plasticity. *Publishing House of Silesian University of Technology, Gliwice.*

[28] Malvar, L. J., Crawford, J. E., and Morrill, K. B. (2007). Use of composites to resist blast. *Journal of Composites for Construction*, 11(6):601–610.

[29] Mander, J. B., Priestley, M. J., and Park, R. (1988). Theoretical stress-strain model for confined concrete. *Journal of Structural Engineering*, 114(8):1804–1826.

[30] Mays, G., Smith, P. D., and Smith, P. D. (1995). *Blast Effects on Buildings: Design of Buildings to Optimize Resistance to Blast Loading.* Thomas Telford.

[31] Mills, C. (1987). The design of concrete structure to resist explosions and weapon effects. In *Proceeding of the 1st international Conference on Concrete for Hazard Protection*, pages 61–73.

[32] Newmark, N. and Hansen, R. (1961). Design of blast resistant structures. In Crede, C. and Harris, C., editors, *Shock and Vibration Handbook*, volume 3. McGraw-Hill.

[33] Ngo, T., Mendis, P., Gupta, A., and Ramsay, J. (2007). Blast loading and blast effects on structures–an overview. *Electronic Journal of Structural Engineering*, 7(S1):76–91.

[34] Rankine, W. J. M. et al. (1870). Xv. on the thermodynamic theory of waves of finite longitudinal disturbance. *Philosophical Transactions of the Royal Society of London*, 160:277–288.

[35] Rigby, S. E., Tyas, A., Bennett, T., Clarke, S. D., and Fay, S. D. (2014). The negative phase of the blast load. *International Journal of Protective Structures*, 5(1):1–19.

[36] Salim, H., Dinan, R., and Townsend, P. (2005). Analysis and experimental evaluation of in-fill steel-stud wall systems under blast loading. *Journal of Structural Engineering*, 131(8):1216–1225.

[37] Salim, H. A., Dinan, R., Kigar, S. A., Townsend, P. T., and Shull, J. (2003). Blast-retrofit wall systems using cold-formed steel studs. In *16th ASCE Engineering Mechanics Conference,* 16–18 July. University of Washington, Seattle, U.S.A.

[38] Smith, P. (2010). Blast walls for structural protection against high explosive threats: A review. *International Journal of Protective Structures*, 1(1):67–84.

[39] Technical Data, 3M Products (2017). *3M Technical Data.* 3M Products, Minnesota, USA.

[40] UFC 3-340-02, 2008 (2008). *Structures to Resist the Effects of Accidental Explosions.* Department of Defense, USA.

[41] Wang, T. and Hsu, T. T. (2001). Nonlinear finite element analysis of concrete structures using new constitutive models. *Computers & Structures*, 79(32):2781–2791.